ELECTRON TRANSFER THROUGH ORGANIC AND BIOLOGICAL MOLECULES

Thesis by

Brian Leigh

In Partial Fulfillment of the Requirements

For the Degree of

Doctor of Philosophy

California Institute of Technology

Pasadena, California

2009

(Defended July 15, 2008)

Acknowledgments

It is difficult to overstate my gratitude to my advisor Harry Gray. He provided great encouragement, sound advice, superior teaching, good company, and lots of excellent ideas. His passion for chemistry is unrivaled. I would have been lost without him.

I would like to thank Jay Winkler for an education in practical chemistry. He has taught me laser spectroscopy, electronics, software, Matlab, and a lot of mathematics. Most of all he has taught me independent problem solving in physical chemistry, an extremely valuable tool.

I am indebted to my past advisor Carl Wamser. If it wasn't for Carl I would have never have pursued chemistry. He is incredibly patient and kind, and has instilled in me a great passion for teaching others.

Katsumi Niki was an excellent collaborator I was fortunate to work with in my time here. He was usually the first person I saw every morning just waiting to talk about electrochemistry and azurin.

I would like to thank Jack Richards for use of his lab space and his time. He has always given good advice and insight into questions I have thrown to him.

Eve Menger, George Hammond, and David Peyton have always been there for any question I have had. Most often it has been the science conversations outside of the lab that have been the most rewarding.

I am grateful for having worked with Judy Kim. Her unbridled enthusiasm for all things science, Raman, and Igor has rubbed off on me. What she lacks in stature she more than makes up for in sheer brain power and unrestrained kindness.

I learned label synthesis, protein labeling, FPLC, and a lot about azurin from Angelo Di Bilio. If it wasn't for his daily devotion to the aging FPLC's in Noyes I would have never have had clean protein.

Bruce Brunschwig has always given me help whenever I have needed it. I thank him for all the time he has spent answering my questions.

Many people in my time at Caltech have added to my education. Jeremiah Miller started me on azurin and spectroscopy, for which I am grateful. All my glass work was done with Oliver Wenger. We had lots of long nights working in the sub-basement. I was fortunate to work with both Kyoko Fujita and Keiko Yokoyama on protein electrochemistry. Yuling Sheng is an amazing biochemist; we would be lost without her skill. Libby Mayo was a great partner in crime; never get on her bad side. Steve Contakes is the best person to share an office with, and his wife makes good brownies. Don Walker has always been there to lend me a hand with whatever I needed help with in lab or out. Alec Durrell has been a great help in lab and I am happy to see the glass work continue with him. Catherine May always looks out for me in the Beckman Institute. Rick Gerhart and Mike Roy have always made me whatever I needed when I needed it, be it made of glass or metal.

This thesis is dedicated to

Robert F. Rice Sr.,

Katsumi Niki,

and George S. Hammond

Abstract

The function of solvent in facilitating long-range coupling in donor/bridge/acceptor complexes is not well understood. There are exceptional challenges inherent to the measurement of the electron transfer coupling properties of solvents. By immobilizing the donor and acceptor in a glass to eliminate the effects of diffusion, statistical methods of analysis can be employed to study electron transfer between randomly dispersed donor and acceptor molecules over long distances. Toluene and 2-methyltetrahydrofuran form glasses that can solubilize donor and acceptor molecules at 77 K. Exponential decay constant of 1.23 per angstrom, for electron tunneling through a frozen toluene glass, and 1.62 per angstrom through 2-methyltetrahydrofuran glass have been found.

Identification of the electronic coupling sites on the surfaces of proteins is usually achieved by inspection of a crystal structure. These coupling spots have been experimentally observed by employing mixed self-assembled monolayer electrodes and a variety of mutants. The electron transport protein azurin has a well defined reduction potential on self-assembled monolayer electrodes (0.16 V vs. saturated Ag/AgCl). When a point mutation is made at position 48, electron transfer ceases. This disruption of electron transfer occurs because the mutation forces conformational changes that disrupt a critical hydrogen bond between asparagine-47 and cysteine-112. This hydrogen bond is a key element for electron transfer into and out of the protein.

Table of Contents

List of Figures and Tables

Chapter 1 – Introduction

Chapter 2 - Electron Transfer through Organic Glasses

Chapter 3 - Electron Transfer and Bridge Energy Levels

Chapter 4 - Electron Transfer Through Biological Molecules

Chapter 1

Introduction

Electron Transfer

Classical theory

Electron transfer is the only reaction that occurs over long distances (>20 Å) with rates that are greater than 10^3 s^{-1}. No bonds are made or broken, only rearrangements of angles and bond lengths in the products are required. The observable kinetics of electron transfer can be described using a small number of experimentally available factors.[1]

The seminal paper for electron transfer theory was published by Marcus in 1956.[2] Classical theory is based on the law of energy conservation and the Franck-Condon principle. The electron transfer reaction only occurs at the transition state, when the reactants and products are of equal energy and the nuclei do not move. This lack of nuclear motion occurs because the nuclei are much larger in mass relative to electrons, and they change their positions much more slowly than do the electrons. In general, classical theory is used to describe strongly coupled (adiabatic) systems.[3]

Semiclassical theory

For weakly coupled systems (nonadiabatic), the transition state must be formed a number of times before the electron is transferred to create the product; this electron transfer reaction is described by semiclassical models (Equation 1.1).[4]

$$k_{ET} = \left(\frac{4\pi^3}{h^2 \lambda kT} \right)^{1/2} H_{AB}^2 \exp\left(\frac{-\left(\Delta G^o + \lambda\right)^2}{4\lambda kT} \right) \qquad (1.1)$$

The rate of the reaction (k_{ET}) is a function of temperature (T), driving force (ΔG^o), reorganization energy (λ), and electronic coupling between the donor and the acceptor (H_{AB}). H_{AB} is sensitive to the intervening medium and decays rapidly with distance.[5-9]

The relationship between ΔG^o and λ results in four different situations (Figures 1.1 and 1.2). These different scenarios for electron transfer are when $\Delta G^o = 0$ (self exchange), the normal region where $0 \leq -\Delta G^o \leq \lambda$, the barrierless condition where $-\Delta G^o = \lambda$, and the inverted region where $-\Delta G^o > \lambda$. The barrierless situation will exhibit the fastest kinetics since the ground state of the products is at the transition state.

Initiation of electron transfer

There are three main processes for initiating electron transfer: thermal, optical, and photoinduced. Thermally activated electron transfer is achieved through vibronic coupling of the two molecules such that the activation energy is achieved and the process proceeds forwards.[10-12] Optical electron transfer (inter-valence charge transfer) is the transfer of an electron between two adjacent metal ions, occurring vertically from the reactant state. Absorption of a photon within the energy gap initiates the electron transfer reaction (Figure 1.3).[13] Photoinduced electron transfer occurs when photoexcitation creates an excited state that is of sufficient energy for electron transfer. Photon absorption results in charge separation, which is then typically followed by thermal charge recombination back to the original ground state unless the charge-separated state can further react.

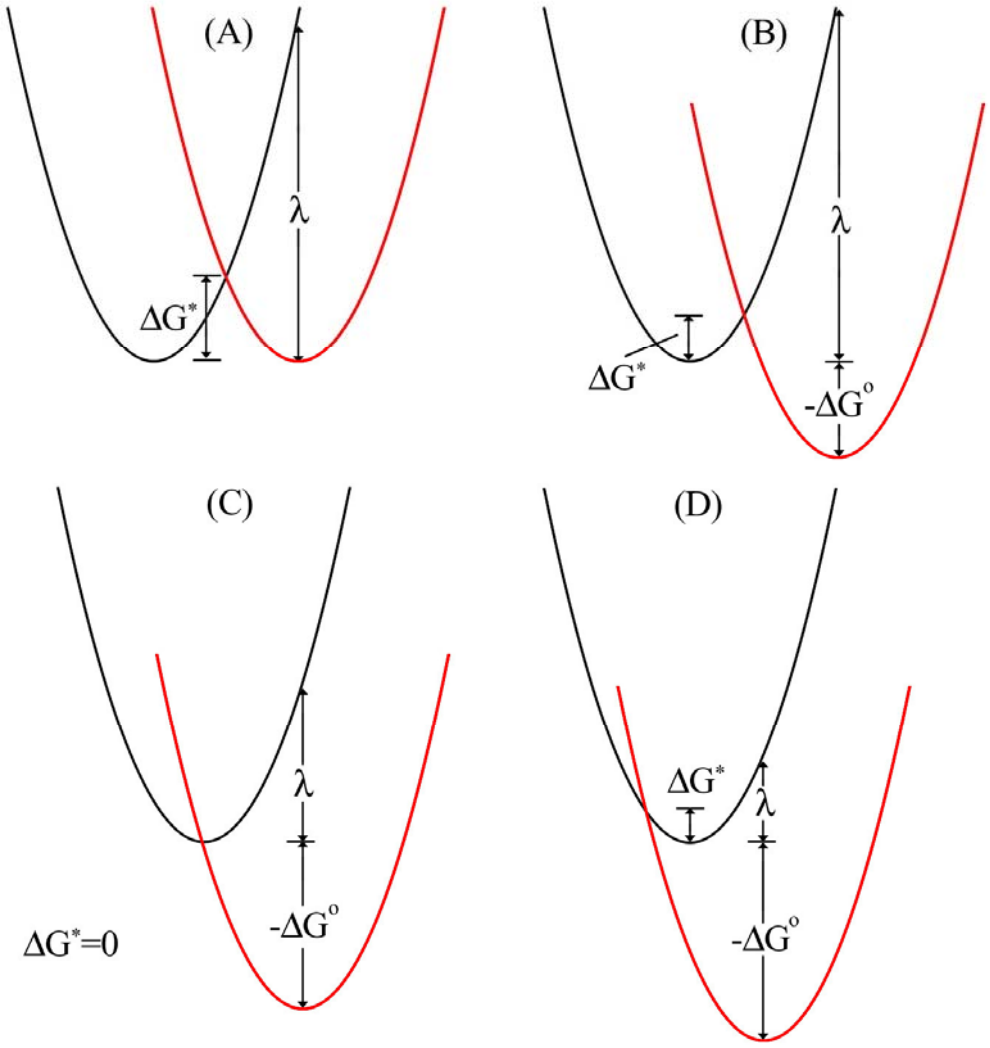

Figure 1.1 Diagrams showing the intersections of the Gibbs energy surfaces for the reactant state (black) and the product state (red): (A) isoergonic reaction were $\Delta G^o = 0$; (B) normal region where $0 \leq -\Delta G^o \leq \lambda$; (C) the barrierless condition where $-\Delta G^o = \lambda$; (D) inverted region where $-\Delta G^o > \lambda$.

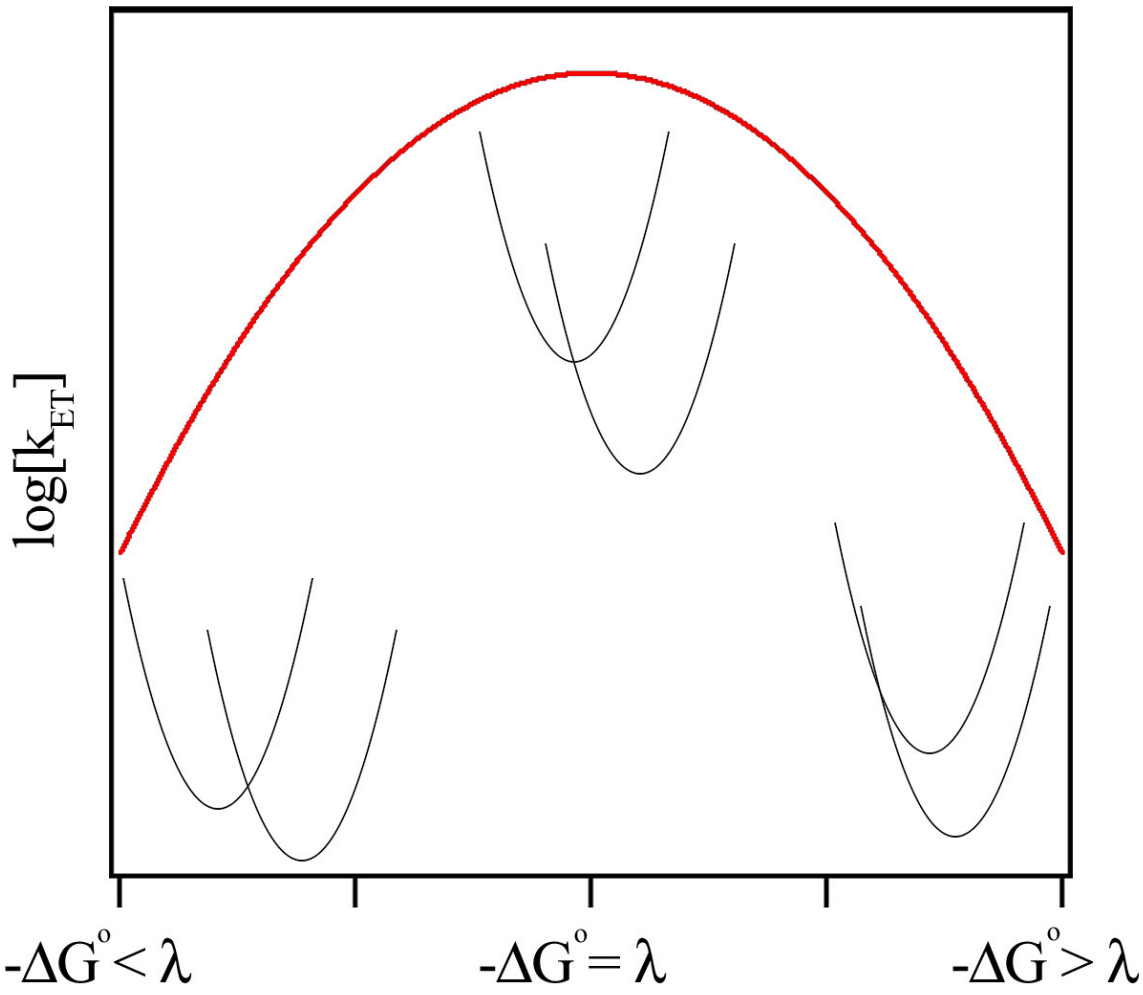

Figure 1.2 Diagram illustrating relationship between driving force (-ΔGº) in relation to reorganization energy (λ) and logarithm of the rate of electron transfer (red). Black curves are Gibbs free energy surfaces from Figure 1.1.

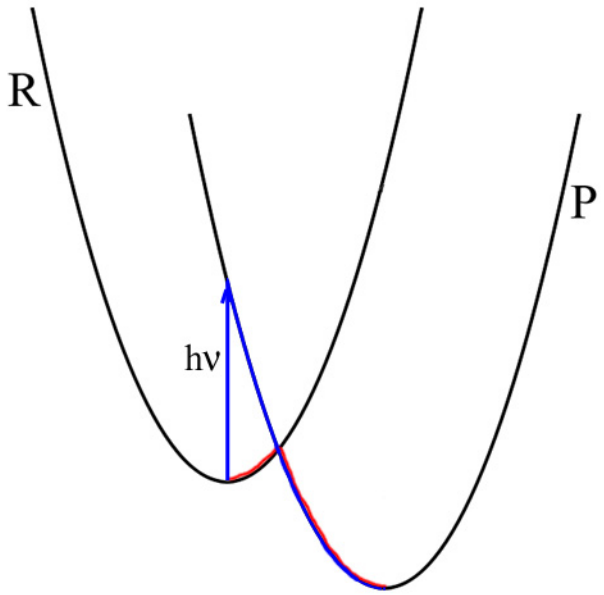

Figure 1.3 Diagrams showing the intersections of the Gibbs energy surface with thermal electron transfer pathway (red) and optical electron transfer (inter-valence charge transfer) (blue).

Self Assembled Monolayers

Self assembled monolayers (SAMs) are surfaces consisting of a single layer of molecules on a substrate. SAMs are usually prepared by adding a solution of the desired molecule onto a substrate surface and washing off the excess, unbound molecules. The desired monolayer molecule typically has a unique region that exhibits a high affinity for the substrate, and not to itself or another monolayer molecule. Once full coverage of the substrate surface area is achieved, the monolayer does not continue to grow since intermolecule forces between the molecules are relatively weak.

Common materials used to make SAMs are alkanethiols. Thiols have a high affinity for gold (145 kJ/mol) and the alkane chains pack well due to van der Waal forces. Alkanethiols have been well characterized.[14, 15]

Proteins have been shown to adsorb onto a variety of different SAMs.[16] Experiments on proteins adsorbed onto SAMs included biosensors,[17] electron transfer kinetics,[18] impedance spectroscopy,[19] and AFM.[20] Many electrochemistry experiments have been run as well.[21, 22]

References

1. Marcus, R. A.; Sutin, N., *Biochim. Biophys. Acta* **1985,** 811, 265.
2. Marcus, R. A., *J. Chem. Phys.* **1956,** 24, 966.
3. Marcus, R. A.; Eyring, H., *Ann. Rev. Phys. Chem.* **1964,** 15, 155.
4. Hopfield, J. J., Electrical Phenomena at the Biological Membrane Level. In Roux, E., Ed. Elsevier: 1977.
5. Oevering, H.; Paddon-Row, M.; Heppener, M.; Oliver, A.; Cotsaris, E.; J.Verhoeven; Hush, N., *J. Am. Chem. Soc.* **1987,** 109, 3258.
6. Johnson, M. D.; Miller, J. R.; Green, N. S.; Closs, G. L., *J. Phys. Chem.* **1989,** 93, 1173.
7. Helms, A.; Heiler, D.; McLendon, G., *J. Am. Chem. Soc.* **1992,** 114, 6227.
8. Miller, J. R.; Peeples, J. A.; Schmitt, M. J.; Closs, G. L., *J. Am. Chem. Soc.* **1982,** 104, 6488.
9. Guarr, T.; McGuire, M. E.; G. McLendon, *J. Am. Chem. Soc.* **1985,** 107, 5104.
10. Hopfield, J. J., *Proc. Natl. Acad. Sci. USA* **1974,** 71, 3640.
11. Li, X.; Hihath, J.; Chen, F.; Masuda, T.; Zang, L.; Tao, N., *J. Am. Chem. Soc.* **2007,** 129, 11535.
12. Zhao, Y.; Han, M.; Liang, W.; Nakamura, H., *J. Phys. Chem. A* **2007,** 111, 2047.
13. Ito, T.; Hamaguchi, T.; Nagino, H.; Yamaguchi, T.; Washington, J.; Kubiak, C. P., *Science* **1997,** 277, 660.
14. Rubinstein, I.; Sabatani, E.; Maoz, R.; Sagiv, J., *Organized Monolayers on Gold Electrodes*. The Electrochemical Society: 1986; p 175.
15. Pale-Grosdemange, C.; Simon, E. S.; Prime, K. L.; Whitesides, G. M., *J. Am. Chem. Soc.* **1991,** 113, 12.
16. DiMilla, P. A.; Folkers, J. P.; Biebuyck, H. A.; Haerter, R.; Lopez, G. P.; Whitesides, G. M., *J. Am. Chem. Soc.* **1994,** 116, 2225.
17. Dong, S.; Li, J., *Bioelectrochemistry and Bioenergetics* **1997,** 42, 7.
18. Armstrong, F. A.; Barlow, N. L.; Burn, P. L.; Hoke, K. R.; Jeuken, L. J. C.; Shenton, C.; Webster, G. R., *Chemical Communications* **2004,** 3, 316.
19. Bordi, F.; Prato, M.; Cavalleri, O.; Cametti, C.; Canepa, M.; Gliozzi, A., *J. Phys. Chem. B* **2004,** 108, 20263.
20. Huang, Y.-W.; Gupta, V. K., *J. Chem. Phys.* **2004,** 121, 2264.
21. Avila, A.; Gregory, B. W.; Niki, K.; Cotton, T. M., *J. Phys. Chem. B* **2000,** 104, 2759.
22. Fujita, K.; Nakamura, N.; Ohno, H.; Leigh, B. S.; Niki, K.; Gray, H. B.; Richards, J. H., *J. Am. Chem. Soc.* **2004,** 126, 13954.

Chapter 2

Electron Transfer through Organic Glasses

Introduction

Many hormones in nature require amidation at the carboxyl terminus or other modification in order for them to be biologically active.[1-4] Peptidylglycine α-hydroxylating monooxygenase (PHM) is an example of an enzyme that catalyzes the amidation reaction utilizing two copper centers.[5] PHM contains two subunits; the CuA site acts as an electron transfer site and the CuB site acts as an oxygen binding site (Figure 2.1).[6, 7] In a typical di-copper protein, both copper sites are saturated by protein ligands. In PHM, however, the two copper centers have solvent occupied coordination sites. The distance between the copper atoms is 11 Å, and crystal structures of PHM in both substrate-bound and unbound configurations show no variation in the Cu-Cu distance, ruling out the possibility that the protein undergoes a conformational change that brings the two metal centers into contact distance (Figure 2.2). Spectroscopic studies have further confirmed that a binuclear copper center is not transiently generated during the enzymatic reaction.[6-9] From inspection of the structures the shortest through-bond electron transfer pathway is 70 residues in length and the shortest pathway involving hydrogen-bonded residues is 24 residues.[5] Catalytic turnover of the enzyme dictates that the electron transfer rate must be at least 100 ms^{-1}. This electron-transfer rate is much faster than that predicted by through-bond tunneling, which should occur through a distance of no more than about 30 Å.[10]

It has been proposed that the path of electron transfer between the two metal centers is directly through the 11 Å of intervening water.[5] Other experimental observations support this idea; for example, in covalently cross-linked azurin complexes, structured water that formed between the two redox centers appeared to increase the

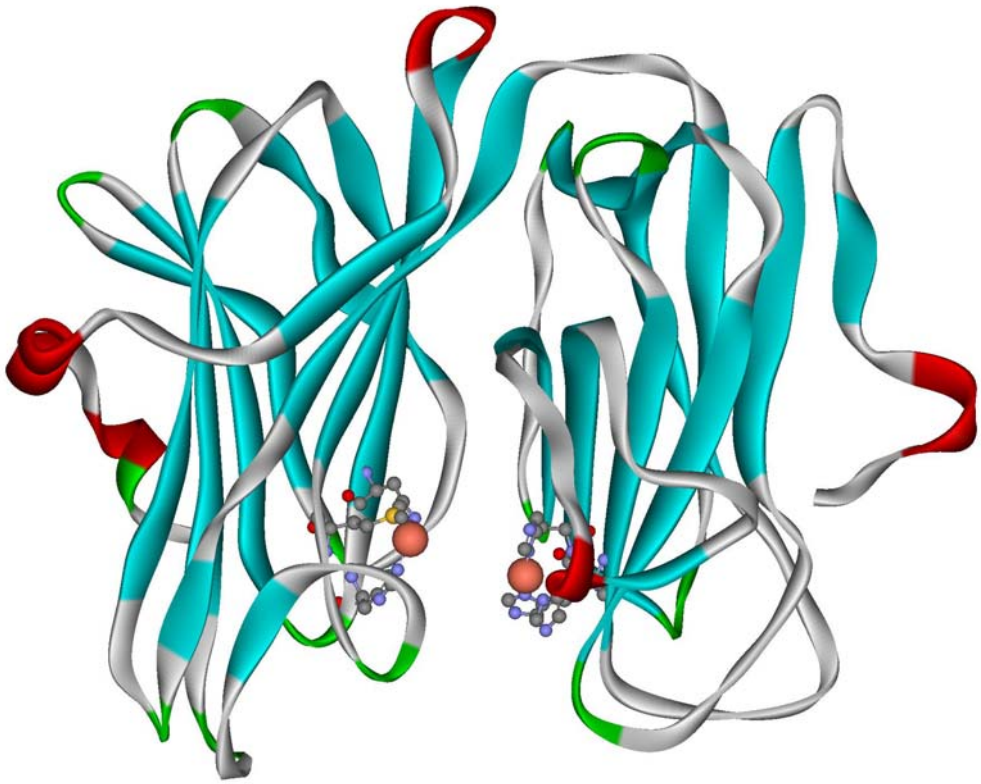

Figure 2.1 Peptidylglycine α-hydroxylating monooxygenase (PHM) from PDB structure 1PHM.

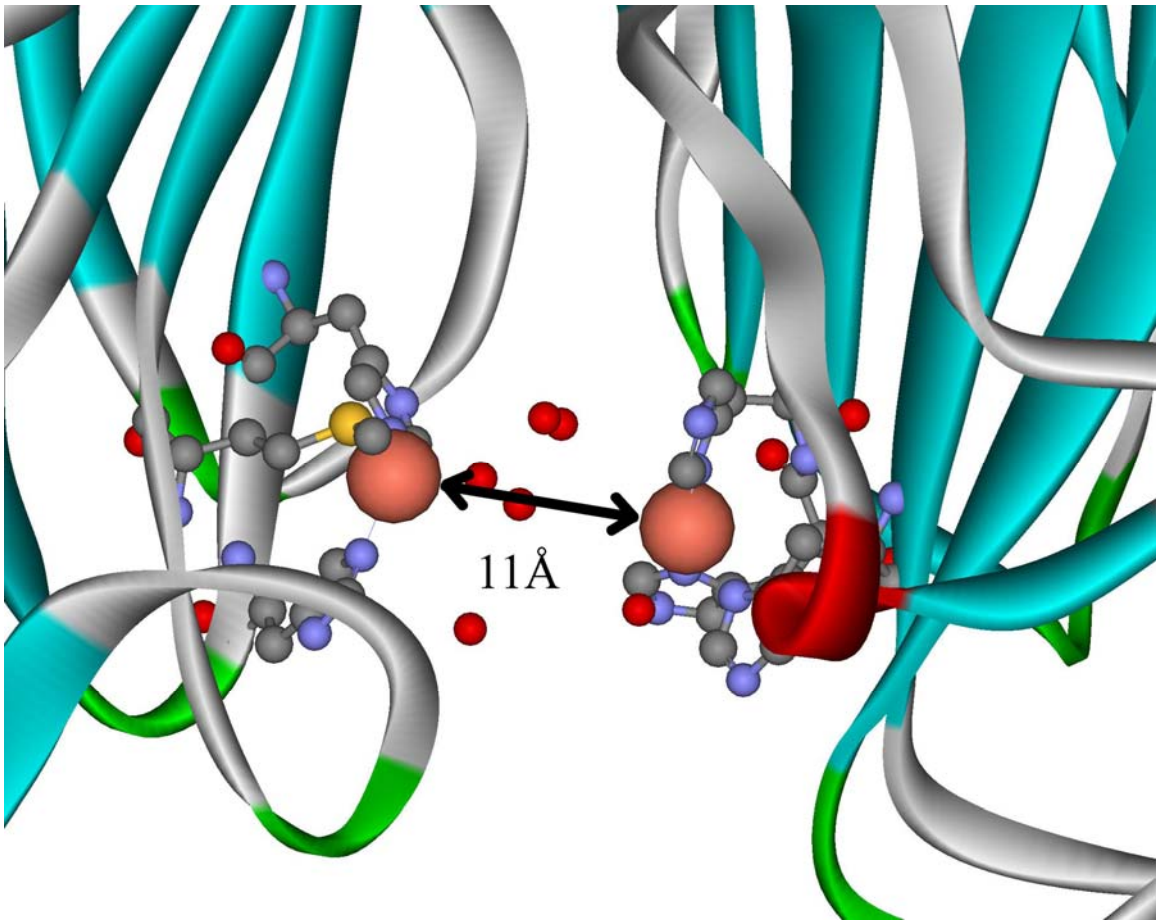

Figure 2.2 Peptidylglycine α-hydroxylating monooxygenase (PHM) active site showing the 11 Å separation between the copper atoms and the interstitial water molecules shown in red.

electron transfer rate.[11] Theoretical work by Beratan *et al*. has proposed that for distances ranging from 9 Å to 12 Å, there exists a structured water motif that can facilitate electron transfer much more readily than through bulk water.[12]

Direct measurements of electron transfer rates through a solvent were previously attempted by using a variety of C-clamp shaped molecules. In these systems, the donor and acceptor molecules were attached to the ends of the C-clamp molecule and thus, held at a well-defined distance. The goal of the study was to allow solvent molecule(s) to insert into the cavity of the "C"-shape such that electron transfer rates across the solvent molecule could be measured. Waldeck *et al.* used an anthracene donor and conjugated dicarboxylic acid acceptor (Figure 2.3).[13] Paddon-Row *et al.* used a dimethoxynaphthalene donor and a dicyanovinyl acceptor (Figure 2.4).[14] In both cases, the distances between the donor and acceptor were controlled via the shape and size of the compound. Various compounds were made by both research groups to systematically modify the size of the "C" opening, and a linear version of the molecule was created as a control molecule. While electron transfer was observed in these molecules, the true composition and local solvent network in the microenvironment between donor and acceptor molecules remained unknown.

Pulse radiolysis was used by Miller to explore statistical distributions of randomly dispersed donor and acceptor molecules in water glasses.[15, 16] Electron transfer in glassed water was further refined by Ponce *et al.* using photochemical processes that do not generate the high energy solvated electron typical of pulsed radiolysis studies.[17] The glass was created by using H_2SO_4/H_2O and HSO_3F/H_2O mixtures at 25% volume/volume ratios at 77 K. The donor molecule was $Ru(tpy)_2^{2+}$ (tpy = 2,2':6,2''-terpyridine), and the

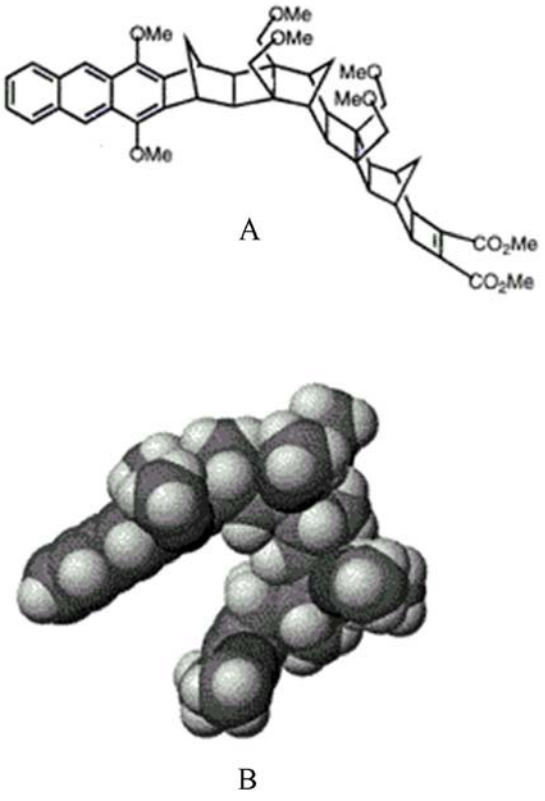

Figure 2.3 Anthracene donor and conjugated dicarboxylic acid acceptor attached to a C-clamp molecule in schematic (A) and three dimensional CPK (B) views.[13]

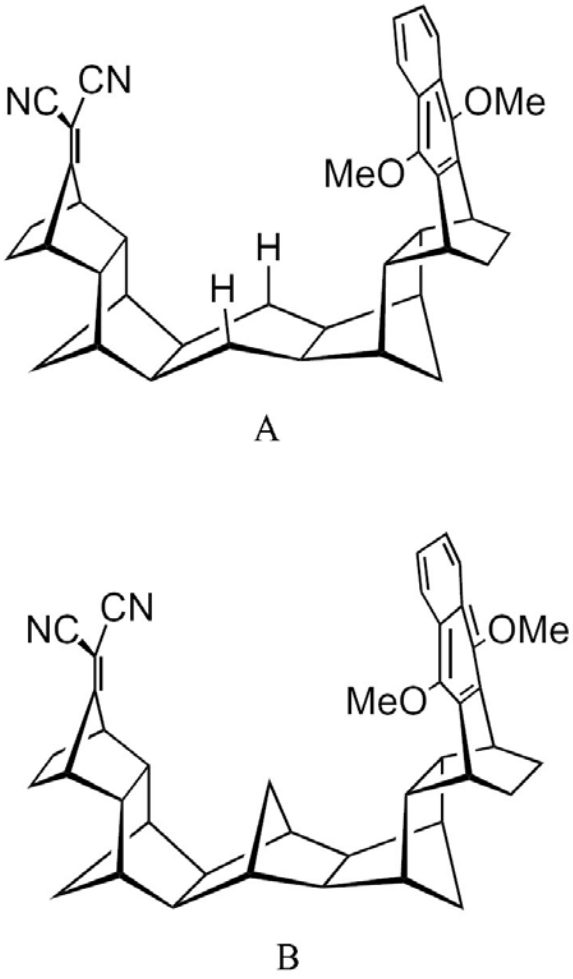

Figure 2.4 Dimethoxynaphthalene donor and a dicyanovinyl acceptor attached to a C-clamp molecules showing both the 7.0 Å donor/acceptor separated construct (A) and the 9.6 Å donor/acceptor separated construct (B).[14]

acceptor molecule was $Fe(OH_2)_6^{3+}$. The excitation wavelength for kinetics measurements was 532 nm while a 514 nm beam was utilized for the relative quantum yield measurements. The decay curves were multi-exponential and fit to equation 2.1, where d is the nearest neighbor in the lattice distance, I_o is the emission intensity in the absence of quencher, $I(t=0)$ is the intensity of emission at time zero, β is the distance decay factor, k_o is the electron transfer rate at distance b, and Q is the acceptor concentration measured in moles per liter and distances in angstroms.[18-20]

$$\ln\left(\frac{I(t)}{I(t=0)}\right) = \ln(I_o(t)) - \sum_{j=1}^{\infty}\left(\frac{[Q]d^3}{2348}\right)^j \frac{1}{j}\sum_i{}'[1-\exp\{k_o t \exp[-\beta(R_i - b)]\})] \qquad (2.1)$$

The variables β and k_o were fit to the scaled kinetic traces and produced excellent fits to the data (Figure 2.5).

Background

We have now applied this technique to measure electron transfer rates in glasses of organic solvents. A number of potential glassing solvents were evaluated for their ability to dissolve various donors and acceptors and to be non-reactive with the donor and acceptor. Glassing solvents such as isopropanol, glycerol, and ethanol/methanol mixtures tended to degrade some of the potential donors and acceptors perhaps due to the reactive alcohol moiety. Ultimately toluene and 2-methyl-tetrahydrofuran (mTHF) had the best solubility characteristics and were also inert to a variety of donor and acceptor molecules.

Multiple donor/acceptor systems were evaluated against six criteria critical for this experiment (Table 2.1). Foremost, it was necessary that up to ~30 μM of donor

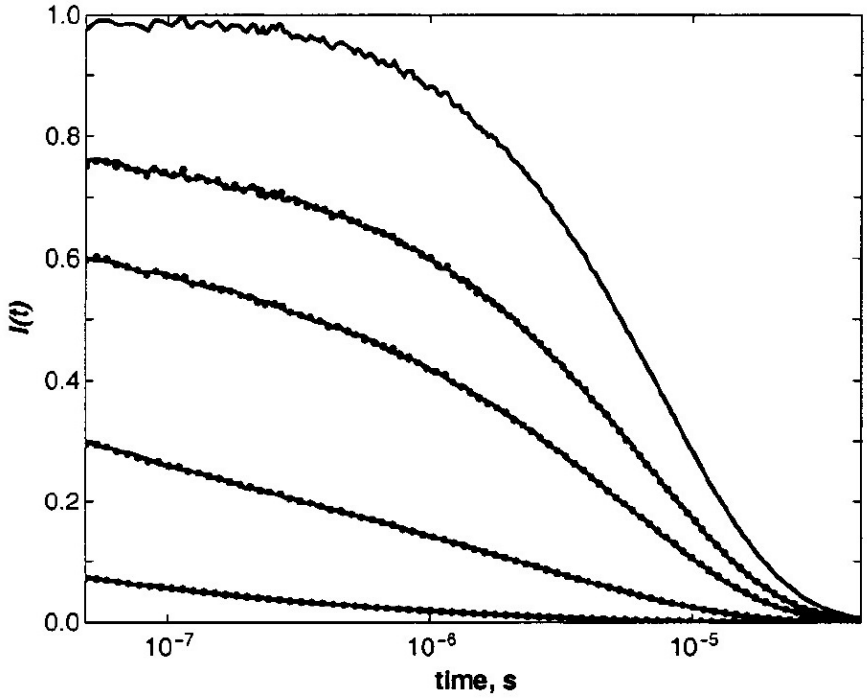

solvent[b]	$[Fe(OH_2)_6^{3+}]$, M	β, Å^{-1}	k_0, s^{-1}
H_2SO_4	0.05	1.74	5.7×10^{13}
	0.10	1.65	1.6×10^{13}
	0.25	1.63	1.1×10^{13}
	0.50	1.71	3.9×10^{13}

Figure 2.5 Emission decay kinetics for $Ru(tpy)_2^{2+}$ in a H_2SO_4/H_2O glass (at 77 K) in the presence of $Fe(OH_2)_6^{3+}$ (upper to lower traces: 0.0, 0.05, 0.10, 0.25, 0.50 M).[17] Dots correspond to calculated decays using equation 2.1 and the parameters listed above.

donor	acceptor	soluble in frozen glass	high driving force	chemically inert	long lifetime	no energy transfer	no counter-ions
$Ru(bpy)_2(CN)_2$	$Fe(acac)_3$	YES	FAIR	YES	YES	NO	YES
$Os(bpy)_2(CN)_2$	$Fe(acac)_3$	YES	FAIR	YES	NO	YES	YES
$Ru(bpy)_2(CN)_2$	$Fe(acac\text{-}F_6)_3$	NO	YES	YES	YES	YES	YES
$Ru(bpy)_2(CN)_2$	4-Mepy	NO	FAIR	YES	YES	YES	YES
$Ru(bpy)_2(CN)_2$	$PMo_{12}O_{40}^{3-}$	NO	FAIR	YES	YES	YES	YES
$Ru(bpy)_2(CN)_2$	$SiMo_{12}O_{40}^{3-}$	NO	FAIR	YES	YES	YES	YES
$Pt_2(P_2O_5H_2)_4^{4-}$	$PMo_{12}O_{40}^{3-}$	NO	YES	YES	YES	YES	YES
$[Ir(\mu\text{-pz})(COD)]_2$	TCNE	YES	YES	NO	YES	YES	YES
$[Ir(\mu\text{-pz})(COD)]_2$	quinone	NO	YES	YES	YES	YES	YES
$[Ir(\mu\text{-pz})(COD)]_2$	Cl_2-quinone	YES	YES	YES	YES	YES	YES

Table 2.1 Some of the combinations of donor-acceptor pairs that were evaluated for use.

compound and up to ~200 mM of acceptor molecule dissolve in the glassy solution at 77 K. Second, the donor/acceptor pair must have a driving force sufficient to offset the low temperature and solvent rigidity. Third, the donor/acceptor pair must be chemically inert with respect to each other. Fourth, the donor must exhibit a relatively long emission lifetime. As the acceptor concentration is increased, the observed donor emission lifetime will subsequently decrease; if the donor lifetime becomes too short as a result of the acceptor, the decay curves will be difficult to interpret. Fifth, there must be essentially no spectral overlap between the absorption spectrum of the acceptor and the emission spectrum of the donor. This lack of overlap is critical to ensure that fluorescence energy transfer does not complicate the observed kinetics. Finally, the donor/acceptor pair must be uncharged such that they will be dispersed in the solution in a random, statistical manner.

Multiple donor-acceptor systems were investigated (Table 2.1). The donor-acceptor pair that fulfilled all six criteria were [Ir(μ-pyrazolyl)(1,5-cyclooctadiene)]$_2$ (D_{IR}) and 2,6-dichloro-1,4-benzoquinone (A_Q) (Figure 2.6). The donor is soluble at 77 K up to 100 mM and the acceptor is soluble in excess of 500 mM. The driving force has been estimated from potentials measured in acetonitrile to be about 1.6 eV.[21-23] The donor has a lifetime of 3.2 μs in toluene and mTHF at 77 K, and neither compound reacts with the solvent or each other on the timescale of the experiments. The iridium donor has an absorption maximum of ~500 nm with a molar absorptivity of 9100 M^{-1} cm^{-1}.[21] The donor phosphorescence exhibits a maximum at ~700 nm. The absorption maximum of the acceptor is at higher energies than both the donor absorption and emission, ensuring

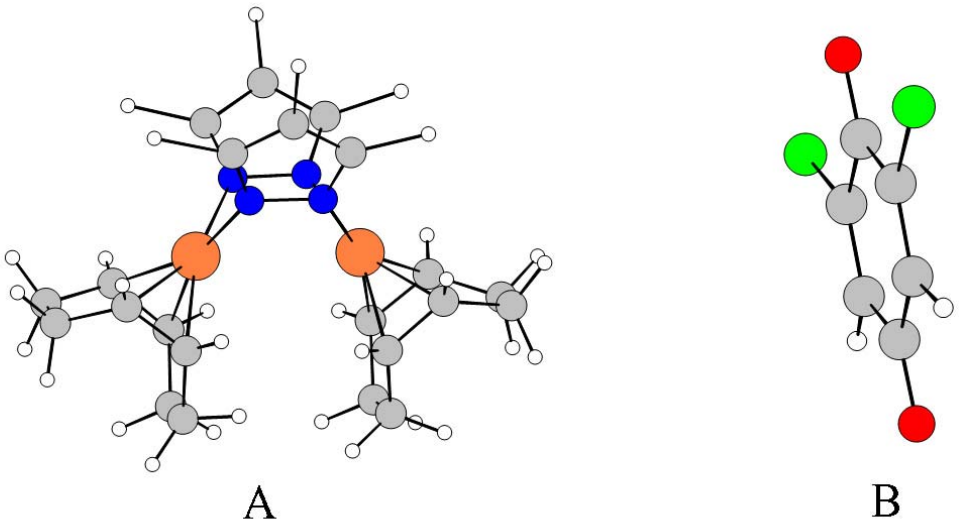

Figure 2.6 [Ir(μ-pyrazolyl)(1,5-cyclooctadiene)]$_2$ donor (A) and 2,6-dichloro-1,4-benzoquinone acceptor (B). The color scheme is as follows: carbon (grey), hydrogen (white), iridium (orange), nitrogen (blue), oxygen (red), and chlorine (green).

that no energy transfer will occur upon excitation with a 520 nm laser source (Figure 2.7). Finally, neither of the molecules has a net charge so a true statistical distribution will be achieved in the glassy solvent.

Experimental

[Ir(μ-pyrazolyl)(1,5-cyclooctadiene)]$_2$ synthesis

The donor was prepared using a previously published synthesis.[24] Bis(1,5-cyclooctadiene)diiridium(I) dichloride and pyrazole were purchased from Sigma-Aldrich and used as is. A THF pyrazole solution was added dropwise to a THF and triethylamine solution of the Bis(1,5-cyclooctadiene)diiridium(I) dichloride. The color of the iridium solution slowly changed from red to purple. After 30 minutes the reaction was pumped to dryness leaving a dark purple/black residue in the flask. The residue was then extracted with a small volume of THF; this crude THF solution containing donor was passed through an alumina column to remove excess pyrazole. The eluent was then slowly evaporated to achieve a highly concentrated solution of donor from which pure donor could be crystallized. Hexane was then layered on top of this concentrated THF solution (approximately 1/3 the volume of the concentrated solution). The flask was then placed into a -20 ºC freezer for three days. Needle-shaped red crystals were then removed via suction filtration using a fine frit (Figure 2.8). Chemical composition was determined by elemental analysis (Desert Analytics, Tucson, AZ 85717) (Table 2.2) and X-ray crystallography (Caltech X-ray crystallography facility) (Figure 2.9).

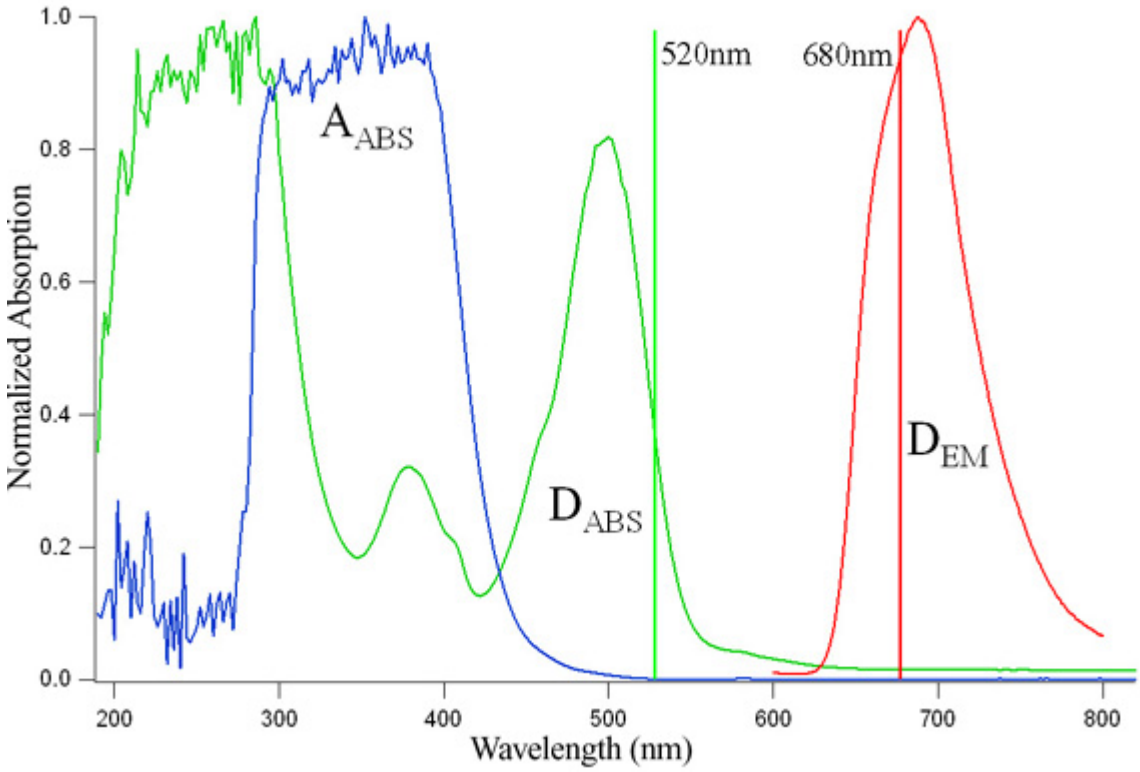

Figure 2.7 Absorption spectrum of the donor in green (D_{ABS}), emission spectrum of the donor in red (D_{EM}), and absorption spectrum of the acceptor in blue (A_{ABS}). The excitation wavelength of 520 nm and observation wavelength of 680 nm are indicated on the graph.

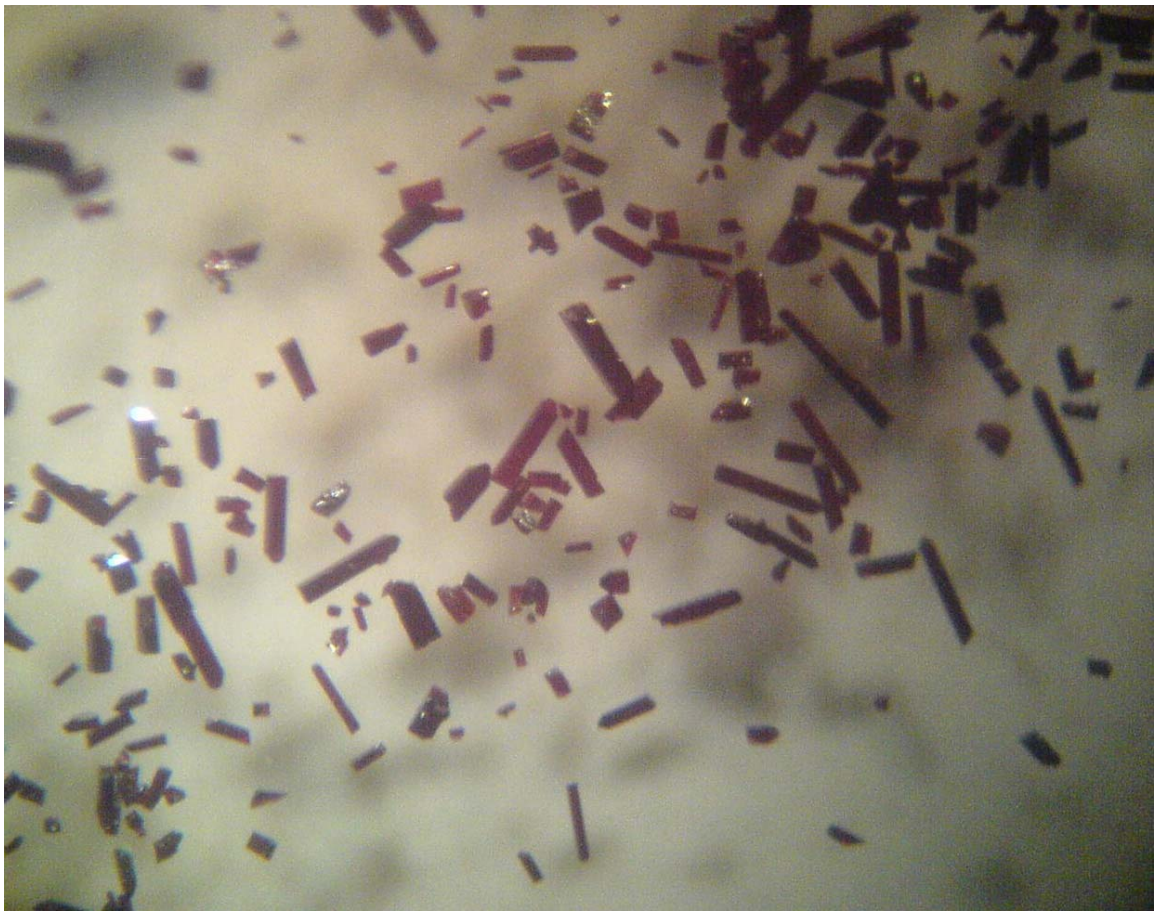

Figure 2.8 [Ir(μ-pyrazolyl)(1,5-cyclooctadiene)]$_2$ red needle donor crystals under 20x magnification.

Sample ID	%C	%H	%N	%Cl	%Ir	%O
Experimental						
[Ir(μ-pyrazolyl)(1,5-cyclooctadiene)]$_2$	35.97	3.65	7.35		46.8	
2,6-dichloro-1,4-benzoquinone	40.44	0.95		39.93		18.57
Calculated						
[Ir(μ-pyrazolyl)(1,5-cyclooctadiene)]$_2$	35.95	4.11	7.62		52.31	
2,6-dichloro-1,4-benzoquinone	40.92	1.15		39.75		18.18

Table 2.2. Experimental and calculated elemental analysis of donor and acceptor molecules.

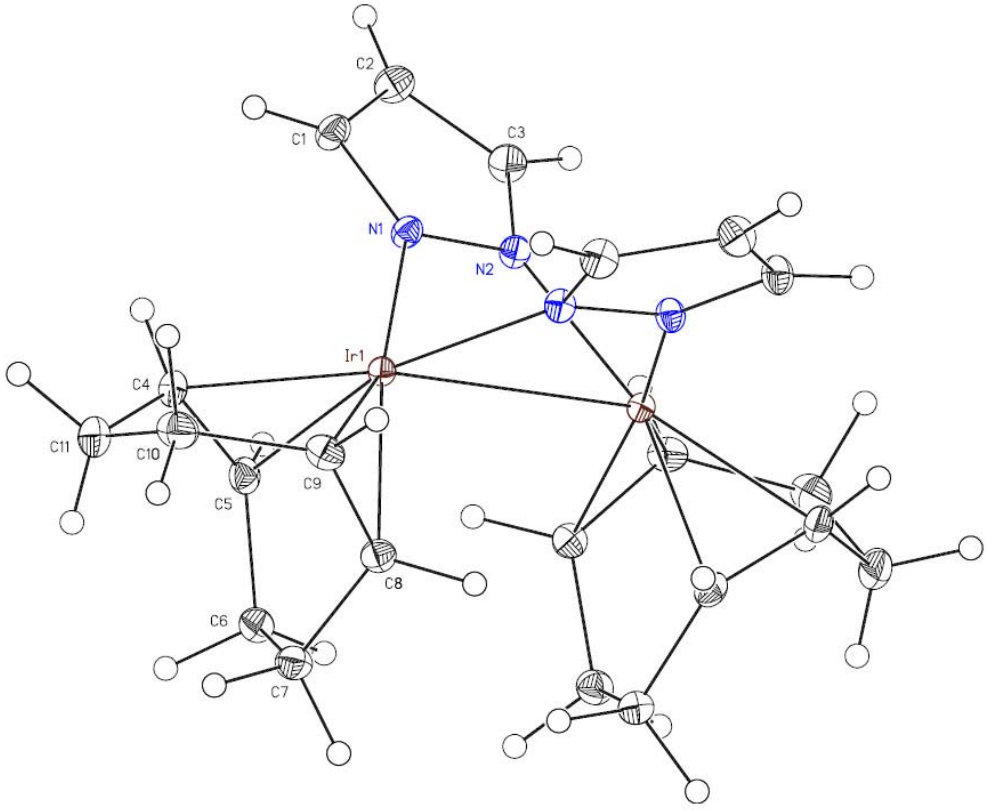

Ir(1)-N(1)	2.0706(11)	N(1)-Ir(1)-N(2)#1	88.53(5)
Ir(1)-N(2)#1	2.0707(12)	N(1)-Ir(1)-C(5)	89.11(5)
Ir(1)-C(5)	2.1201(14)	N(2)#1-Ir(1)-C(5)	160.92(5)
Ir(1)-C(9)	2.1221(14)	N(1)-Ir(1)-C(9)	159.32(6)
Ir(1)-C(4)	2.1299(15)	N(2)#1-Ir(1)-C(9)	89.90(5)
Ir(1)-C(8)	2.1330(14)	C(5)-Ir(1)-C(9)	98.81(6)
Ir(1)-Ir(1)#1	3.17696(14)	N(1)-Ir(1)-C(4)	92.51(5)
		N(2)#1-Ir(1)-C(4)	160.21(6)
		C(5)-Ir(1)-C(4)	38.86(6)
		C(9)-Ir(1)-C(4)	82.19(6)
		N(1)-Ir(1)-C(8)	161.76(5)
		N(2)#1-Ir(1)-C(8)	95.00(5)
		C(5)-Ir(1)-C(8)	81.71(6)
		C(9)-Ir(1)-C(8)	38.84(6)
		C(4)-Ir(1)-C(8)	90.17(6)
		N(1)-Ir(1)-Ir(1)#1	64.09(3)
		N(2)#1-Ir(1)-Ir(1)#1	63.93(3)
		C(5)-Ir(1)-Ir(1)#1	98.14(4)
		C(9)-Ir(1)-Ir(1)#1	132.56(4)
		C(4)-Ir(1)-Ir(1)#1	133.56(4)
		C(8)-Ir(1)-Ir(1)#1	101.50(4)

Figure 2.9 Crystal structure of [Ir(μ-pyrazolyl)(1,5-cyclooctadiene)]$_2$ and table of selected bond lengths [Å].

2,6-dichloro-1,4-benzoquinone purification

2,6-dichloro-1,4-benzoquinone was purchased from Sigma-Aldrich. Solutions prepared from this source were found to have variable purity and as a result, the acceptor was recrystallized from ethanol prior to use. The resulting yellow needle-like crystals were dried under a vacuum for several hours. Chemical composition and ethanol removal were confirmed by elemental analysis (Table 2.2).

Solvent preparation

Toluene was acquired from the Peters group solvent system and was held in a dry solvent bomb. The toluene was used within an hour and excess toluene was discarded. The 2-methyl-tetrahydrofuran was acquired form Sigma-Aldrich in a "septa seal" bottle. It was found that the mTHF became wet with time and was consequently stored in a bomb under nitrogen and over a piece of sodium metal.

Sample holder and dewar configuration

Sample tubes were made by the Caltech glass shop. Tubes are 30 cm long and 0.7 cm in diameter. A glass liquid nitrogen dewar with a square finger was also constructed by the Caltech glass shop. A teflon collet and lid were made to hold the sample tube in the dewar (Figure 2.10). An external frame that rigidly held the dewar in place on a laser table or in the fluorimeter was also constructed. Sample positioning was highly reproducible. Rubber size 11 seals were used to cap the sample tubes. Helium gas was bubbled through the liquid nitrogen during the experiment to retard boiling during

Figure 2.10 Picture and dimensions of finger dewar, collet, and lid used for 77 K measurements and dewar holder.

measurements. Dry air was constantly blown onto the finger dewar to prevent the formation of ice.

Samples were created from the same donor and acceptor stock solutions at the same time to minimize sample variances. A 400 mM acceptor stock solution was diluted with a 200 μM donor stock solution and excess solvent in order to create samples with 30 μM donor and 0, 50, 100, 150, and 200 mM acceptor. These solutions were transferred to sample holders that had been cleaned with aqua regia, rinsed with nano-pure water, and stored in an oven. The samples then underwent three cycles of freeze-pump-thaw to remove oxygen. The resulting samples were stored in liquid nitrogen and used within the next four hours. Prior to spectroscopic measurements, the samples were completely thawed and vitrified by immersion into liquid nitrogen in the sample dewar. Once the samples were glassed, the liquid nitrogen was topped off and boiling of the liquid nitrogen was eliminated by submerging a helium gas tube to the bottom of the dewar, and then slowly raised to a level above the sample path.

Kinetics measurements

Kinetic traces were acquired using the Beckman Institute Laser Resource Center's nanosecond transient emission/absorption setup. Excitation of the sample was achieved by a Spectra-Physics model P 190-10 Nd:YAG laser coupled to a Spectra-Physics MOPO operating at 10 Hz. Sample emission was collected using a Instruments SA (ISA Edison, NJ) model DH10 (1200 grooves/mm) double monochromator and Hamamatsu R928 PMT with a 5 stage socket made by Products for Research (model R928/17149.00301.0040 Bridgewater, NJ). A 650 nm long pass filter was placed in front

of the entrance slit to remove scattering signal from the excitation beam. Signal from the PMT was amplified with a Phillips Scientific 100 MHz bipolar amplifier (100x). Data was collected with a LeCroy 9354A digitizing oscilloscope.

Relative quantum yield measurements

Excitation of the sample was achieved by a Coherent Innova 70 argon ion laser emitting 514 nm light. Luminescence was collected and dispersed using a Spex 750 (3/4 meter) spectrograph coupled to a Princeton Instruments liquid nitrogen cooled CCD camera. A 650 nm long pass filter was placed in front of the spectrograph entrance slit to prevent laser scatter from entering the spectrometer. The sample was regularly thawed, reglassed, and rotated to average away scatter from cracks that form in the 77 K glass. A statistical average of the intensity at 580 nm was determined. Quantum yield measurements exhibited an error of less than 2% (standard deviation/mean).

Data analysis

The relatively long excited state lifetime allowed us to probe electron transfer over long distances (~20 Å). The luminescence quantum yield was drastically reduced and the decays became faster and highly nonexponential upon addition of acceptor (0.05-0.20 M). Since a substantial amount of luminescence quenching occurs on a sub-nanosecond timescale, the 10 ns time resolution of our instrument prevented direct measurement of $I(t=0)$. Therefore, kinetic traces were integrated and the areas under the decay curves were adjusted to reflect the relative quantum yield data that was obtained. Integrated intensity values of each of the traces were then scaled to the decay curve of the

pure donor sample, which was adjusted to have an intensity of 1 at time zero (Figure 2.11 and 2.12). Semiclassical theory was invoked to describe how the rate of electron transfer decays exponentially with distance (Equation 2.2, 2.3, Chapter 1). For a given driving force (ΔG), reorganization energy (λ), and temperature (T), the rate or electron transfer, k_{ET}, depends on distance between donor and acceptor (r), $H_{AB}{}^{0}$ (contact coupling), and a distance decay parameter (β).

$$k_{ET} = \left(\frac{4\pi^3}{h^2 \lambda kT}\right)^{1/2} H_{AB}^2 \exp\left(\frac{-(\Delta G + \lambda)^2}{4\lambda kT}\right) \qquad (2.2)$$

$$H_{AB} = H_{AB}^{o} \cdot \exp\left(-\frac{\beta \cdot r}{2}\right) \qquad (2.3)$$

If the donor and acceptor molecules are randomly distributed, translational motion is slow with respect to electron transfer, the rate of electron transfer is independent of molecular orientation, and the electron transfer rate of the system has an exponential distance dependence, then Equation 2.4 can be used to describe the kinetics of the system.[19, 20]

$$\ln\left(\frac{I(t)}{I(t=0)}\right) = \frac{t}{\tau_o} - \frac{[A]}{132.12\text{MÅ}^3} \cdot \int_{r_o}^{\infty} \left(1 - \exp\left(-k_{ET}^{o} \cdot t \cdot \exp\left(-\beta(r - r_o)\right)\right)\right) \cdot r^2 dr \qquad (2.4)$$

Equation 2.4 describes the luminescence decay, $I(t)$, in terms of luminescence intensity at time zero, $I(t=0)$, the lifetime of the donor in the absence of acceptor (τ_o), the

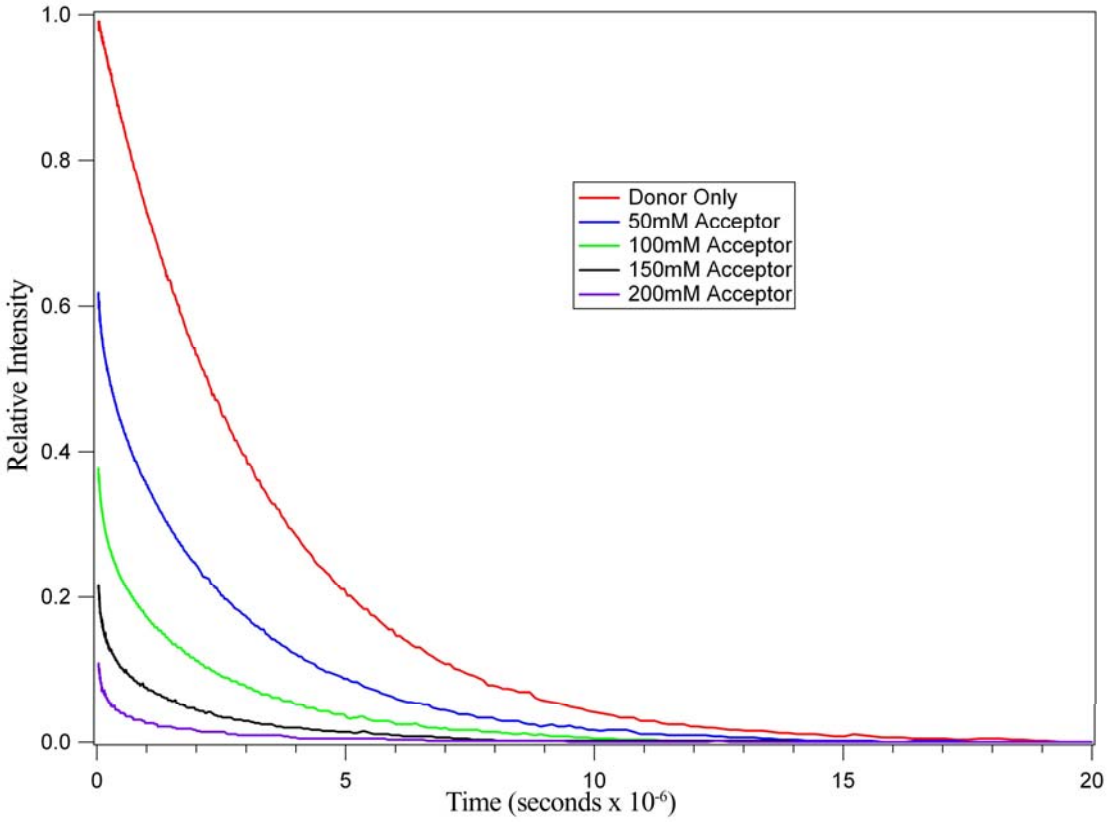

Figure 2.11 Scaled kinetic traces of [Ir(μ-pyrazolyl)(1,5-cyclooctadiene)]$_2$ and 2,6-dichloro-1,4-benzoquinone acceptor in 2-methyl-tetrahydrofuran at 77 K.

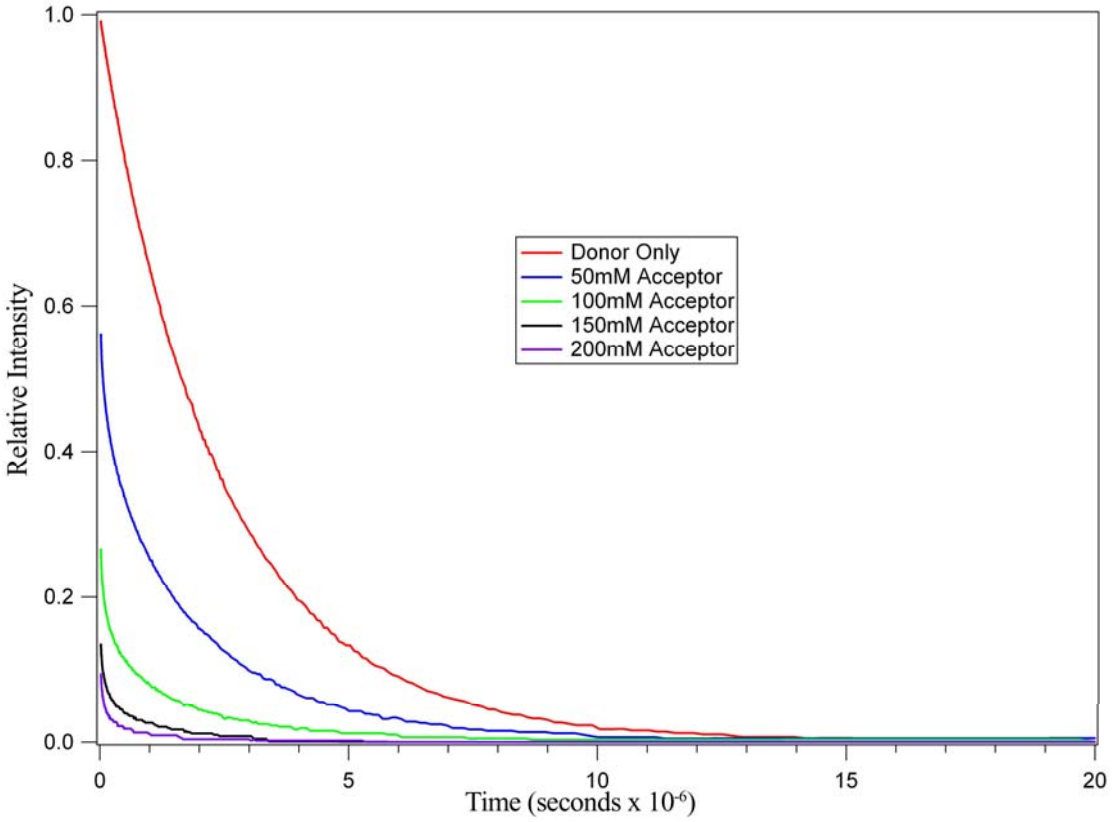

Figure 2.12 Scaled kinetic traces of [Ir(μ-pyrazolyl)(1,5-cyclooctadiene)]$_2$ and 2,6-dichloro-1,4-benzoquinone acceptor in toluene at 77 K.

concentration of acceptor in molarity [A], van der Waals contact distance (r_o), the electron transfer rate at contact distance between the donor and acceptor (k^o_{ET}), and the distance decay factor (β). The van der Waals contact distance was determined by modeling crystal structures of the donor and acceptor together and finding the shortest distance between the two centers of the molecules; r_o was found to be 4 Å.

Discussion

Measurements of luminescence quantum yields relative to an unquenched sample allowed proper scaling of the time resolved data,[25, 26] thereby reducing the number of unknowns in Equation 2.4 to two parameters: the distance decay parameter β and the electron transfer rate k^o_{ET} at donor/acceptor contact distance r_o. We find that the following β-values adequately describe electron transfer in both glasses (Table 2.3); toluene 1.27Å^{-1} ± 0.07 (Figure 2.13) and mTHF 1.60Å^{-1} ± 0.07 (Figure 2.14). The electron transfer rate constants at contact distance are near 10^{13} s^{-1}. Thus, tunneling 20 Å through toluene is about 750 times faster than tunneling through mTHF and roughly 450 times faster than tunneling through water (β = 1.68 ± 0.07 Å^{-1} and $k^o_{ET} \sim 10^{13}$ s^{-1}) (Figure 2.15).[17]

Coupling between donor and acceptor is mediated by intervening bridges, which may consist of a covalent bonding network or solvent molecules. A superexchange model describes H_{DA} as a product of nearest neighbor interactions (Equation 2.5) between the donor and the bridge states (h_{Db}), adjacent bridge states (h_{bb}), and the bridge and acceptor states (h_{bA}).[27]

	Acceptor Concentration (M)	β ($Å^{-1}$)	k^0_{ET} (s^{-1})
Toluene	0.05	1.23	1.2×10^{13}
	0.10	1.32	4.1×10^{13}
	0.15	1.33	8.3×10^{13}
	0.20	1.19	18×10^{13}
MTHF	0.05	1.50	0.3×10^{13}
	0.10	1.62	2.5×10^{13}
	0.15	1.64	2.7×10^{13}
	0.20	1.65	0.3×10^{13}

Table 2.3 Best-fit values of β and k^o_{ET} (Equation 2.4) extracted from luminescence decay kinetics and quantum yields of [Ir(μ pyrazolyl)(1,5 cyclooctadiene)]$_2$ quenched by electron transfer to 2,6-dichloro-1,4-benzoquinone in glasses at 77 K.

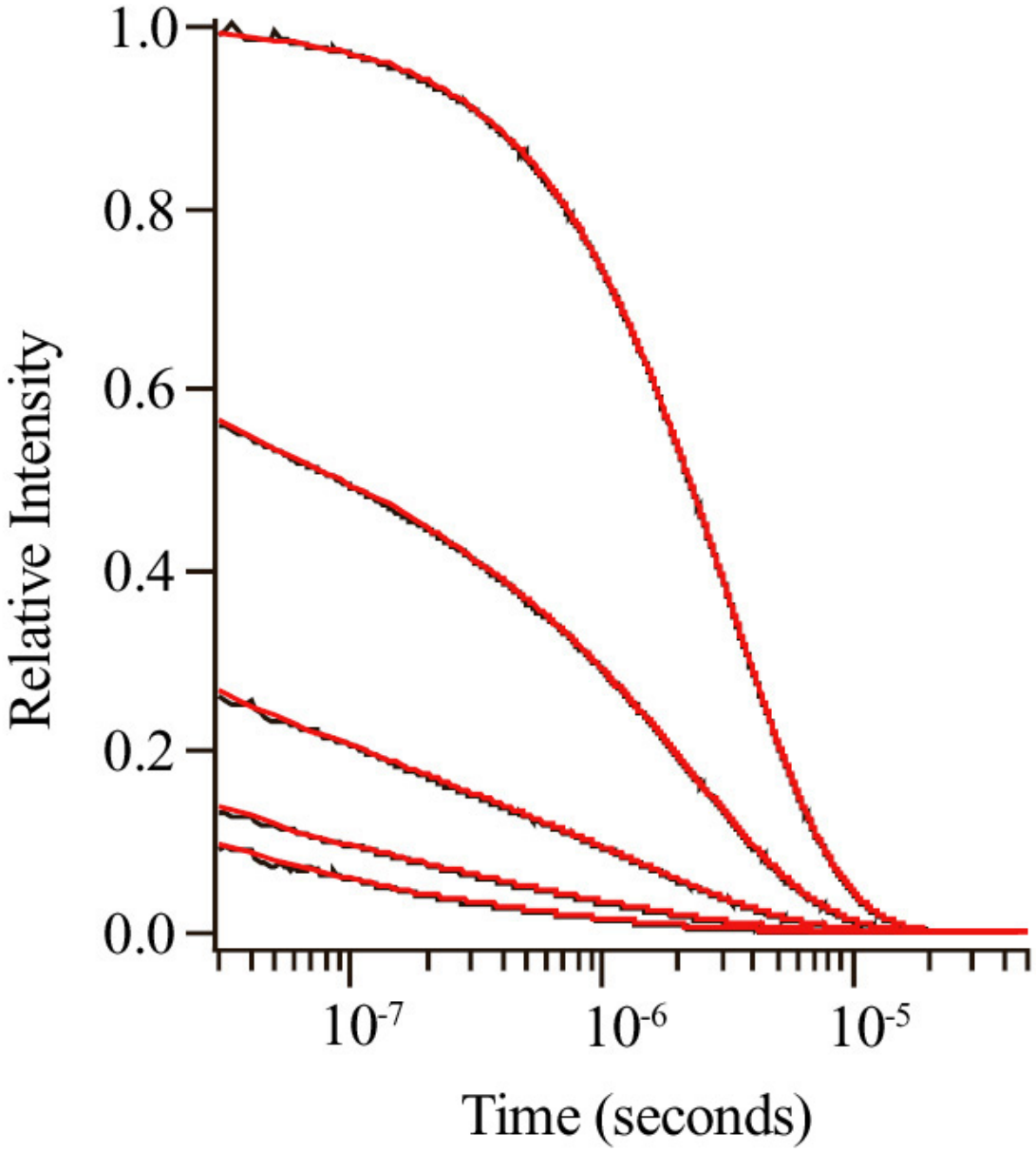

Figure 2.13 Luminescence decay kinetics (black) for [Ir(μ-pyrazolyl)(1,5-cyclooctadiene)]$_2$ in toluene glass at 77 K in the presence of 2,6-dichloro-1,4-benzoquinone (upper to lower traces: 0.0, 0.05, 0.10, 0.15, 0.20 M). The smooth red line is the calculated decay using Equation 2.4 and the parameters listed in Table 2.3

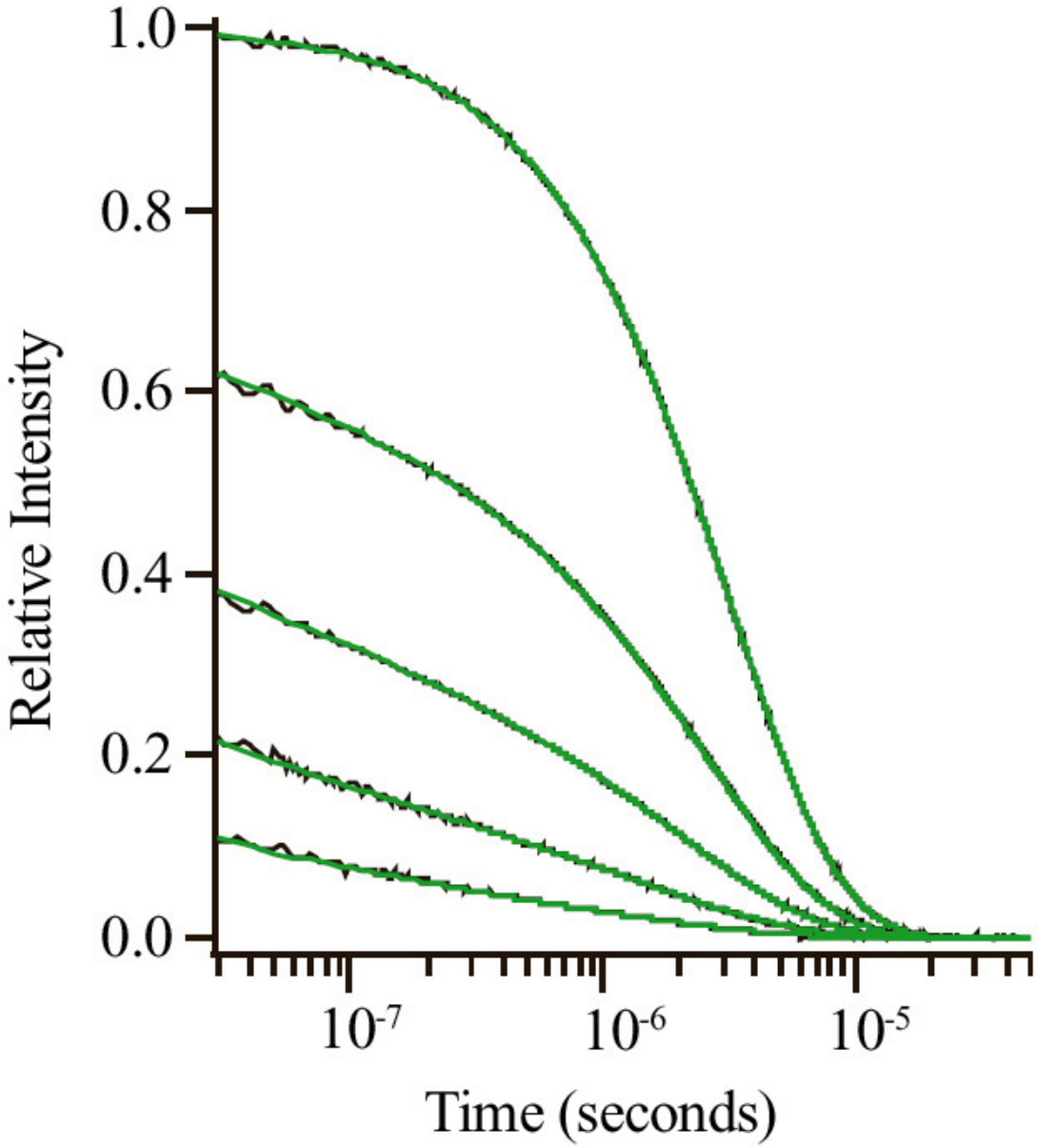

Figure 2.14 Luminescence decay kinetics (black) for [Ir(μ-pyrazolyl)(1,5-cyclooctadiene)]$_2$ in MTHF glass at 77 K in the presence of 2,6-dichloro-1,4-benzoquinone (upper to lower traces: 0.0, 0.05, 0.10, 0.15, 0.20 M). The smooth green line is the calculated decay using Equation 2.4 and the parameters listed in Table 2.3

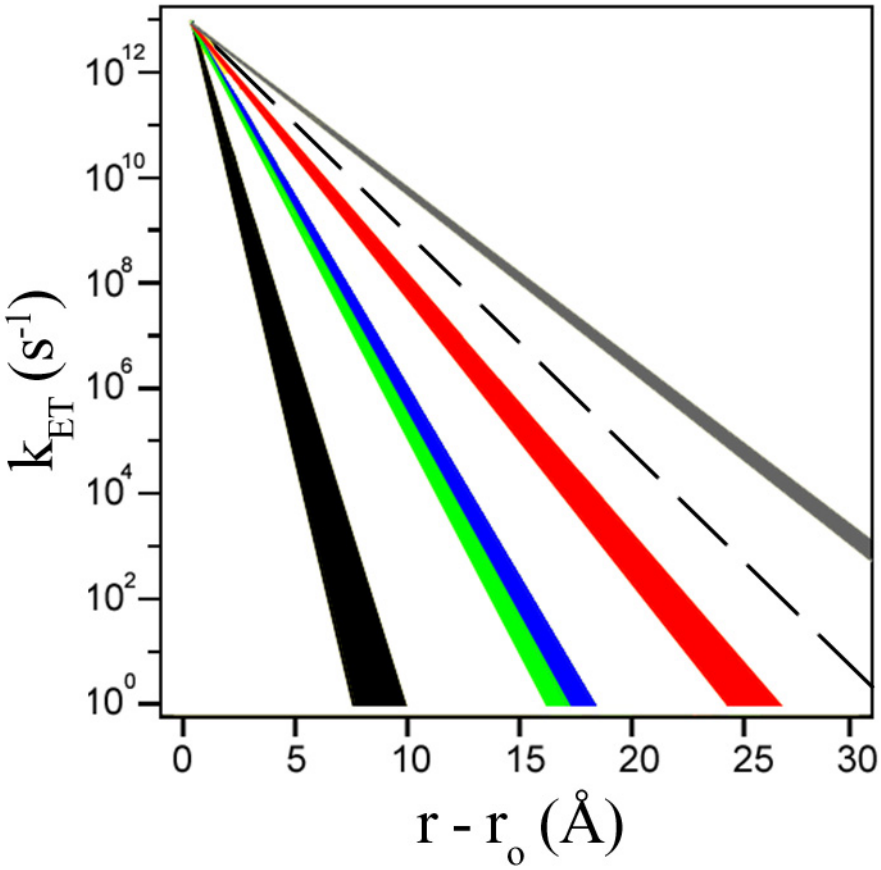

Figure 2.15 Tunneling time table of vacuum (black), mTHF (green), water (blue), toluene (red), and polyxylene bridged systems (gray).[28] Dotted line is $\beta = 1$.

$$H_{DA} = \frac{h_{Db}}{\Delta\varepsilon} \cdot \left(\frac{h_{bb}}{\Delta\varepsilon} \right)^{n-1} \cdot h_{bA} \qquad (2.5)$$

$\Delta\varepsilon$ is the tunneling energy gap, or the energy difference between the donor/acceptor state at the transition state configuration and the energy of the one-electron reduced states of the bridge. n is the number of identical bridge units. Decreasing $\Delta\varepsilon$ is expected to lead to greater donor/acceptor coupling and more efficient ET.[29] According to McConnell's model, H_{DA} decreases exponentially with increasing donor/acceptor distance. Hydrogen bonds have been known to mediate coupling between individual bridge units, and experimental studies have shown that electron transfer across hydrogen bonds can be efficient.[12, 30-32] Based on hydrogen bonding strength and in the absence of any other effects, decreasing electron transfer efficiency should correlate with decreasing ability to form a hydrogen bond. This means the efficiency of water > mTHF > toluene; which is exactly the opposite of what is observed. Band gap differences between the individual solvents provide reasonable approximations to the differences in the tunneling energy gaps. The lowest energy absorption maxima in the various solvents are 151 nm for water[33], 188 nm for mTHF[34] and 260 nm for toluene.[35] Thus, in toluene, $\Delta\varepsilon$ will be about 1.8 - 2.0 eV smaller than in mTHF and roughly 3.4 eV smaller than in water (Figure 2.16).

Polyene and phenylenevinylene bridged donor/acceptor systems exhibit remarkably efficient electron transfer rates over long distances. β values on the order of 0.2 $Å^{-1}$ and below have been found.[28, 36, 37] In these systems, the bridge state energies strongly depend on the length of the bridge, and the contribution from each additional bridge state is altered as a result of conjugation. In solvent-mediated electron transfer

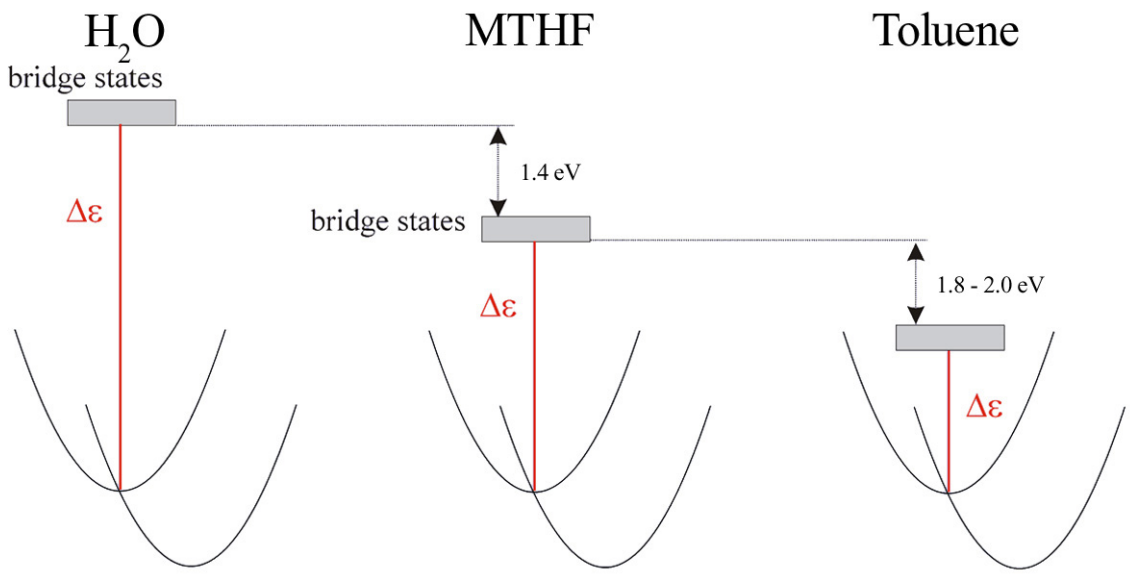

Figure 2.16 Schematic of the tunneling energy gaps of water, mTHF, and toluene. The lowest energy absorption maxima in the various solvents are 151 nm for water[33], 188 nm for mTHF[34] and 260 nm for toluene.[35]

from free donor to free acceptor, this complication arising from the effects of conjugation is eliminated. Electron transfer rates along a polypeptide backbone in a β-strand conformation also exhibits an exponential distance dependence (β of 1.1 $Å^{-1}$) [38] which is close to that found for alkane chains (β of 1.0 $Å^{-1}$).[39-41] Electron tunneling through mTHF should be similar to tunneling through a β-strand backbone or alkane chain since the composition of the medium is similar (C-C single bonds). Analogously, tunneling though toluene should be similar to polyxylenes, based solely on the composition of the medium (aromatic C-C bonds). In both the mTHF and toluene systems, tunneling through the van der Waal gap imparts a penalty to electron transfer rates.

Future work

Protein environments are extremely complex. Nature utilizes van der Waal forces, salt bridges, disulfide bonds, and ligands to metals for a variety of purposes, including providing well-defined structures, catalysis reactions, and electron transfer reactions. Most ubiquitous of all these interactions is the hydrogen bond. Electron transfer through hydrogen bonds has been studied.[12, 42, 43] The experiments on electron transfer through glasses described here may be applied to learn more about the nature of the hydrogen bond. We have found multiple analogs of mTHF and toluene that have the ability to from hydrogen bonds, dissolve the donor and acceptor in sufficient quantities, and form glasses at 77 K. These experiments are ongoing.

Conclusion

We have investigated electron transfer though mTHF and toluene glasses. We have determined that the exponential decay constants are 1.60 $Å^{-1}$ and 1.27 $Å^{-1}$ respectively and that there is a penalty for tunneling through van der Waal contacts.

References

1. Bradbury, A. F.; Smyth, D. G., *Trends Biochem. Sci.* **1991,** 16, 112.
2. Eipper, B. A.; Milgram, S. L.; Husten, E. J.; Yun, H.-Y.; Mains, R. E., *Protein Sci.* **1993,** 2, 489.
3. Eipper, B. A.; Stoffers, D. A.; Mains, R. E., *Annu. Rev. Neurosci.* **1992,** 15, 57.
4. Merkler, D. J., *Enzyme Microb. Technol.* **1994,** 16, 450.
5. Prigge, S. T.; Kolhekar, A. S.; Eipper, B. A.; Mains, R. E.; Amzel, L. M., *Science* **1997,** 278, 1300.
6. Eipper, B. A.; Quon, A. S. W.; Mains, R. E.; Boswell, J. S.; Blackburn, N. J., *Biochemistry* **1995,** 34, 2857.
7. Boswell, J. S.; Reedy, B. J.; Kulathila, R.; Merkler, D.; Blackburn, N. J., *Biochemistry* **1996,** 35, 12241.
8. Brenner, M. C.; Klinman, J. P., *Biochemistry* **1989,** 28, 4664.
9. Scott, R. A.; Sullivan, R. J.; DeWolf, W. E.; Dolle, R. E., *Biochemistry* **1988,** 27, 5411.
10. Bell, J.; Meskini, R. E.; D'Amato, D.; Mains, R. E.; Eipper, B. A., *Biochemistry* **2003,** 42, 7133.
11. van Amsterdam, I. M. C.; Ubbink, M.; Einsle, O.; Messerschmidt, A.; Merli, A.; Cavazzini, D.; Rossi, G. L.; Canters, G. W., *Nature Structural Biology* **2002,** 9, 48.
12. Lin, J.; Balabin, I. A.; Beratan, D. N., *Science* **2005,** 310, 1311.
13. Read, I.; Napper, A.; Kaplan, R.; Zimmt, M. B.; Waldeck, D. H., *J. Am. Chem. Soc.* **1999,** 121, 10976.
14. Lokan, N. R.; Craig, D. C.; Paddon-Row, M. N., *Synlett* **1999,** 4, 397.
15. Miller, J. R., *J. Phys. Chem.* **1975,** 79, 1070.
16. Miller, J. R., *Chem. Phys. Lett.* **1973,** 22, 180.
17. Ponce, A.; Gray, H. B.; Winkler, J. R., *J. Am. Chem. Soc.* **2000,** 122, 8187.
18. Blumen, A.; Manz, J. J., *J. Chem. Phys.* **1979,** 71, 4694.
19. Blumen, A. J., *J. Chem. Phys.* **1980,** 72, 2632.
20. Inokuti, M.; Hirayama, F. J., *J. Chem. Phys.* **1965,** 43, 1978.
21. Marshall, J. L.; Stobart, S. R.; Gray, H. B., *J. Am. Chem. Soc.* **1984,** 106, 3027.
22. Smith, D. C.; Gray, H. B., *Coord. Chem. Rev.* **1990,** 100, 169.
23. Fukuzumi, S.; Koumitsu, S.; Hironaka, K.; Tanaka, T., *J. Am. Chem. Soc.* **1987,** 109, 305.
24. Atwood, J.; Beveridge, K.; Bushnell, G.; Dixon, K.; Eadie, D.; Stobart, S.; Zaworotko, M., *Inorg. Chem.* **1984,** 23, 4050.
25. Weidemaier, K.; Tavernier, H. L.; Swallen, S. F.; Fayer, M. D., *J. Phys. Chem. A* **1997,** 101, 1887.
26. Swallen, S. F.; Weidemaier, K.; Tavernier, H. L.; Fayer, M. D., *J. Phys. Chem.* **1996,** 100, 8106.
27. McConnell, H. M., *J. Chem. Phys.* **1961,** 35, 508.
28. Villahermosa, R. PhD, California Institute of Technology, 2002.
29. Paddon-Row, M. N.; Shephard, M. J.; Jordan, K. D., *J. Am. Chem. Soc.* **1993,** 115, 3312.
30. Wuttke, D. S.; Bjerrum, M. J.; Winkler, J. R.; Gray, H. B., *Science* **1992,** 256, 1007.

31. de Rege, P. J. F.; Williams, S. A.; Therien, M. J., *Science* **1995,** 269, 1409.
32. Yang, J.; Seneviratne, D.; Arbatin, G.; Andersson, A. M.; Curtis, J. C., *J. Am. Chem. Soc.* **1997,** 119, 5329.
33. Bernas, A.; Ferradini, C.; Jay-Gerin, J. P., *Chem. Phys.* **1997,** 222, 151.
34. Bremner, L. J.; Curtis, M. G.; Walker, I. C., *J. Chem. Soc., Faraday Trans.* **1991,** 87, 1049.
35. Ginsburg, N.; Robertson, W. W.; Matsen, F. A., *J. Chem. Phys.* **1946,** 14, 511.
36. Joachim, C.; Launay, J. P.; Woitellier, S., *J. Chem. Phys.* **1990,** 147, 131.
37. Davis, W. B.; Svec, W. A.; Ratner, M. A.; Wasielewski, M. R., *Nature* **1998,** 396, 60.
38. Langen, R.; Chang, I.; Germanas, J.; Richards, J.; Winkler, J.; Gray, H. B., *Science* **1995,** 268, 1733.
39. Oevering, H.; Paddon-Row, M.; Heppener, M.; Oliver, A.; Cotsaris, E.; Verhoeven, J.; Hush, N., *J. Am. Chem. Soc.* **1987,** 109, 3258.
40. Johnson, M. D.; Miller, J. R.; Green, N. S.; Closs, G. L., *J. Phys. Chem.* **1989,** 93, 1173.
41. Smalley, J.; Finklea, H.; Chidsey, C.; Linford, M.; Creager, S.; Ferraris, J.; Chalfant, K.; Zawodzinsk, T.; Feldberg, S.; Newton, M., *J. Am. Chem. Soc.* **2003,** 125, 2004.
42. Krasilnikov, P. M.; Mamonov, P. A.; Knox, P. P.; Paschenko, V. Z.; Rubin, A. B., *Biochimica et Biophysica Acta, Bioenergetics* **2007,** 1767, 541.
43. Trifonov, A.; Buchvarov, I.; Wagenknecht, H.-A.; Fiebig, T., *Chem. Phys. Lett.* **2005,** 409, 277.

Chapter 3

Electron Transfer and Bridge Energy Levels

Introduction

A β value of 1.1 $Å^{-1}$ for proteins provides a good first approximation to a broad set of data from ruthenium-modified proteins.[1-3] These studies have established that the secondary and tertiary structure of a protein have important effects on long distance electronic coupling. For example, weak coupling in the photosynthetic reaction center maintains the electron/hole separation that is critical for its function.[4] The sensitivity of this coupling, H_{DA}, on $\Delta\varepsilon$ (Chapter 2),[5] could potentially be exploited by minimizing $\Delta\varepsilon$ for photoinduced charge-separation while maximizing $\Delta\varepsilon$ for thermal charge recombination reactions. This ability to modify H_{DA} via alterations in $\Delta\varepsilon$ may be a useful tool for the optimal photogeneration of charge separated species and efficient artificial photochemical energy storage.

Background

Electron transfer through randomly dispersed toluene molecules occurs efficiently, and reasonably compares to electron transfer through covalently linked alkane (Figure 2.15). The relatively small value of $\beta = 1.27$ $Å^{-1}$ for toluene is likely a result of intramolecular aromaticity, which compensates for the weak coupling between individual toluene solvent molecules (h_{bb}) relative to the case of mTHF. The β value of 0.76 $Å^{-1}$ for the covalently linked xylyl bridges likely results from strong coupling between individual bridge units combined with small tunneling energy gaps.[6]

Superexchange theory suggests that the β of a system depends on the size of the bridge unit (δ), the coupling between the repeating bridge units (h_{bb}), and energy gap

between the donor/acceptor electron transfer transition state and the electron affinity or ionization potential of the bridge (Δε) (Equation 3.1).[5, 7, 8]

$$\beta = \left(\frac{2}{\delta}\right)\ln\left(\frac{\Delta\varepsilon}{h_{bb}}\right) \qquad (3.1)$$

Photoinitiated electron transfer between an iridium dimer and quinine acceptor (Chapter2) occurs as a result of electron tunneling through the bridge. The energy gap (Δε) is a function of the potential of the donor/acceptor pair and the electron affinity of the bridge. By modifying the bridge material so that the electron affinity of the bridge molecule is lower, yet ensuring that the coupling strength and the repeating bridge size remain unaltered, a smaller value of β could be obtained to enhance the electron transfer rate.

Multiple commercially available mTHF and toluene analogs were investigated, such as 2-(dichloromethyl)-tetrahydrofuran, 2-(chloromethyl)tetrahydrofuran, 2-(bromomethyl)tetrahydrofuran, 2-(iodomethyl)tetrahydrofuran, tetrahydrofuran-3-carboxaldehyde tetrahydro-2-furancarbonitrile, benzyl-fluoride, benzyl-chloride, benzyl-bromide, benzyl-iodide, difluoromethylbenzene, dichloromethylbenzene, dibromomethylbenzene, trifluoromethylbenzene, trichloromethylbenzene, 2,3,4,5,6-pentafluorotoluene, 2,3,4,5,6-pentachlorotoluene, 2,3,4,5,6-pentabromotoluene, perfluorotoluene, 2-fluorotoluene, 3-fluorotoluene, 4-fluorotoluene (Figure 3.1). All of these solvents, but one, were unsuitable for the experiment. A majority did not glass, and

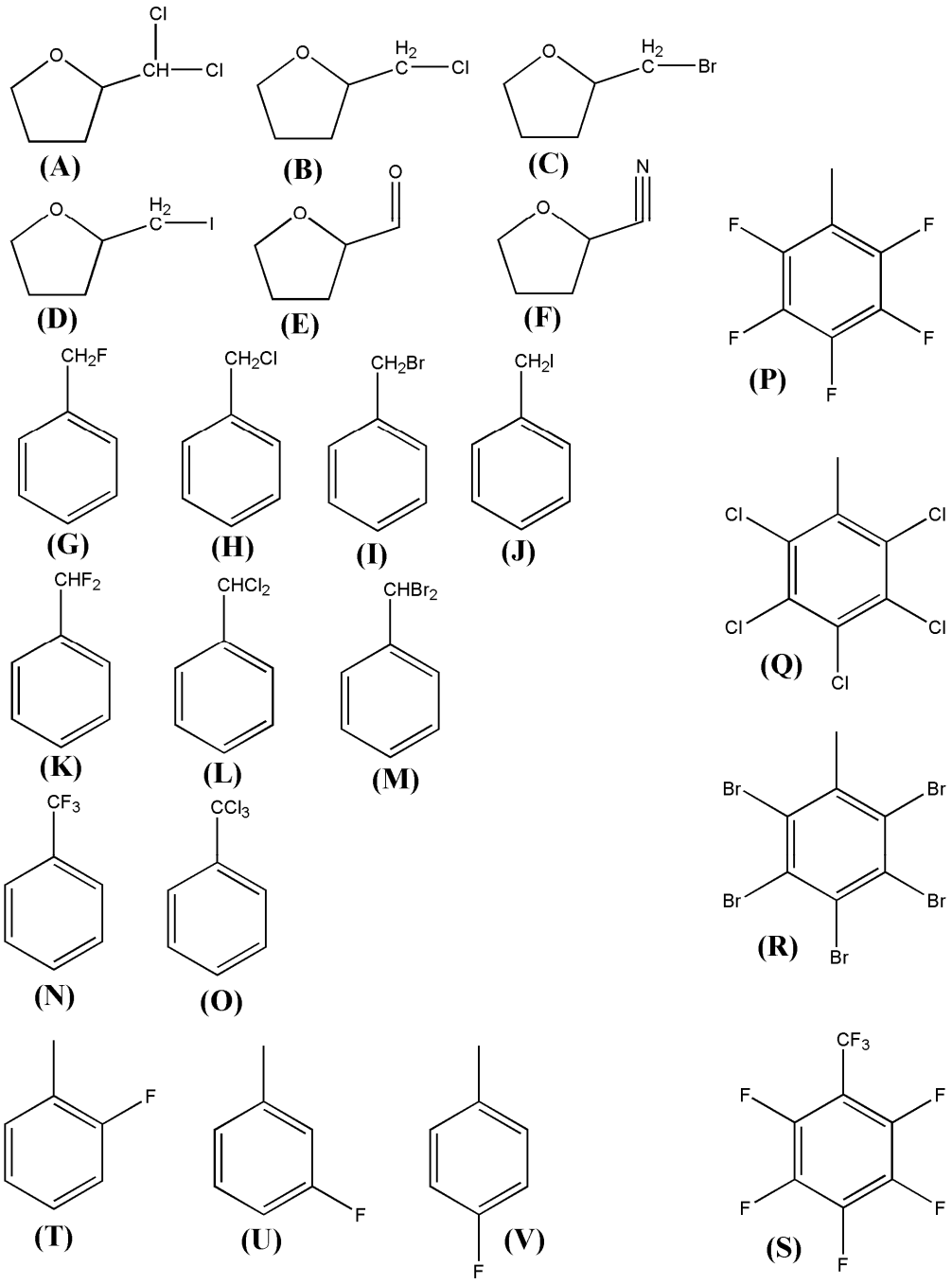

Figure 3.1 MTHF and toluene analogs 2-(dichloromethyl)-tetrahydrofuran (A), 2-(chloromethyl)tetrahydrofuran (B), 2-(bromomethyl)tetrahydrofuran (C), 2-(iodomethyl)tetrahydrofuran (D), tetrahydrofuran-3-carboxaldehyde (E), tetrahydro-2-furancarbonitrile (F), benzyl-fluoride (G), benzyl-chloride (H), benzyl-bromide (I), benzyl-iodide (J), difluoromethylbenzene (K), dichloromethylbenzene (L), dibromomethylbenzene (M), trifluoromethylbenzene (N), trichloromethylbenzene (O), 2,3,4,5,6-pentafluorotoluene (P), 2,3,4,5,6-pentachlorotoluene (Q), 2,3,4,5,6-pentabromotoluene (R), perfluorotoluene (S), 2-fluorotoluene (T), 3-fluorotoluene (U), 4-fluorotoluene (V).

those that did form a glass lacked the ability to dissolve the donor or acceptor in any appreciable amount. Only 3-fluorotoluene (Figure 3.1, (U)) successfully formed a glass at 77 K, dissolved the donor and acceptor in sufficient concentrations (~0.5 M), and remained inert to the donor and acceptor molecules. Hence, 3-fluorotoluene was investigated as a modified bridge molecule to potentially enhance the electron transfer rate.

Experimental

Donor and acceptor synthesis and purification

[Ir(μ-pyrazolyl)(1,5-cyclooctadiene)]$_2$ and 2,6-dichloro-1,4-benzoquinone were obtained as described in Chapter 2.

Solvent preparation

The 3-fluorotoulene 99% was acquired form Sigma-Aldrich in a "septa seal" bottle. The solvent was found to be sufficiently dry and was used as is.

Sample holder and dewar configuration

The identical sample holder set up was used as described in Chapter 2.

Kinetics measurements

The kinetic measurement was obtained as described in Chapter 2.

Relative quantum yield measurements

Quantum yield measurements were obtained on the same sample used in kinetics experiments, and within hours of performing kinetics measurements. The relative quantum yields were obtained using a custom built dewar holder that sat inside the sample chamber of a Fluorolog Model FL3-11 fluorometer with a Hamamatsu R928 PMT (Figure 2.10). Positional reproducibility was high, and resulted in error of less than 1% (standard deviation/mean). Entrance and exit slits were set at 1 mm and integration time was set to 1 second, with 30 measurements acquired per sample. Excitation was 514 nm and the luminescence was measured at 680 nm. Standard deviation for the quantum yield measurements was approximately 10%.

Data analysis

Data analysis was preformed using the same methods described in Chapter 2. Kinetics of donor luminescence in 3-fluorotoluene was highly nonexponential in the presence of acceptor and the decay curves were similar to those of donor in toluene (Figure 3.2). Matlab 13 (MathWorks Natick, MA) and Igor Pro 5.01 (Wavemetrics Lake Oswego, OR) were used to fit the scaled kinetics to Equation 2.4 (Figure 3.3, Table 3.1).

Discussion

The exponential decay constant (β) for 3-fluorotoluene was found to be 1.25 $Å^{-1}$ ± 0.08, which is essentially identical to the value for toluene of 1.27 $Å^{-1}$ ± 0.07 (Chapter 2). Assuming that all relevant molecular properties of 3-fluorotoluene are identical to those of toluene with the exception that electron affinity is potentially lower in 3-fluorotoluene,

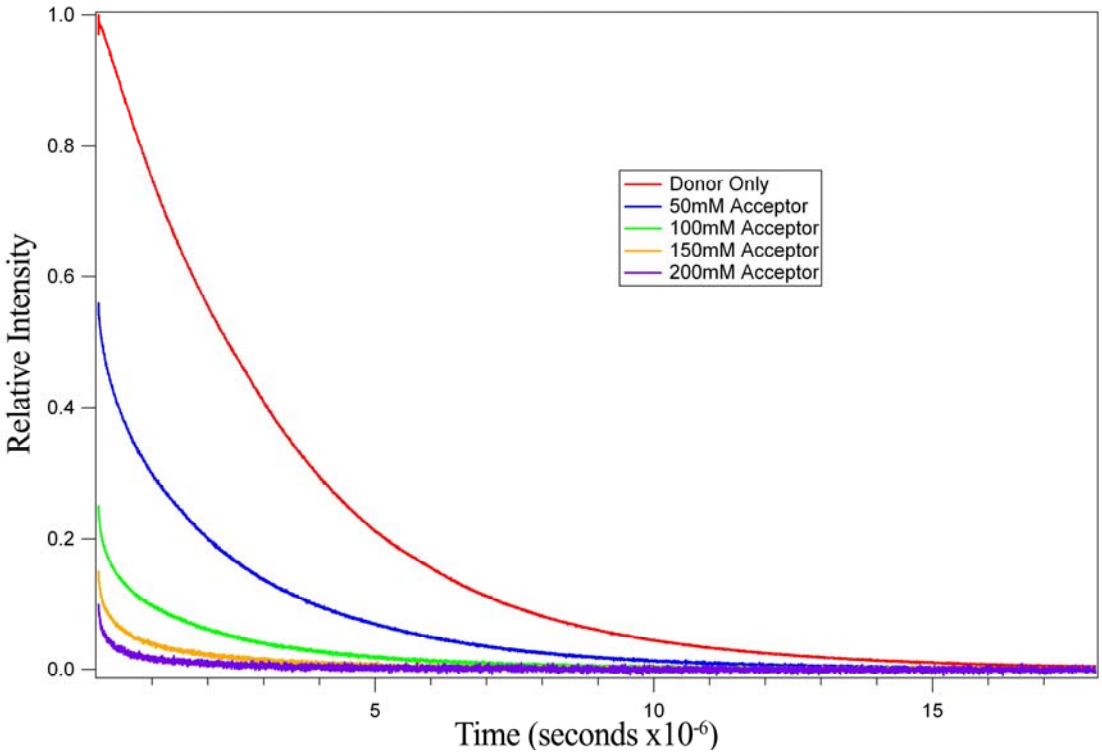

Figure 3.2 Scaled kinetics traces of [Ir(μ-pyrazolyl)(1,5-cyclooctadiene)]$_2$ and 2,6-dichloro-1,4-benzoquinone acceptor in 3-fluorotoluene at 77 K.

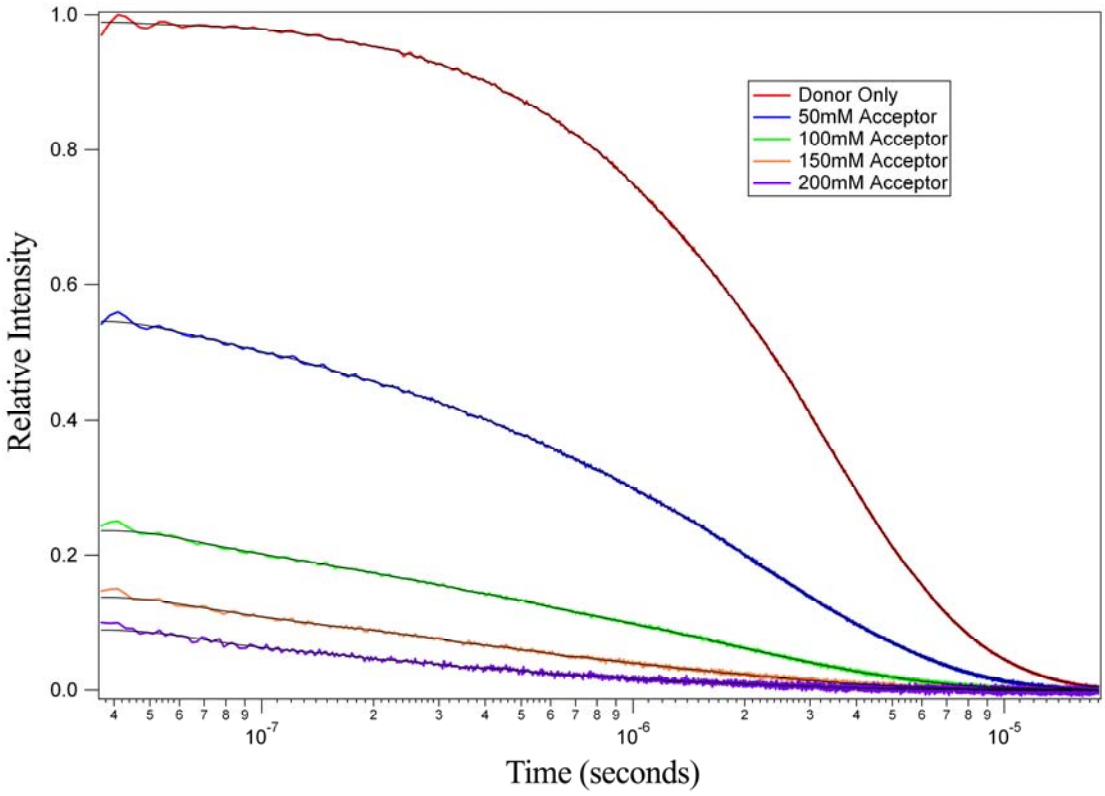

Figure 3.3 Luminescence decay kinetics (black) for [Ir(μ-pyrazolyl)(1,5-cyclooctadiene)]$_2$ in 3-fluorotoluene glass at 77 K in the presence of 2,6-dichloro-1,4-benzoquinone (upper to lower traces: 0.0, 0.05, 0.10, 0.15, 0.20 M). The smooth black line is the calculated decay using Equation 2.4 and the parameters listed in Table 3.1.

	Acceptor Concentration (M)	β ($Å^{-1}$)	k^{o}_{ET} (s^{-1})
3-Fluorotoluene	0.05	1.31	2.9×10^{13}
	0.10	1.14	4.0×10^{13}
	0.15	1.25	0.3×10^{13}
	0.20	1.29	0.8×10^{13}

Table 3.1 Best-fit values of β and k^{o}_{ET} (Equation 2.4) extracted from luminescence decay kinetics and quantum yields of [Ir(μ pyrazolyl)(1,5 cyclooctadiene)]$_2$ quenched by electron transfer to 2,6-dichloro-1,4-benzoquinone in 3-fluorotoluene at 77 K.

the hypothesis was that electron transfer in 3-fluorotoluene should be faster than in toluene. No information on the electron affinity of 3-fluorotoluene could be found in the literature. However, it is known that the energy of the LUMO scales linearly with electron affinity in small molecules.[9] DFT calculations of mTHF, toluene, and 3-fluorotoluene were performed using Jaguar (Shrödinger, Inc.). Results from this calculation indicated that there is very little difference in the energy levels of toluene and 3-fluorotoluene (Figure 3.4); this finding is consistent with the experimental observation that the β values for toluene and 3-fluorotoluene are identical within the errors of this experiment. It appears that the single fluorine atom on the benzene ring of toluene does not enhance the electron withdrawing capabilities of 3-fluorotoluene to lower the electron affinity sufficiently and hence, we are unable to observe the effect of a change in $\Delta\varepsilon$ on electron transfer rates.

Conclusion

We have determined that the exponential decay constant for 3-fluorotoluene is 1.25 $Å^{-1} \pm 0.08$. This value is identical to the value found for toluene, and this similarity may be due to the lack of a dramatic effect of a single fluorine atom on the electron affinity of toluene.

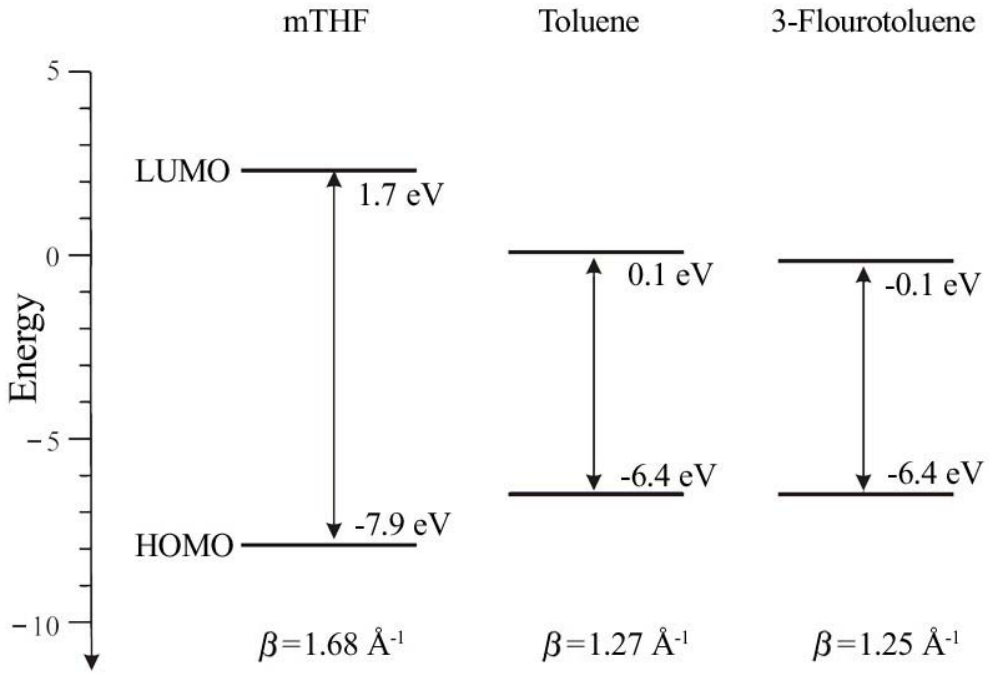

Figure 3.4 HOMO and LUMO energy levels for mTHF, toluene and 3-fluorotoluene from DFT (B3LYP) calculations.

References

1. Langen, R.; Chang, I.; Germanas, J.; Richards, J. H.; Winkler, J. R.; Gray, H. B., *Science* **1995,** 268, 1733.
2. Winkler, J. R.; Gray, H. B., *Chem. Rev.* **1992,** 92, 369.
3. Langen, R.; Colón, J. L.; Casimiro, D. R.; Karpishin, T. B.; Winkler, J. R.; Gray, H. B., *J. Biol. Inorg. Chem.* **1996,** 1, 221.
4. Feher, G.; Allen, J. P.; Okamura, M. Y.; Rees, D. C., *Nature* **1989,** 339, 111.
5. McConnell, H. M., *J. Chem. Phys.* **1961,** 35, 508.
6. Villahermosa, R. PhD, California Institute of Technology, 2002.
7. Skourtis, S. S.; Beratan, D. N., *Adv. Chem. Phys.* **1999,** 106, 377.
8. Wenger, O. S.; Leigh, B. S.; Villahermosa, R.; Gray, H. B.; Winkler, J. R., *Science* **2005,** 307, 99.
9. Zhan, C.; Nichols, J. A.; Dixon, D. A., *J. Phys. Chem. A* **2003,** 107, 4184.

Chapter 4

Electron Transfer Through Biological Molecules

Introduction

Azurin is a well known copper containing protein with a 50+ year history. In 1956 it was reported that *Pseudomonas aeruginosa* contained a blue protein.[1] It was first proposed in 1958 that this intense blue color arose from copper bound to a polypeptide chain.[2] The absorption maximum of this blue species was centered at about 600 nm and the color intensity was about 80 times greater than that of the same concentration of copper in the form of cuprammonium ion.[2] It was also discovered that the blue color disappears reversibly if a reducing agent such as sodium dithionite is added, or irreversibly if the protein is denatured chemically or thermally. Dialysis against cyanide was performed, and the blue color could be made to disappear and then reappear upon addition of a Cu^{2+} solution to the apo-protein.[3] These properties were further investigated, and the protein responsible for the blue color, azurin, was isolated and found to be common in other species such as *Pseudomonas, Bordetella,* and *Alcaligenes*.[4-7] It was eventually determined that azurin acts as an electron shuttle between cyctochrome c_{551} and nitrite reductase in denitrifying pathways.[7, 8]

Background

Azurin from *Pseudomonas aeruginosa* contains 128 residues, and has a molecular weight of about 14 kDa.[9] It contains 12 β-sheet strands (43 residues), 4 α-helices (21 residues, and a disulfide bridge (Figure 4.1). This structure is very stable and has a denaturation temperature of around 80 ºC.[10] The stability of the molecule is attributed to the ridged β-sheet motif it has (Figure 4.2).

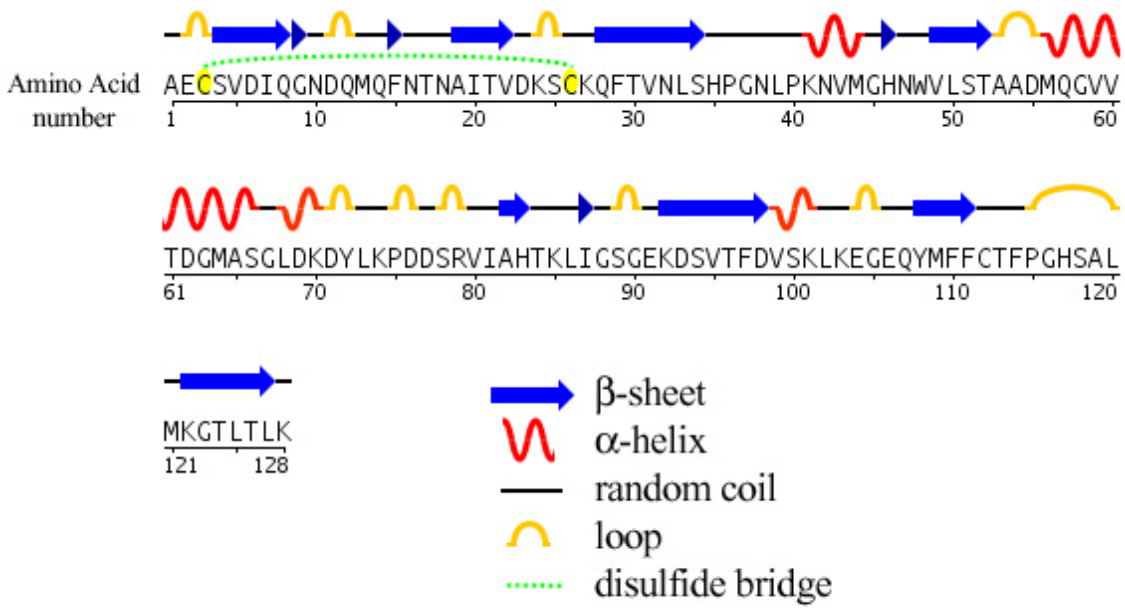

Figure 4.1 Polypeptide sequence of azurin from *Pseudomonas aeruginosa*, highlighting how β-sheet, α-helix, random coil, loops, and disulfide bridges map onto the sequence. Short arrowheads indicate sections of extended strands that participate in the beta ladder.[11] Data obtained from 4AZU PDB file.

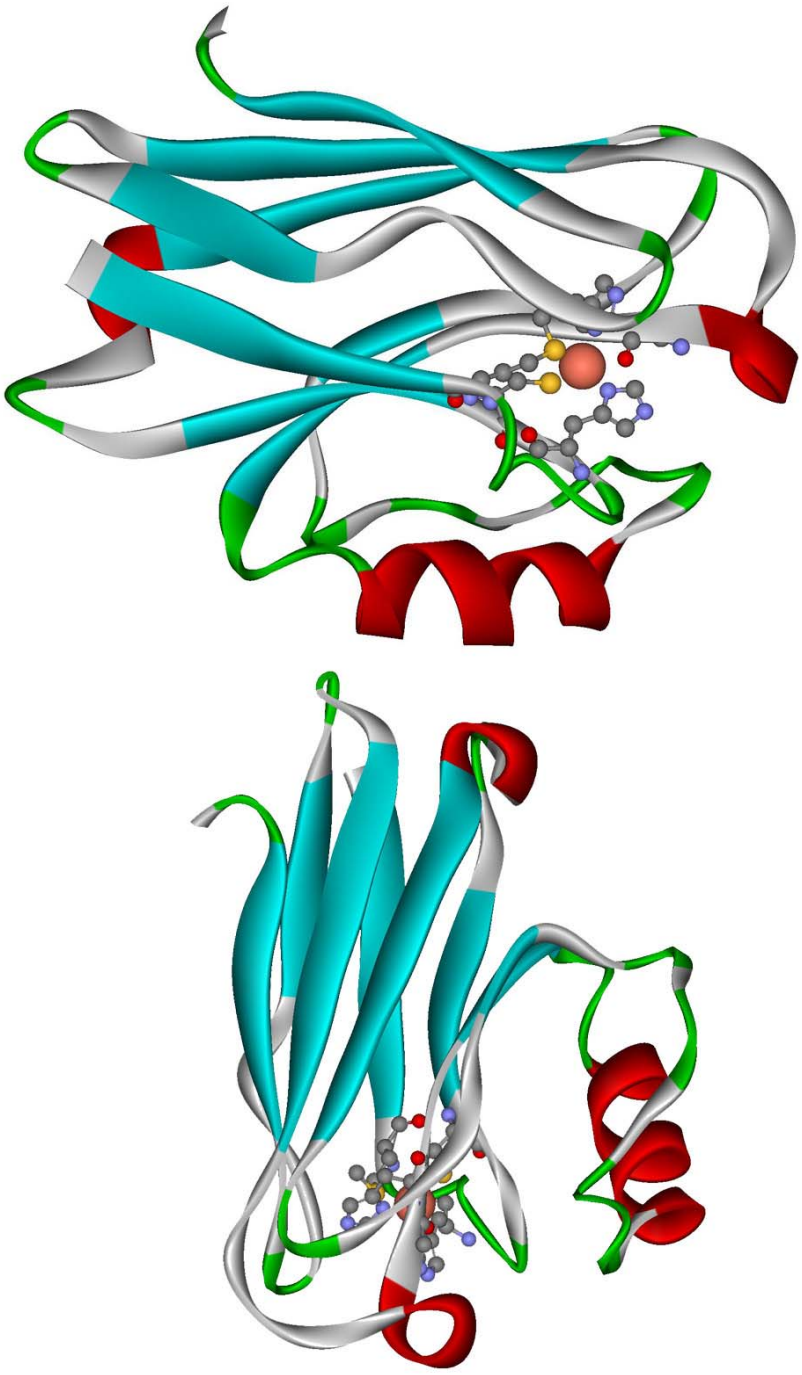

Figure 4.2 Structure of azurin from *Pseudomonas aeruginosa* in two views to illustrate β-sheet/β-barrel structural motif. The copper atom and ligands are shown. Data obtained from 4AZU PDB file.

The redox active site of azurin is a type 1 copper center. The copper is ligated by two histidine residues (H46 and H117) and a cysteine residue (C112) in a trigonal planar structure. There are also two weakly interacting axial ligands, methionine (M121) and the backbone carbonyl of glycine (G45) (Figure 4.3). The reduction potential of this center (and many mutants) has been determined to be 0.31 V vs. NHE.[12-15]

The electron transfer pathway in azurin is of great interest. One approach that has shed light on electron transfer pathways in proteins is the study of self-assembled monolayers (SAMs) on electrodes. An example of a protein that has been studied in this manner is cytochrome *c* (cyt *c*). It has been established that cyt *c* can be immobilized electrostatically on carboxy terminated SAMs (HOOC-SAMs).[16, 17] This system has been investigated by surface enhanced resonance Raman spectroscopy, and it was reported that when cyt *c* is immobilized on the SAM, it retains its native structure and orientates such that the heme edge is towards the SAM electrode.[18] In addition to the structure of cyt *c* on the SAM, the region within the protein that couples to the SAM has been elucidated by the use of multiple cyt *c* mutants on the HOOC-SAM.[16, 17]

This successful technique to determine the electron transfer pathway "hot spot" in cyt *c* was used to investigate electron transfer pathways in azurin and the Cu_A soluble domain of cytochrome *c* oxidase from *Thermus thermophilus* (CcO) with the goal of determining one or more strong coupling sites. One region of azurin considered important for electron transfer is the environment surrounding H117. This ligating histidine residue is solvent exposed and is thought to be responsible for electron self-exchange reactions[15, 19-22] as well as intermolecular electron transfer with nitrate

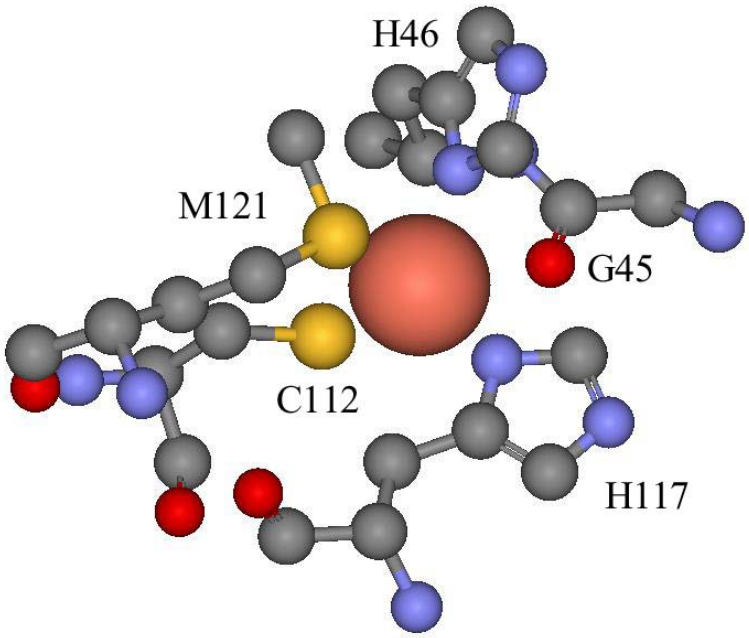

Figure 4.3 Redox active site of azurin. The copper atom is ligated by two histidines (H46 and H117), a cysteine (C112), a methionine (M121) and the backbone carbonyl of glycine (G45). Data obtained from (4AZU PDB file).

reductase.[23] A separate hydrophobic patch is believed to be responsible for coupling to cyt c_{551}.[23]

Another important electron transfer protein is Cu_A, which is a binuclear copper subunit of CcO. The soluble domain of Cu_A contains 121 residues (called soluble Cu_A) and has a molecular weight of approximately 15 kDa (Figures 4.4 and 4.5). This protein acts as the site at which cyt *c* binds to CcO and transfers electrons into the protein to be further utilized to reduce dioxygen to water. The two copper atoms in Cu_A are bridged by 2 cysteine residues creating a "diamond core" structure (Figure 4.6). It has been suggested that the solvent exposed residue H157 is a likely region of coupling to cytochrome *a* in CcO.[24]

This chapter describes the study of azurin and soluble Cu_A immobilized on SAM electrodes. Previous work has utilized alkane-terminated SAMs to immobilize azurin and obtain a voltammetric response.[25] Ulstrap *et al*. has published a comprehensive report on azurin on CH_3-SAM/gold electrodes.[26, 27] Wild-type azurin and the following four azurin mutants were studied to investigate the role of the important native residue, tryptophan 48, in the electron transfer reaction: W48F/Y72F/H83Q/Q107H/Y108F (all-Phe), W48F/Y72F/H83Q/Y108F/K122W/T124H (all-Phe-W122), W48F/Y72F/H83Q/Q107H/Y108W (all-Phe-W108), and Y72F/H83Q/Q107H/Y108F (all-Phe-W48).[22, 28] The soluble domain of Cu_A was also investigated to help elucidate the electron transfer hot spot in this system.

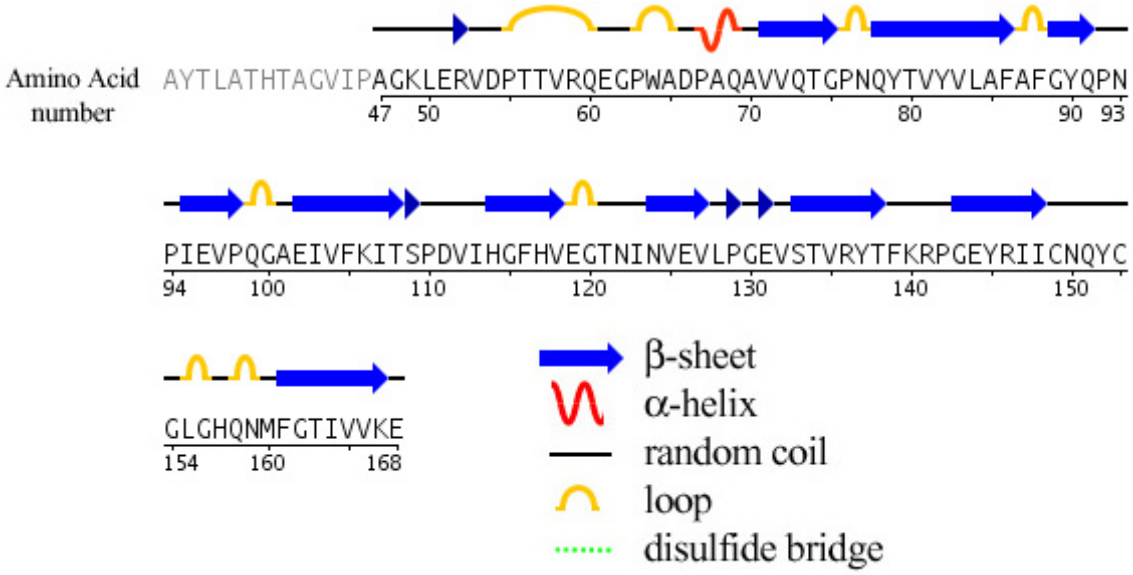

Figure 4.4 Polypeptide sequence of soluble Cu_A from *Thermus thermophilus*, highlighting how β-sheet, α-helix, random coil, loops, and disulfide bridges map onto the sequence. Short arrowheads indicate sections of extended strands that participate in the beta ladder.[11] Data obtained from 2CUA PDB file. The transmembrane domain is not included.

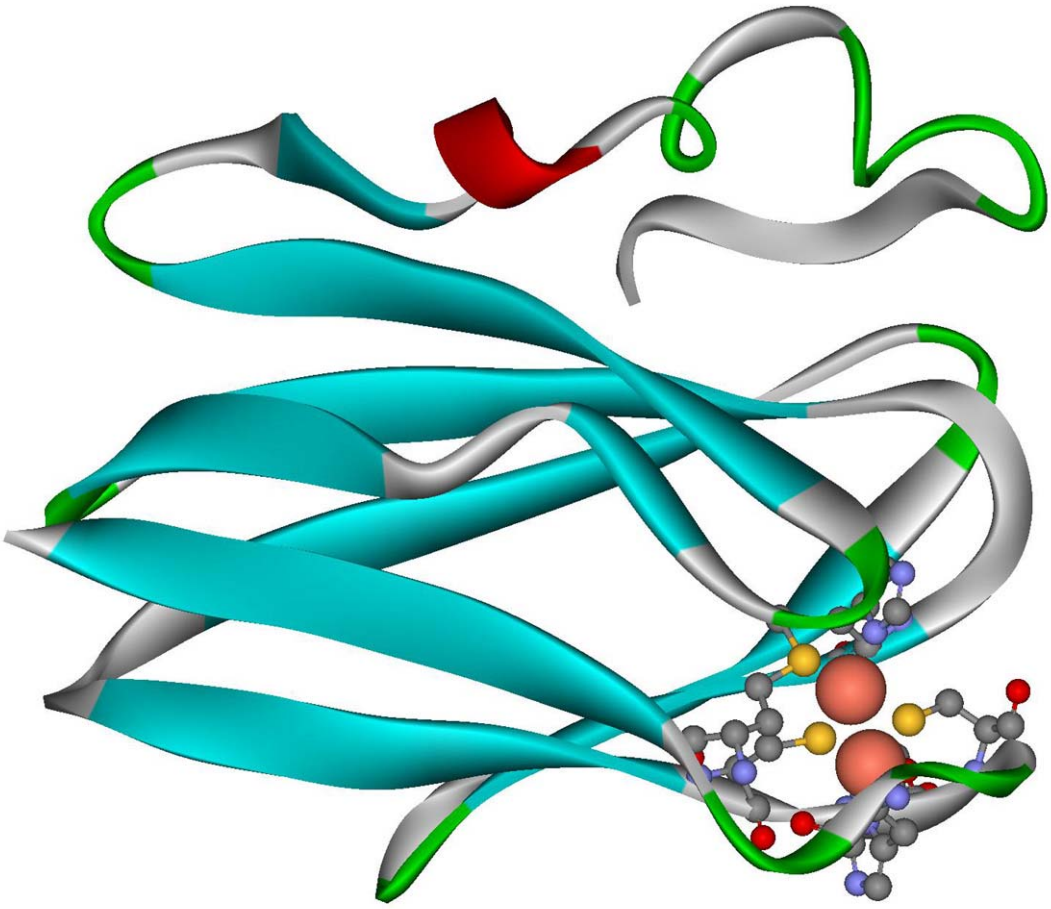

Figure 4.5 Structure of Cu_A from *Thermus thermophilus*. Data obtained from 2CUA PDB file. The copper centers and ligands are indicated.

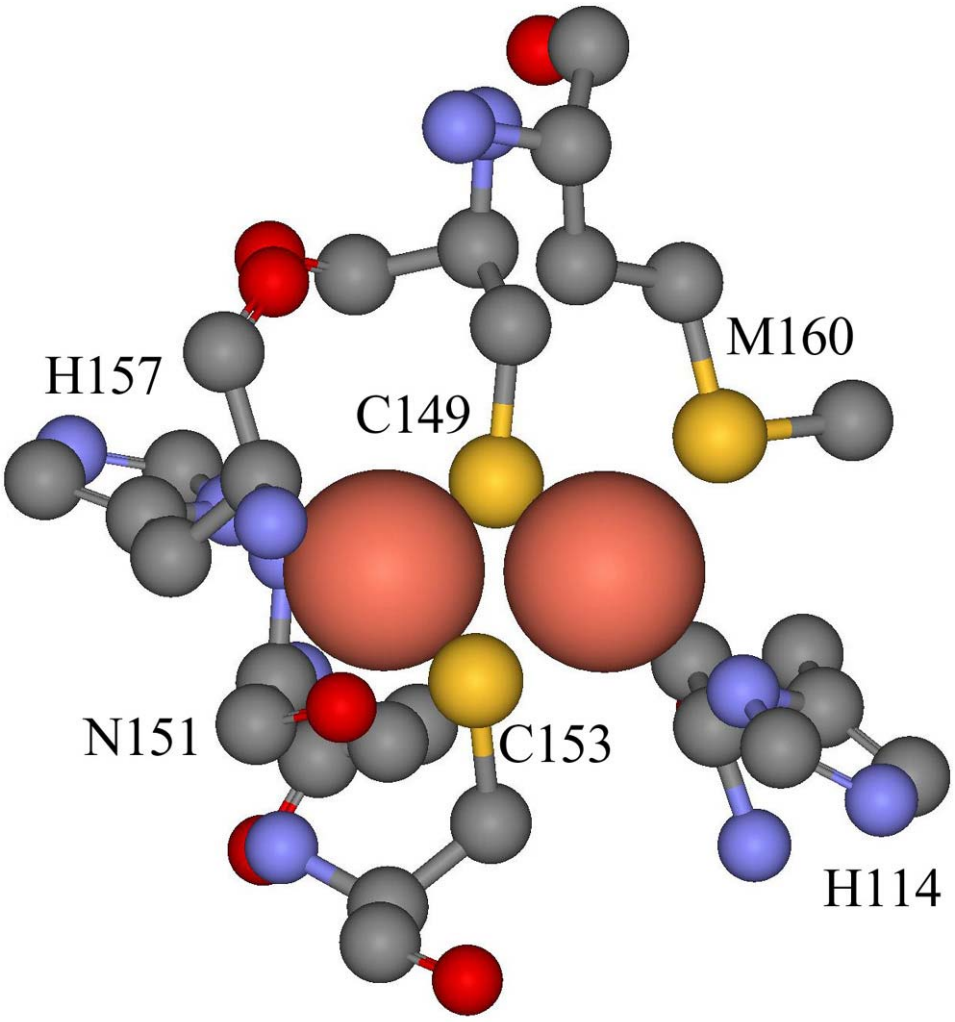

Figure 4.6 Redox active site of Cu_A binuclear center; bridging cysteines (C149, C153), The first copper atom (Cu_A#1) utilizes histidine (H114) and methionine (M160) as ligands while the second copper atom (Cu_A#2) incorporates histidine (H157) and carbonyl oxygen (N151) as ligands.

Experimental

Azurin site directed mutagenesis

Azurin was expressed from a plasmid from the Richard's group.[29] Primers were obtained from Invitrogen (Table 4.1). HPLC grade water (1 ml) was added to the primer to obtain a primer concentration of 50 ng/µl. Primers were vortexed, allowed to sit for 10 minutes, then vortexed again. A QuikChange site-directed mutagenesis kit from Stratagene (La Jolla, CA) was used to make new plasmids via polymerase chain reaction (PCR) following a timing sequence in a thermal cycler (Table 4.2).

Azurin plasmid amplification

Mutant plasmid was obtained by transforming PCR product into XL1-Blue Super competent cells (Stratagene La Jolla, CA). Cells were thawed and kept on ice and combined with 1 µl of PCR product. Cells were then warmed to 42 ºC in a warm water bath for 45 seconds, and then placed back on ice for 5 minutes. Cells were then transferred to 200 µl of NZY+ broth in a 10-ml falcon tube. (NZY+ broth per liter: 10 g of NZ amine (casein hydrolysate), 5 g of yeast extract, 5 g of NaCl. Add deionized H_2O to a final volume of 1 liter. Adjust to pH 7.5 using NaOH. Autoclave. Add the following filer-sterilized supplements prior to use: 12.5 ml of 1 M $MgCl_2$, 12.5 ml of 1 M $MgSO_4$, 20 ml of 20 % (w/v) glucose) Culture was placed in a shaker at 37 ºC for 1 hour and was then plated to an LB agar plate that had 70 mg/liter ampicillin. (LB agar medium per 500 ml: 5 g of NaCl, 5 g of tryptone, 2.5 g of yeast extract, 10 g of agar. Add deionized H_2O to a final volume of 500 ml. Autoclave. Let cool to 55 °C and add 500 µl of 70 mg/ml

W48F/Y72F/H83Q/Q107H/Y108F Primers			
Y72F	5'	GAT AAA GAC TTC CTG AAG CCG	3'
H83Q	5'	GTT ATC GCC CAG ACC AAG CTG	3'
W48F	5'	GGT CAC AAC TTC GTT CTG TCC	3'
Q107H	5'	GAA GGT GAA CAC TAC ATG TTC	3'
Y108F	5'	GGT GAA CAC TTC ATG TTC TTC	3'
W48F/Y72F/H83Q/Y108F/K122W/T124H Primers			
Y72F	5'	GAT AAA GAC TTC CTG AAG CCG	3'
H83Q	5'	GTT ATC GCC CAG ACC AAG CTG	3'
W48F	5'	GGT CAC AAC TTC GTT CTG TCC	3'
Y108F	5'	GGT GAA CAG TTC ATG TTC TTC	3'
K122W	5'	GCA CTG ATG TGG GGT ACC CTG	3'
T124H	5'	ATG TGG GGT CAC CTG ACT CTG	3'
W48F/Y72F/H83Q/Q107H/Y108W Primers			
Y72F	5'	GAT AAA GAC TTC CTG AAG CCG	3'
H83Q	5'	GTT ATC GCC CAG ACC AAG CTG	3'
W48F	5'	GGT CAC AAC TTC GTT CTG TCC	3'
Q107H	5'	GAA GGT GAA CAC TAC ATG TTC	3'
Y108W	5'	GGT GAA CAC TGG ATG TTC TTC	3'
Y72F/H83Q/Q107H/Y108F Primers			
Y72F	5'	GAT AAA GAC TTC CTG AAG CCG	3'
H83Q	5'	GTT ATC GCC CAG ACC AAG CTG	3'
Q107H	5'	GAA GGT GAA CAC TAC ATG TTC	3'
Y108F	5'	GGT GAA CAC TTC ATG TTC TTC	3'

Table 4.1 Primers used to generate mutant azurin: W48F/Y72F/H83Q/Q107H/Y108F (all-Phe), W48F/Y72F/H83Q/Y108F/K122W/T124H (all-Phe-W122), W48F/Y72F/H83Q/Q107H/Y108W (all-Phe-W108), and Y72F/H83Q/Q107H/Y108F (all-Phe-W48). The 5' to 3' antisense sequence is not included. Primers must be applied in the order in which they are listed as some primers rely on previous site directed mutagenesis to bind.

Step	Temp (°C)	Time
1	95	30 Sec
2	95	30 Sec
3	55	1 Min
4	68	8 Min
5	Loop to Step 2 - 15 times	
6	2	hold
7	End	

Table 4.2 PCR thermal cycler temperature and time table.

filter-sterilized ampicillin. Pour into petri dishes, ~25 ml/100-mm plate). Plates were allowed to incubate inverted for 24 hours at 37 ºC. A single colony was selected and transferred to a falcon tube with 5 ml LB media. Culture was then allowed to incubate for 24 hours at 37 ºC. Media was then centrifuged at 5000 rpm, decanted and the pellet was saved.

Azurin plasmid isolation

Plasmid was isolated using QIAprep Miniprep (Qiagen Valencia, CA) plasmid DNA purification kit. Isolation of plasmid was performed exactly as outlined in the instruction manual. After plasmid isolation, 15 µl of product was submitted to the Caltech DNA Sequencing Facility. Sequences were confirmed for correct mutation and were either expressed or used as a new template for the next mutation.

Azurin protein expression

Expression of azurin was performed in Novagen BL-21(DE3) cells. Single-use tubes of BL-21 were thawed and placed on ice. Each tube received 1 µl of the plasmid to be expressed and was allowed to sit on ice for 5 minutes. Transformation was achieved by placing the cells in a hot water bath at 42 ºC for 30 seconds, and then placed on ice for another 5 minutes. 80 µl of NZY+ broth was then added and mixed gently. Mixture was placed in a falcon tube and incubated at 37 ºC for 1 hour and poured onto an agar plate that had 70 mg/liter ampicillin. Plates were incubated inverted for 24 hours at 37 ºC. A single colony was selected and transferred to a falcon tube with 10 ml LB media and left to incubate at 37 ºC for 12 hours. 1 ml of this culture was then added to 1 liter of TB

media with 70 mg/liter ampicillin (6 liters were grown at a time). Liter growth flasks were then placed into a shaker and incubated at 37 ºC for 16 hours. After 16 hours, isopropyl β-D-1-thiogalactopyranoside (IPTG) was then added (1ml of 0.4 M), and incubation was continued for another 4 hours.

After a total of 20 hours of growth plus induction, the cells were pelleted via centrifugation at 6000 RPM. The cell pellet was resuspended in 25 mM pH 7.2 potassium phosphate buffer. About 10 mg of lysozyme (Sigma L-6876) and 40 µl of DNAse I (RNAse free, Roche Basel, Switzerland [10 units/µl]) were added, and the solution was allowed to sit on ice for an hour. The solution was then centrifuged at 9500 RPM for 30 minutes and the supernatant was collected. The supernatant was brought to 50 mM sodium acetate (NaOAc) using a 1M NaOAc pH 4.3 stock buffer solution. At this pH, azurin remains in solution while other proteins precipitate out of solution. Solid $CuSO_4$ was then added to bring this solution to 20mM $CuSO_4$; addition of $CuSO_4$ changed the solution to a blue color. This blue solution was centrifuged for 10 minutes at 5000 RPM to isolate crude azurin in the supernatant, which was stored at 4 ºC for 24 hours.

Purification of azurin

The blue crude azurin solution was concentrated using Amicon Ultra-15 10,000 NMWL from Millipore (Danvers, MA) to a protein concentration of 1mM in 25 mM NaOAc pH 4.5 buffer. Protein can be stored as such at 4 ºC indefinitely. A Mono-S column (Pharmacia) was used to purify azurin. The Mono-S column was attached to a Pharmacia fast protein liquid chromatography system (FPLC) and washed with 10

column volumes of 300 mM NaOAc pH 4.5 buffer and 10 column volumes of 25 mM NaOAc pH 4.5 to ensure that the column was free of contaminants. About 1 ml of the 1 mM azurin was loaded onto the Mono-S column and eluted at a flow rate of 1 ml/min over the next hour using the buffers and parameters listed in Table 4.3. Azurin came off the FPLC around 48 ml into the run. Fractions were assessed using UV-Vis absorption spectroscopy via the LMCT band of azurin at 628 nm ($\varepsilon = 5900\ M^{-1}cm^{-1}$). Combined fractions were then re-concentrated using an Amicon and samples were sent to the Protein and Peptide Mass Analysis Laboratory at Caltech to verify the mass. Purity was also verified by checking the A_{628}/A_{280} ratio ($A_{628}/A_{280} = 1.18$).

Cu_A expression

The soluble Cu_A plasmid from *Thermus thermophilus* was developed by Slutter in the Richards lab.[30] The wild-type plasmid was transformed into BL-21(DE3) cells and the protocol for overexpression of Cu_A is identical to that described above for azurin.

Purification of Cu_A

Cu_A was purified using an FPLC and Mono-Q column (Pharmacia). The Mono-Q column is attached to the FPLC and washed with 10 column volumes of 25 mM diethanolamine (DEA), 200 mM NaCl at pH 9.0, and with 10 column volumes of 25 mM DEA at pH 9.0 to ensure that the column was free of contaminants. Cu_A was exchanged into 25 mM DEA buffer using an Amicon concentrator. About 1 ml of 1 mM Cu_A was loaded onto the Mono-Q column and eluted at a flow rate of 1 ml/min over the next hour using the buffers and parameters listed in Table 4.4.

Mono-S FPLC Buffer Program

Buffer A	25mM NaOAC pH 4.5
Buffer B	300mM NaOAC pH 4.6

ml	%A	%B
0	100	0
10	100	0
12	85	15
60	85	15
62	0	100
80	0	100

Table 4.3 Mono-S FPLC buffer and eluent composition table.

Mono-Q FPLC Buffer Program

Buffer A	25 mM DEA, pH 9.0
Buffer B	25 mM DEA, 200 mM NaCl pH 9.0

ml	%A	%B
0	100	0
15	100	0
20	80	20
40	80	20
45	0	100
60	0	100

Table 4.4 Mono-Q FPLC Buffer and eluent composition table.

Gold bead-SAM electrode synthesis

Gold electrodes were made by melting 99.999% gold wire (Alfa Aesar/Johnson Matthey Ward Hill, MA) in a hydrogen flame. The tip of the wire was slowly placed into the flame until a gold bead formed at the end of the wire. At this point the wire was cleaned by placing it in boiling concentrated H_2SO_4 for about 2 hours. The gold bead was then subjected to an oxidation-reduction cycle (ORC) in 1 M H_2SO_4 between -0.3 and 1.5 V for 20 cycles at a scan rate of 20 mV/s until a well-defined Au(111) voltammogram was obtained (Figure 4.7).[31] Any gold bead not exhibiting a voltammogram like Figure 4.7 was excluded. The gold bead electrodes were then rinsed with Milli-Q water, sonicated in Milli-Q water for 2 minutes to remove any trace of acid, and re-rinsed with Milli-Q water.

Mixed SAMs were prepared by immersing gold bead electrodes into ethanol solutions containing a fixed ratio of alkanethiol to hydroxy alkanethiols to achieve H_3C-/HO- head group ratios of the following: pure methyl, 3:1, 1:1, and 1:3 mole ratios. SAM surface compositions were not experimentally determined. The mixed alkanethiol and ω-hydroxy alkanethiols were as follows: (i) [$H_3C(CH_2)_8SH$ + $HO(CH_2)_8SH$], (ii) [$H_3C(CH_2)_{11}SH$ + $HO(CH_2)_{11}SH$], (iii) [$H_3C(CH_2)_{13}SH$ + $HO(CH_2)_{11}SH$], and (iv) [$H_3C(CH_2)_{15}SH$ + $HO(CH_2)_{11}SH$]. Gold electrodes were then immersed into a 200 μM solution of thiols in ethanol. The electrode was left undisturbed for 3-5 hours in the dark to allow the thiols to adsorb to the gold surface.

Nonanethiol, $CH_3(CH_2)_8SH$, dodecanethiol, $CH_3(CH_2)_{11}SH$, hexadecanethiol, $CH_3(CH_2)_{15}SH$, and 11-mercapto-1-undecanol, $HS(CH_2)_{11}OH$, were purchased from Aldrich Chemical Co. (St. Louis, MO). Tetradecanethiol, $CH_3(CH_2)_{13}SH$, was purchased

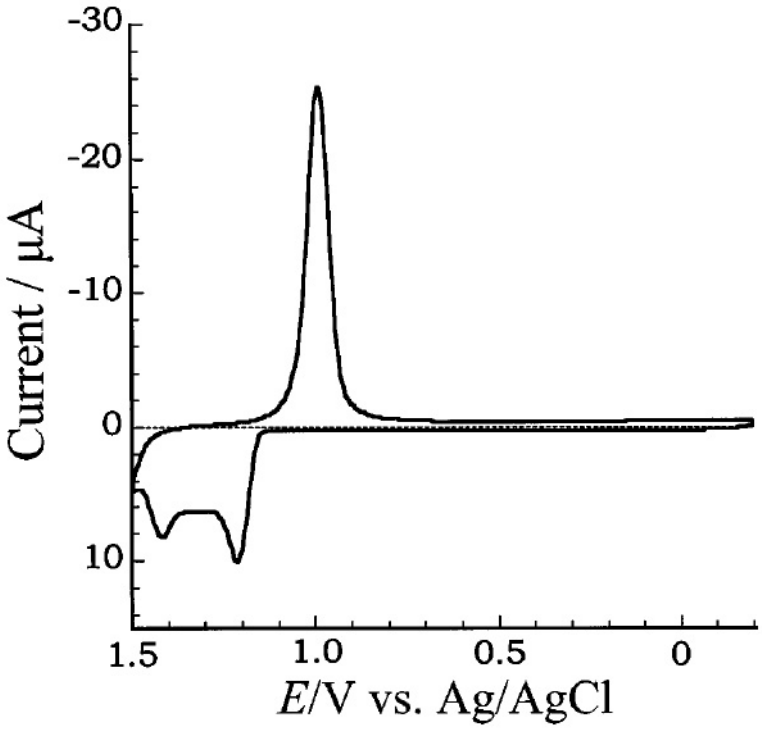

Figure 4.7 Voltammogram of clean Au(111) bead electrode. The oxidation-reduction cycle was performed in 1 M H_2SO_4 between -0.3 and 1.5 V for 20 cycles at a scan rate of 20 mV/s. The reference electrode contained saturated Ag/AgCl and the counter electrode was a Pt electrode.

from Fluka Chemie AG (Buchs, Switzerland). 8-Mercapto-1-octanethiol, $HS(CH_2)_8OH$, and 8-mercaptooctanoic acid, $HOOC(CH_2)_7SH$, were purchased from Dojindo Molecular Technology (Gaithersburg, MD). Thiols were used without further purification.

Further cleaning and activation of the new SAM surfaces was required. ORC was preformed between 0.5 and -0.2 V in 10 mM NaOAc pH 4.6 until the cyclic voltammogram (CV) that was obtained from the bare SAM was nearly flat and without features in the relevant region (Figure 4.8). To adsorb protein onto the SAM surfaces, the SAM electrodes were immersed in 100 μM protein solutions overnight in a refrigerator. The electrodes were thoroughly rinsed with Milli-Q water to remove excess protein from the surface prior to electrochemical measurements.

Electrochemical measurements

The electrochemical cell was cleaned by immersion it into boiling Milli-Q water, and used as soon as it cooled. After each electrochemical experiment, each SAM electrode was subjected to cathodic stripping to determine the amount of SAM on the electrode. Cathodic stripping was performed in 0.5 M KOH solution in the potential range -0.5 to -1.3 V.[31, 32]

The cell electrolyte was deoxygenated with an argon sparge and kept under an argon atmosphere during the experiment (Figure 4.9). The solution used for both azurin and Cu_A is 10 mM ammonium acetate (NH_4OAc) at pH 4.6. The counter electrode was a platinum coil and reference electrode was a saturated Ag/AgCl electrode (0.197 vs. NHE). All measurements were performed using a model 660 Electrochemical Workstation (CH-Instrument, Austin, TX) at room temperature (Figures 4.10 to 4.13).

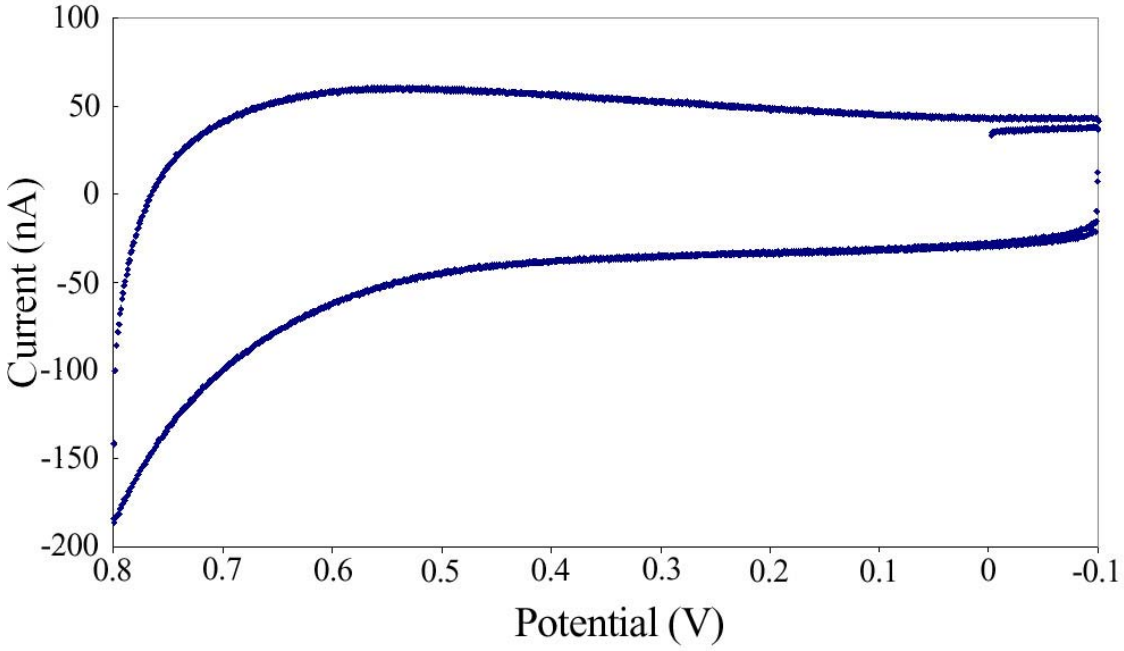

Figure 4.8 Cyclic voltammogram of gold/SAM electrode without protein. Potential range of interest is flat and free of any features.

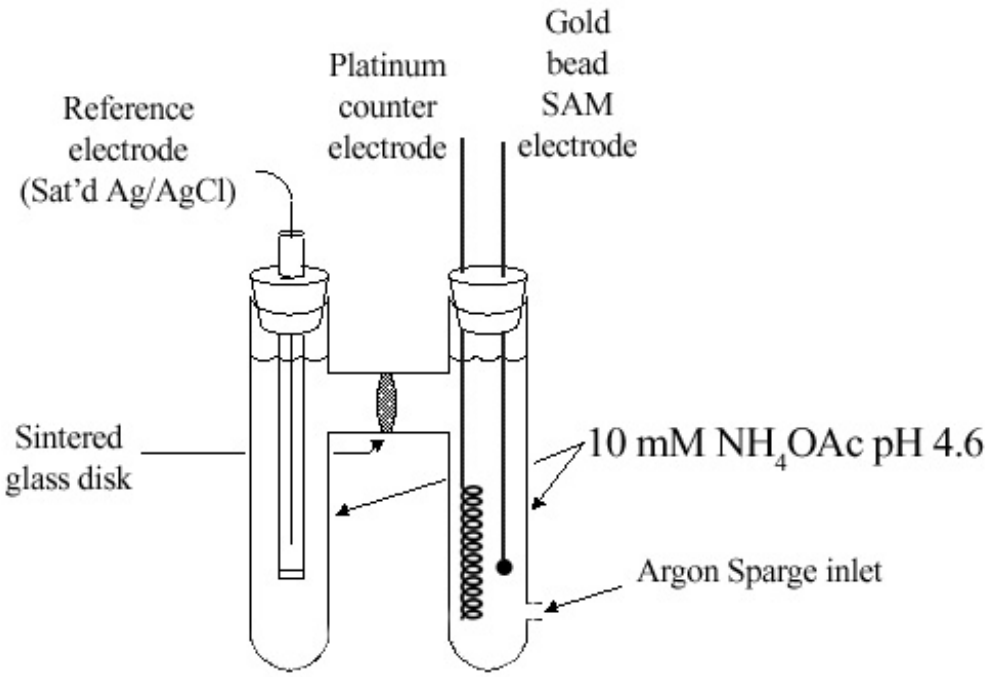

Figure 4.9 Diagram of electrochemical cell used for experiments.

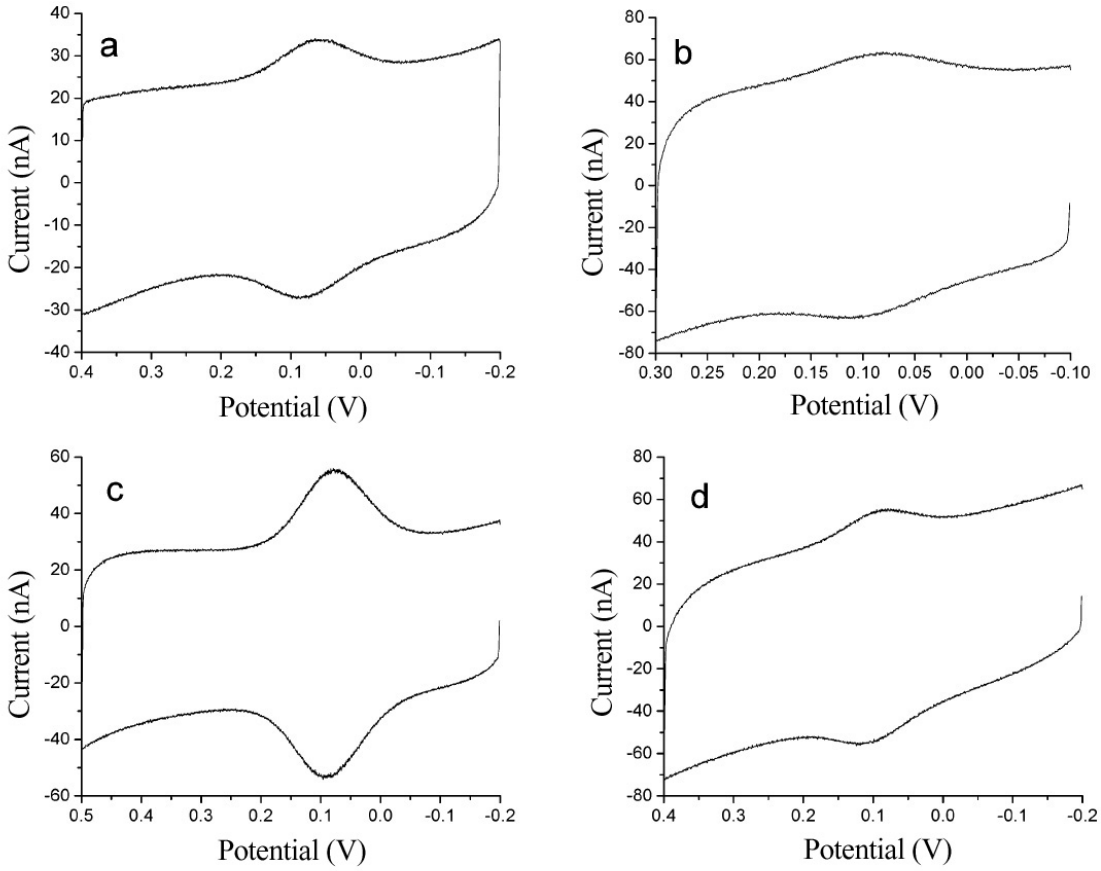

Figure 4.10 Cyclic voltammograms of the CuA domain on a [$CH_3(CH_2)_8SH$ + $HO(CH_2)_8SH$] SAM in 10 mM NH_4OAc buffer solution at pH 4.6. Scan rate 50 mV/s; potential vs. Ag/AgCl. $CH_3(CH_2)_8SH$ + $HO(CH_2)_8SH$ mixing ratio (a) 100:0; (b) 3:1; (c) 1:1; (d) 1:3.

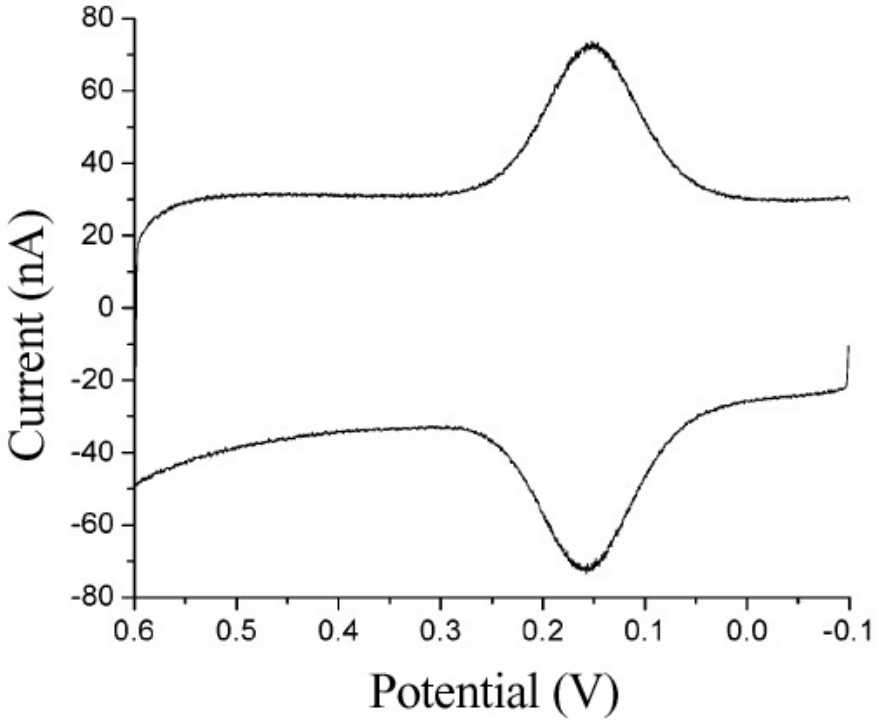

Figure 4.11 Cyclic voltammogram of wild-type azurin on a 1:1 [$CH_3(CH_2)_8SH$ + $HO(CH_2)_8SH$] SAM in 10 mM NH_4OAc solution at pH 4.6. Scan rate 50 mV/s; potential vs. Ag/AgCl.

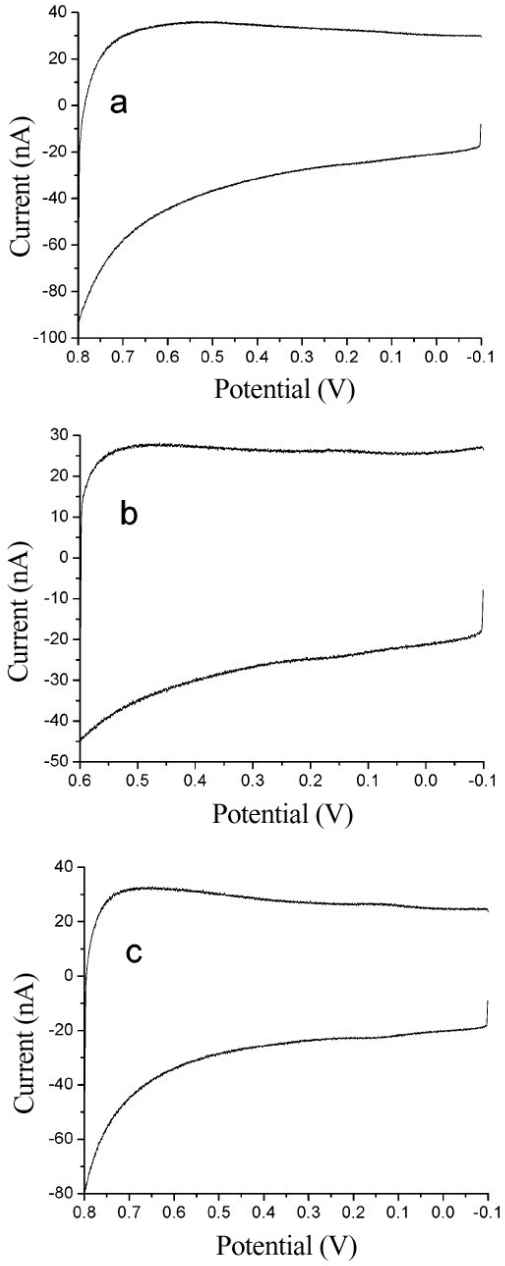

Figure 4.12 Cyclic voltammograms of azurin mutants on a 1:1 [$CH_3(CH_2)_8SH$ + $HO(CH_2)_8SH$] SAM in 10 mM NH_4OAc solution at pH 4.6. Scan rate 50 mV/s; potential vs. Ag/AgCl. CVs are (a) W48F/Y72F/H83Q/Q107H/Y108F mutant (All Phe); (b) W48F/Y72F/H83Q/Q107H/Y108W mutant (All Phe-W108); (c) W48F/Y72F/H83Q/Y108F/K122W/T124H mutant (All Phe-W122).

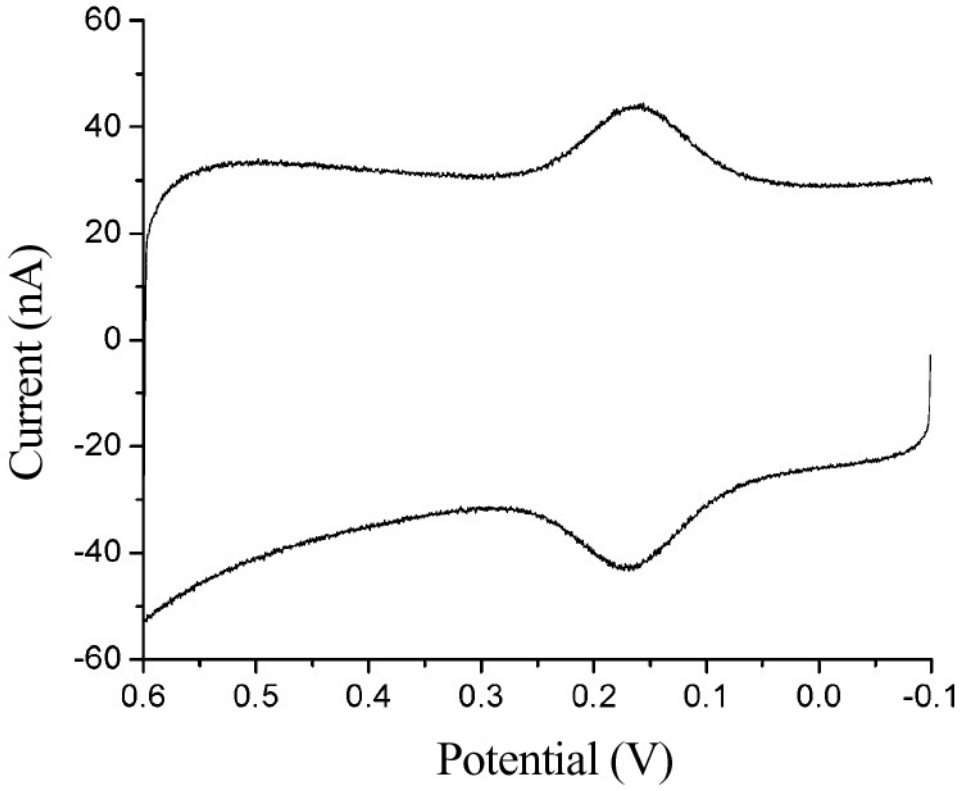

Figure 4.13 Cyclic voltammogram of azurin mutant on a 1:1 [$CH_3(CH_2)_8SH$ + $HO(CH_2)_8SH$] SAM in 10 mM NH_4OAc solution at pH 4.6. Scan rate 50 mV/s; potential vs. Ag/AgCl. CV is of Y72F/H83Q/Q107H/Y108F mutant (All-Phe-W48).

Discussion

Surface Coverage

Well defined voltammetric responses were obtained from the mixed SAM electrodes. By varying the ratio of the -CH_3 and -OH SAM head groups, effects of surface coverage (Γ) could be observed. By measuring the diameter of the gold bead (assuming perfect sphere), the surface area for protein binding can be determined. Crystal structures of both azurin and Cu_A can be used to calculate and average binding footprint of each protein. Assuming that each protein donates or receives a single electron, the number of electrons can be counted and the surface coverage of the SAM electrode can be determined (Figure 4.14). The coverage of the electrode was found to be dependent on the ratio of the -CH_3 and –OH groups. The 1:1 mixed [$CH_3(CH_2)_8SH$ + $HO(CH_2)_8SH$] monolayer yielded a Γ_{Azurin} of 65%. This value was much larger than a Γ_{Azurin} of 10% which had been previously reported on –CH_3 terminated SAMs.[27] It was also found that the 1:1 mixed monolayer gave the best surface coverage for Cu_A (40% coverage).

The surface coverage was also found to be dependent on the length of the SAM alkane chain (Figure 4.15). We did not find a monotonic decrease of Γ_{Azurin} with chain length that correlates with the solubility of the alkanethiols in water. Instead, other effects such as increased conformational flexibility of the longer chains and incomplete coverage may contribute to the observed chain-length dependence.

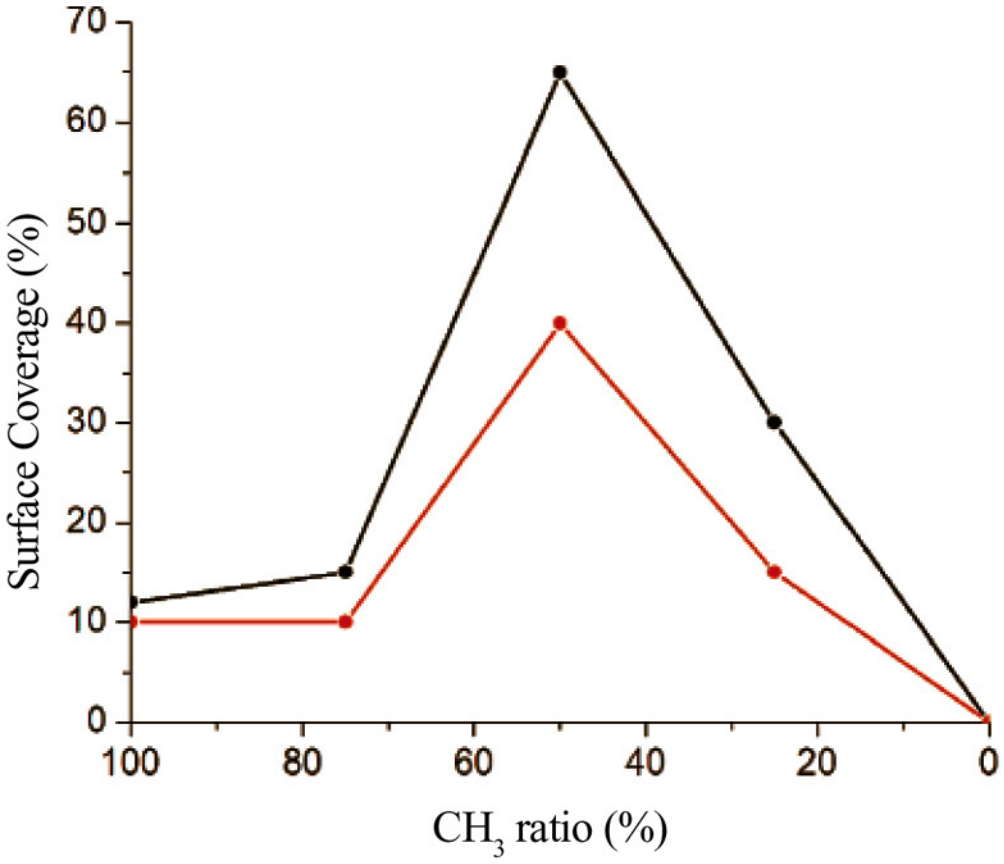

Figure 4.14 Variation in the amount of immobilized azurin (black dots) and the Cu_A domain of cytochrome *c* oxidase from *T. thermophilus* (red dots) on mixed $[CH_3(CH_2)_8SH + HO(CH_2)_8SH]$ SAMs in 10 mM NH_4OAc solution at pH 4.6.

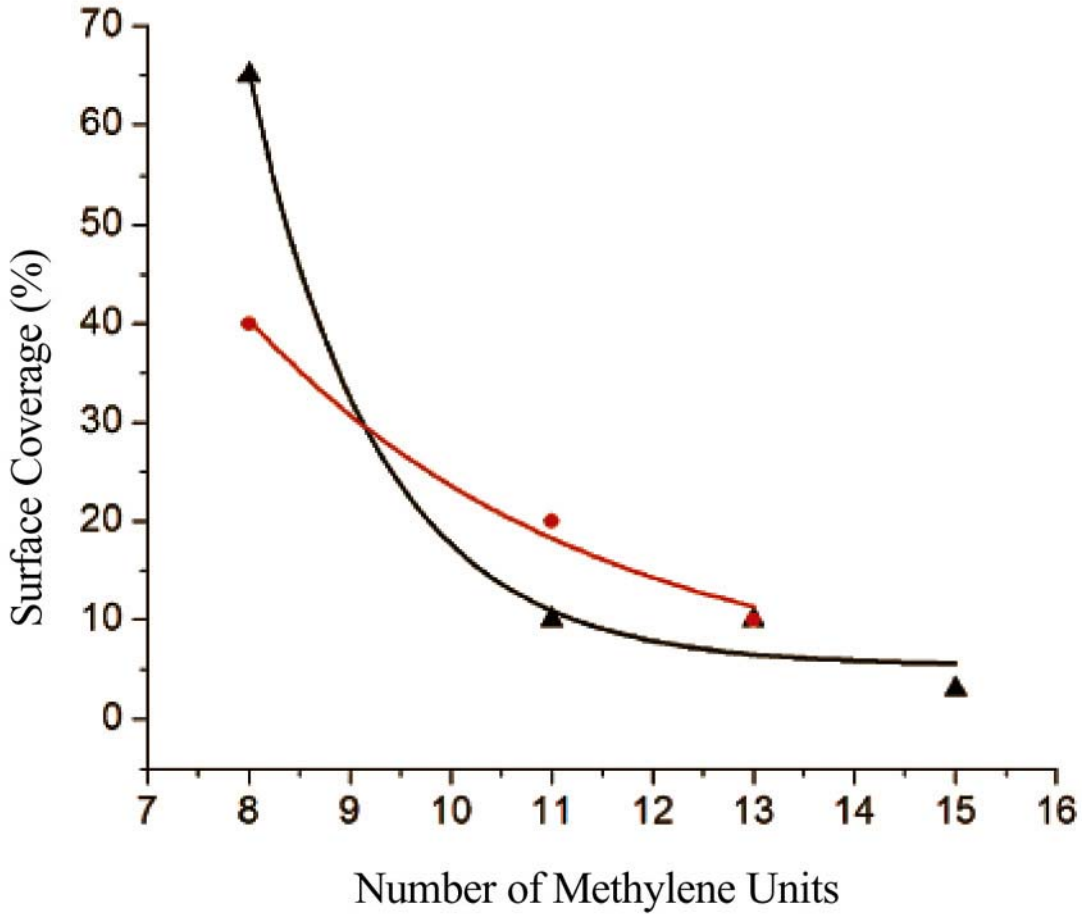

Figure 4.15 Amount of immobilized azurin (black triangles) and the Cu_A domain of cytochrome *c* oxidase from *T. thermophilus* (red dots) on 1:1 mixed (alkanethiol + ω-hydroxy-alkanethiol) SAMs with various chain lengths in 10 mM NH_4OAc solution at pH 4.6.

Formal potentials - Azurin

The formal potential obtained from the midpoint of the peak-to-peak oxidation and reduction potential of wild-type azurin is 0.15 V vs. saturated Ag/AgCl, and is independent of the CH_3/OH-head group ratio. This value agrees well with the results from Ulstrup *et al.* on alkanthiol SAMs,[26, 27] but it is 40-50 mV more positive than other values.[14, 25, 33] The potential of the Y72F/H83Q/Q107H/Y108F (all-Phe-W48) mutant is 0.16 V vs. saturated Ag/AgCl, which is very similar to that of wild-type azurin. High-resolution crystal structures of wild-type and the all-Phe-W48mutant indicate that the redox center and local hydrogen bonding network of the redox center are unperturbed in these two systems.

Formal potentials - Cu_A

The formal potential obtained from the midpoint of the peak-to-peak oxidation and reduction potential of the soluble Cu_A is 0.10 V vs. saturated Ag/AgCl, which is approximately 0.006 V more negative than the value determined at pH 8 in solution.[34]

Electron transfer through SAMs - Azurin

Electron transfer between spatially fixed reactants has a first-order rate constant k_{et} (Equation 4.1),[35] where $\kappa(r)$ is the transmission coefficient when reactants are at

$$k_{et} = \kappa(r)\nu_n \cdot \exp[-(\lambda + \Delta G^o)^2 / 4\lambda RT \qquad (4.1)$$

distance r, ν_n is the nuclear frequency factor ($\nu_n = 10^{13}$ s^{-1}), λ is the reorganization energy, and ΔG^o is the free energy of the reaction. For long-range electron transfer $\kappa(r) << 1$, and $\kappa(r)\nu_n$ is 10^{-13} s^{-1} at $r = r_o$ (Equation 4.2).

$$\kappa(r)\nu_n = \nu_n \cdot \exp[-\beta(r - r_o)] \qquad (4.2)$$

In electrochemistry, $\Delta G^o = 0$ and λ_{el} is one-half of the self exchange reaction ($\lambda_{el} = \lambda_{11}/2$); the rate then becomes (Equation 4.3)

$$k_{et} = \kappa(r)\nu_n \cdot \exp(-\lambda_{el} / 4RT) \qquad (4.3)$$

Coupling between gold and the redox center can be written as Equation 4.4

$$H_{AB}{}^2 \propto \kappa_{protein}\kappa_{inter}\kappa_{SAM} \qquad (4.4)$$

$\kappa_{protein}$, κ_{inter}, and κ_{SAM} are the transmission coefficients for the protein, between the protein and the SAM, and through the SAM. $\kappa_{protein}$ and κ_{SAM} have been well established experimentally.[17, 36-40] Electron transfer rates for protein immobilized on SAMs are given by:

$$k_{et} = k_o \cdot \exp[-(d_{protein}\beta_{protein} + d_{inter}\beta_{inter})] \cdot \exp[-(n+3)\beta_{SAM}] \qquad (4.5)$$

$$k_o = \nu_n \cdot \exp(-\lambda_{el} / 4RT) \qquad (4.6)$$

where $d_{protein}$ represents the distance from the redox center to the coupling site on the surface of the protein and d_{inter} is the distance between the surface coupling site on the protein and the head of the SAM. $\beta_{protein}$, β_{inter}, and β_{SAM} represent the exponential decay of the protein, interstitial space between the SAM and protein, and the SAM. The number of methylene groups in the SAM is represented by n.

The rate constant (k_{et}) through $HO(CH_2)_{11}S$- SAM is 63 s^{-1}.[31] The β_{SAM} is 0.71 ± 0.01 $Å^{-1}$, which is independent for any redox species when $n > 6$.[17] The maximum rate constant (k_o), when $r = r_o$ and $\Delta G^o = 0$, is estimated to be 5.4 x 10^{11} s^{-1} at 298 K assuming $\upsilon_n = 10^{13}$ s^{-1} and $\lambda_{el} = 0.3$ eV. Assuming that $\beta_{protein} \approx 1.0$/bond, $\beta_{SAM} = 1.1$/bond, d_{inter} = 3 Å, and $\beta_{inter} = 2.7$ $Å^{-1}$ Equation 4.7 can be derived.[39-41]

$$63 = 5.4 \times 10^{11} \cdot \exp[-(d_{protein}\beta_{protein} + 3)] \cdot \exp(-14 \times 1.1) \qquad (4.7)$$

From this equation, the number of bonds through which the electron tunnels is $d_{protein}\beta_{protein} = (r - r_o) = 4.5$ bonds. If λ_{el} is lowered to 0.1 eV, the number of bonds tunneled through is 6.5. Based on this analysis, we estimate that the number of bonds the electron tunnels through in azurin is between 4 to 5 bonds. This result suggests that the coupling "hot spot" is relatively near the redox center of the protein.

Electron transfer through SAMs - Cu_A

The λ_{el} for Cu_A from pulse radiolysis kinetic experiments is 0.4 eV.[42] This low reorganization energy indicates that the number of bonds through which electron tunneling occurs in Cu_A is about 5, which is very similar to the case of azurin.

Chain length effects

The electron transfer rate constants as a function of the number of methylene groups in the SAM were evaluated and found to have a linear relationship between the logarithm of the electron transfer rate and chain length for $n \geq 9$ (Figure 4.16).[43] For $n < 9$ it is proposed that the coupling of the electron transfer hot spot is perturbed. The calculated value of β for the methylene group is 1.1.

Tryptophan 48 mutants

Mutations at position 48 in azurin (W48F) effectively turned off electron transfer into and out of the redox center. Tryptophan 48 has been thought to play a role in the electron transfer pathway of azurin.[22, 28] This residue is in the center of the protein in a very hydrophobic region.[44] It is located directly opposite of the redox center from H117 which has been implicated to be the coupling site for electron transfer (Figure 4.17).[15, 19-23] W48 is located approximately 13 Å from H117, and 10 Å from the redox center, towards the center of the protein. We believe that a mutation at position 48 causes distortions along the polypeptide backbone and affects the orientation of the nearest neighbor residues; because the tryptophan is in an optimized environment for its shape, any new amino acid side chain will perturb the local environment. One of these nearest neighbors is asparagine 47, which makes a hydrogen bond through the amide nitrogen to the sulfur of the copper-ligating residue, cysteine 112. Any mutation to position-48 subsequently causes small distortions to the N47 hydrogen bond to C112. These subtle

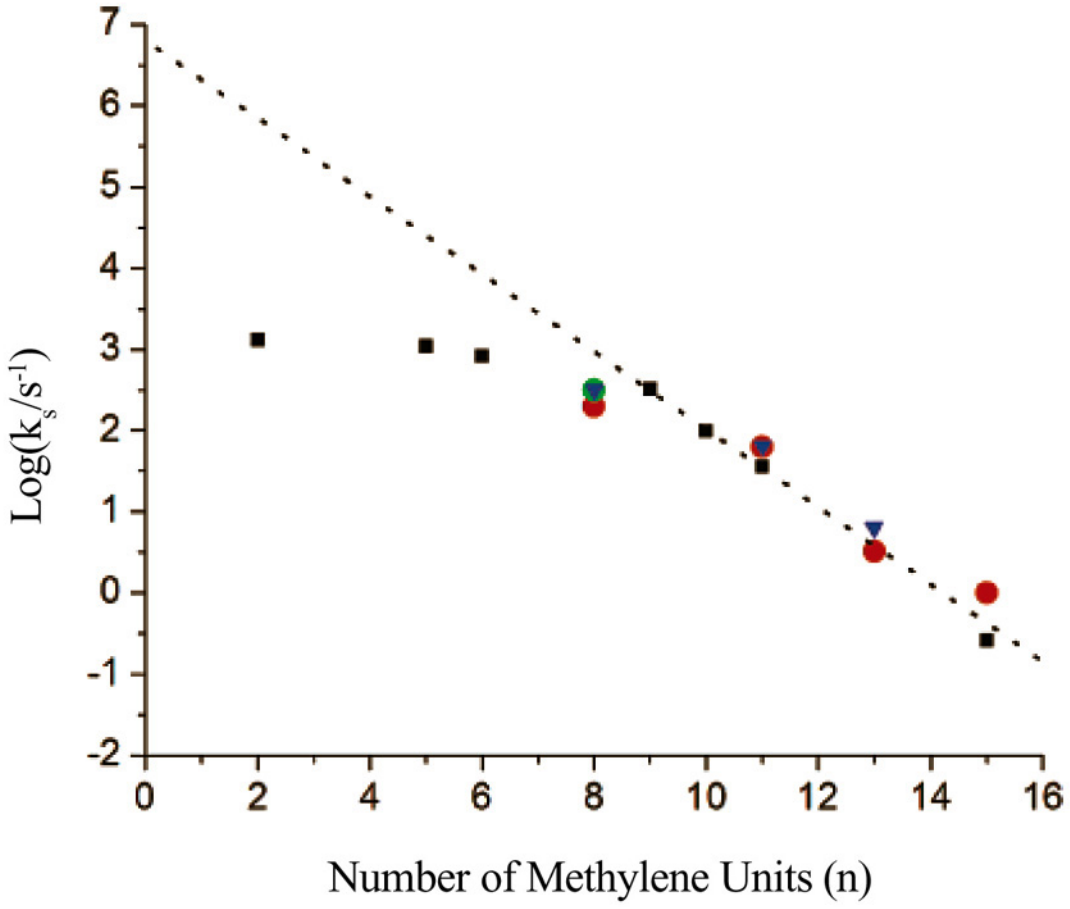

Figure 4.16 Electron transfer rates vs. SAM chain lengths for azurin (red dots), the Y72F/H83Q/Q107H/Y108F (all-Phe-W48) mutant (green dots), and the Cu_A domain (blue downward triangles) immobilized on mixed monolayers of (alkanethiol + ω-hydroxy alkanethiol). Results for cyt *c* on carboxylic acid terminated alkanethiol SAM (black squares) are also included. Fit of the experimental data to an exponential decay factor $\beta = 1.1$ per CH_2 (·····) gives $R^2 = 0.97$ when $n \geq 9$.

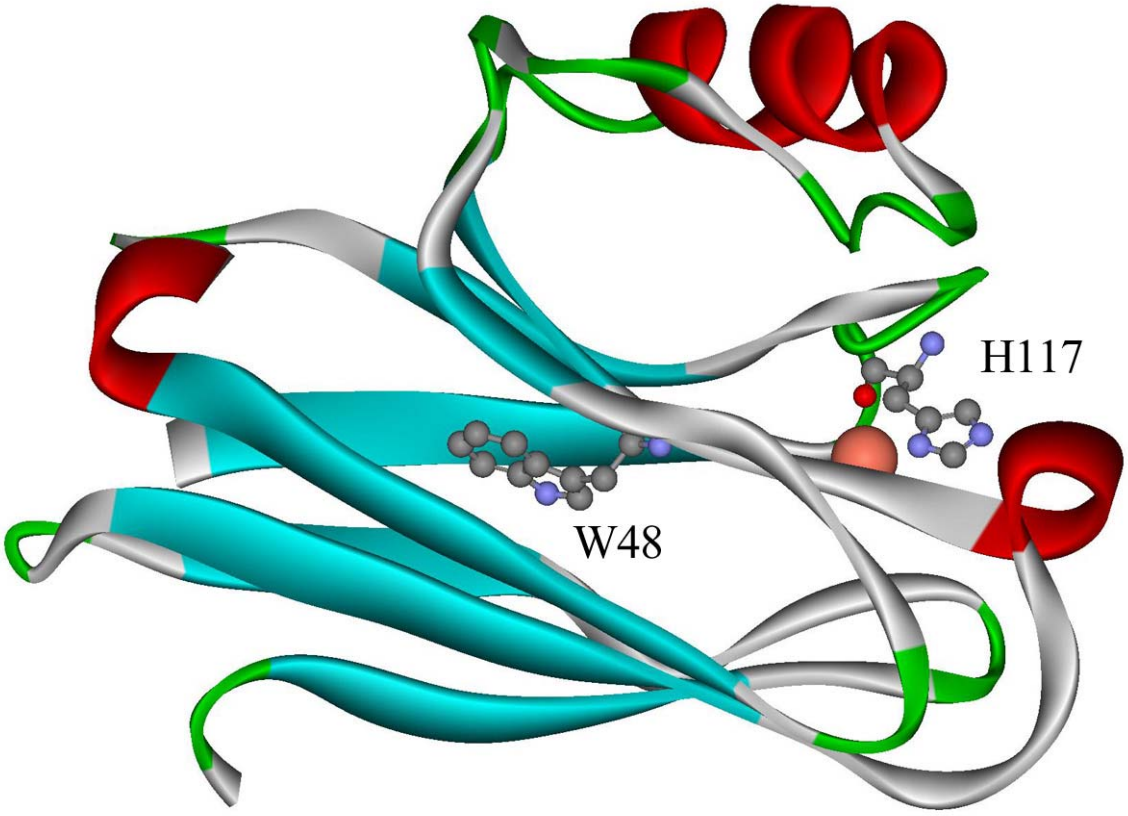

Figure 4.17 Ribbon structure of azurin (4AZU) showing copper redox center, H117, and W48.

but significant changes are evident when overlaying the crystal structures of wild-type azurin and the all-Phe mutant azurin (Figure 4.18).

In further work (unpublished) we have explored mutations at position 47 (N47X/F48W/Y72F/H83Q/Q107H/Y108F, where position 47 has been changed to N47A N47D, N47K, N47R, N47L, and N47T). All but 2 of these mutants are redox inactive even though these mutants contain tryptophan at position 48. Mutations N47D (218 mV) and N47T (250 mV) maintain the pathway into the redox center. Molecular modeling has shown that mutations of aspartate and threonine not only fit into the area vacated by asparagine, but they also have complimentary charges to mimic the two hydrogen bonds asparagine makes with threonine 113, specifically the hydrogen bond to the backbone T113 nitrogen (Figure 4.19). Maintaining this hydrogen bonding network near T113 may be important for preserving the critical hydrogen-bonding structure around C112.

Amine based SAMs

Mixed SAMs (CH_3/HO-head groups) have produced excellent response from both azurin and Cu_A. The 1:1 ratio produced the largest surface coverage for both proteins. In order to investigate whether the critical interaction between the protein and SAM is a general hydrogen bond formed between the protein and SAM head group, or the specific presence of an alcohol group, similar mixed SAM systems were created with amine (NH_2) terminated thiols. The mixed amine SAMs resulted in cyclic voltammograms that mimicked the ones produced from the hydroxy terminated mixed SAMs (Figure 4.20). This result implies that it is the general hydrophobic/hydrophilic nature of the SAMs that allows for successful binding of proteins to it. The identities of the specific hydrogen-

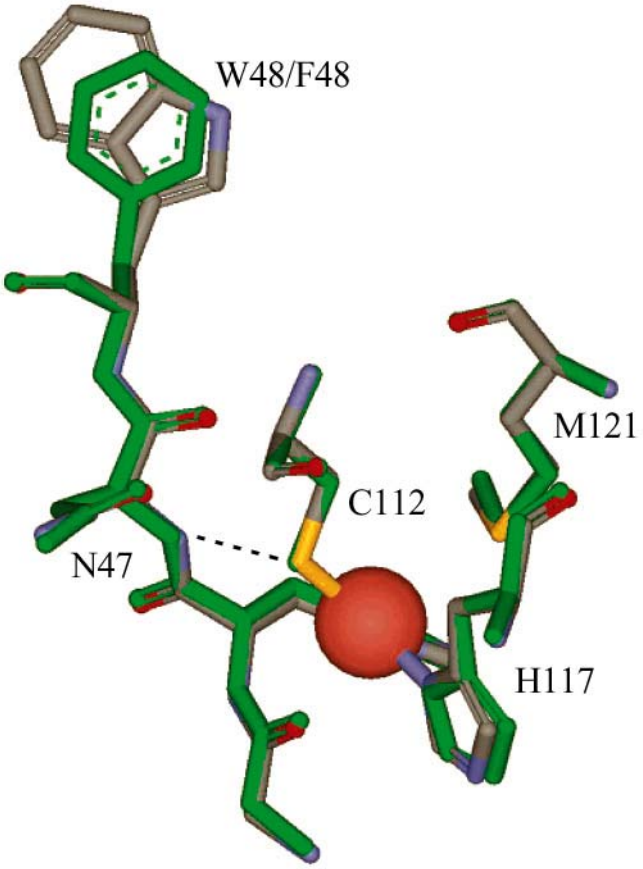

Figure 4.18 Overlay of the copper centers of wild-type and all-Phe (in green) azurins, black dashed line is N47-C112 hydrogen bond.

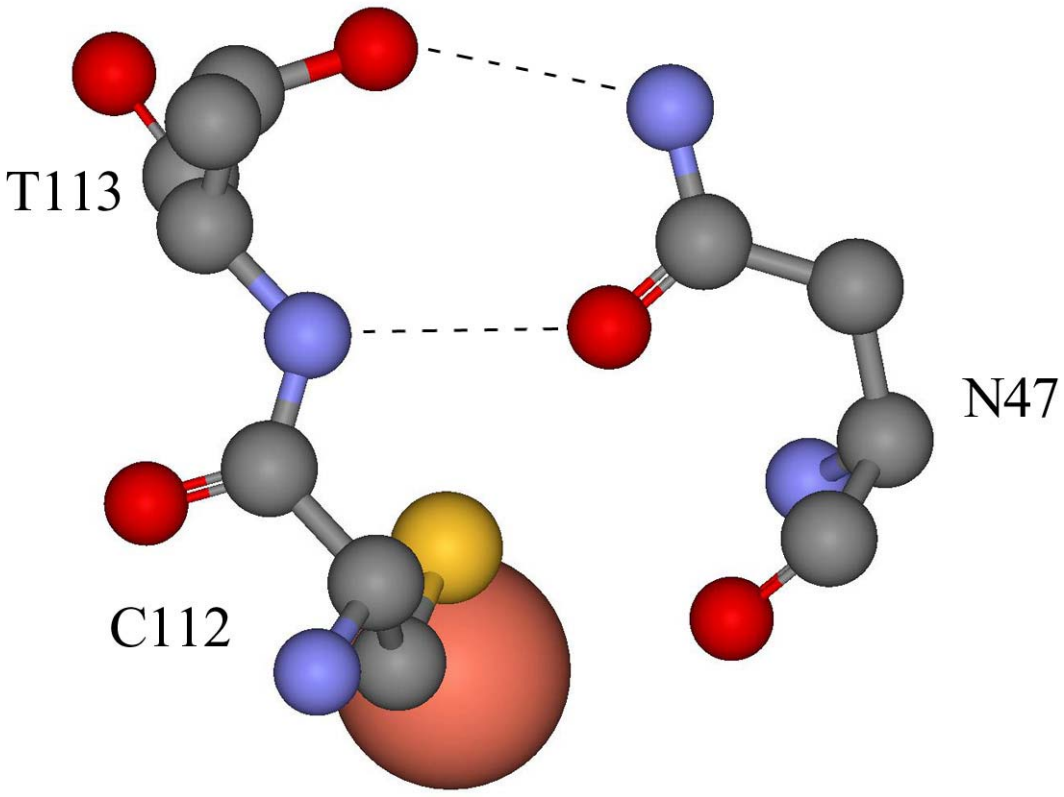

Figure 4.19 N47 side chain hydrogen bonding to T113 side chain and backbone nitrogen, dashed lines are T113-N47 hydrogen bonds.

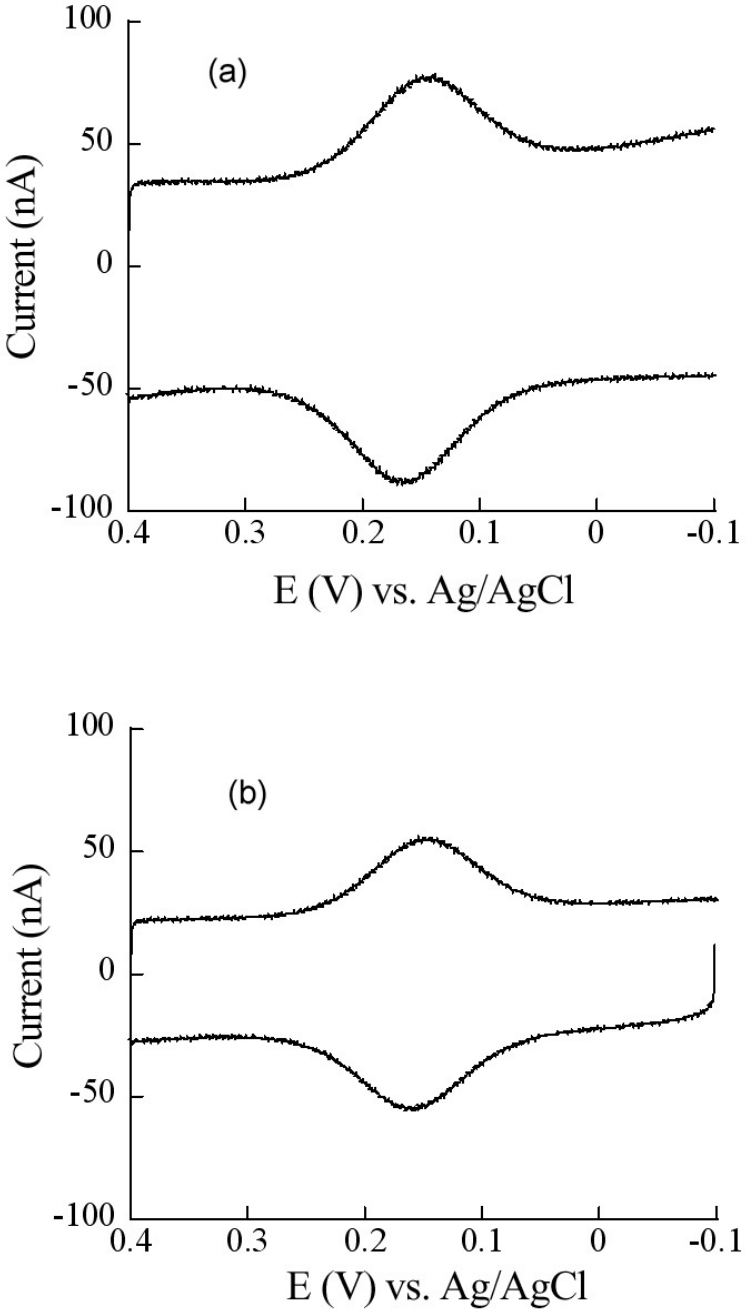

Figure 4.20 Cyclic voltammograms of azurin on $[CH_3(CH_2)_8SH + H_2N(CH_2)_8SH]$ mixed SAM in 10 mM NH_4OAc solution at pH 4.6. Scan rate 50 mV/sec. $[CH_3(CH_2)_8SH : H_2N(CH_2)_8SH]$ at a ratio of (a) 1:1 and (b) 1:3.

bonding atoms that constitute the SAM are less critical; both amines and hydroxyl groups gave similar results.

Ionic strength dependence on potentials

The effect of ionic strength on redox potentials and kinetics of wild-type azurin and the Trp48-all-Phe mutant was studied. It is feasible that a high salt concentration in the region where the protein couples to the SAM could cause a charge-screening effect that may interfere with the electron transfer reaction. However, the experiments indicated that no such effect occurred in our salt concentration range of up to 100 mM; the results demonstrated no major modification in the voltammograms with high salt concentration (Figure 4.21).

pH dependence on potential

Well-defined electrochemical response curves have been obtained from wild-type azurin, making it a perfect testing tool to explore pH effects on electron transfer. Equation 4.8 was used to study the effect of pH on potential.[45]

$$E_m = E_{m1} + \frac{60}{n_e}\log\frac{K_{RED} + [H^+]}{K_{OX} + [H^+]} \qquad (4.8)$$

In the equation K_{OX} and K_{RED} are the proton dissociation constants for a group with two redox states. E_{m1} is the mid point potential at acidic pH, and the number of electrons, n_e, is 1. By fixing $n_e = 1$, we obtain $pK_{OX} = 5.7$ (±0.1), $pK_{RED} = 8.1$ (±0.1) (wild-type); and $pK_{OX} = 5.7$ (±0.1), $pK_{RED} = 8.3$ (±0.1) (W48-all-Phe) (Figure 4.22). The potentials at low pH are more than 150mV higher than at high pH, which contrasts to what is found in

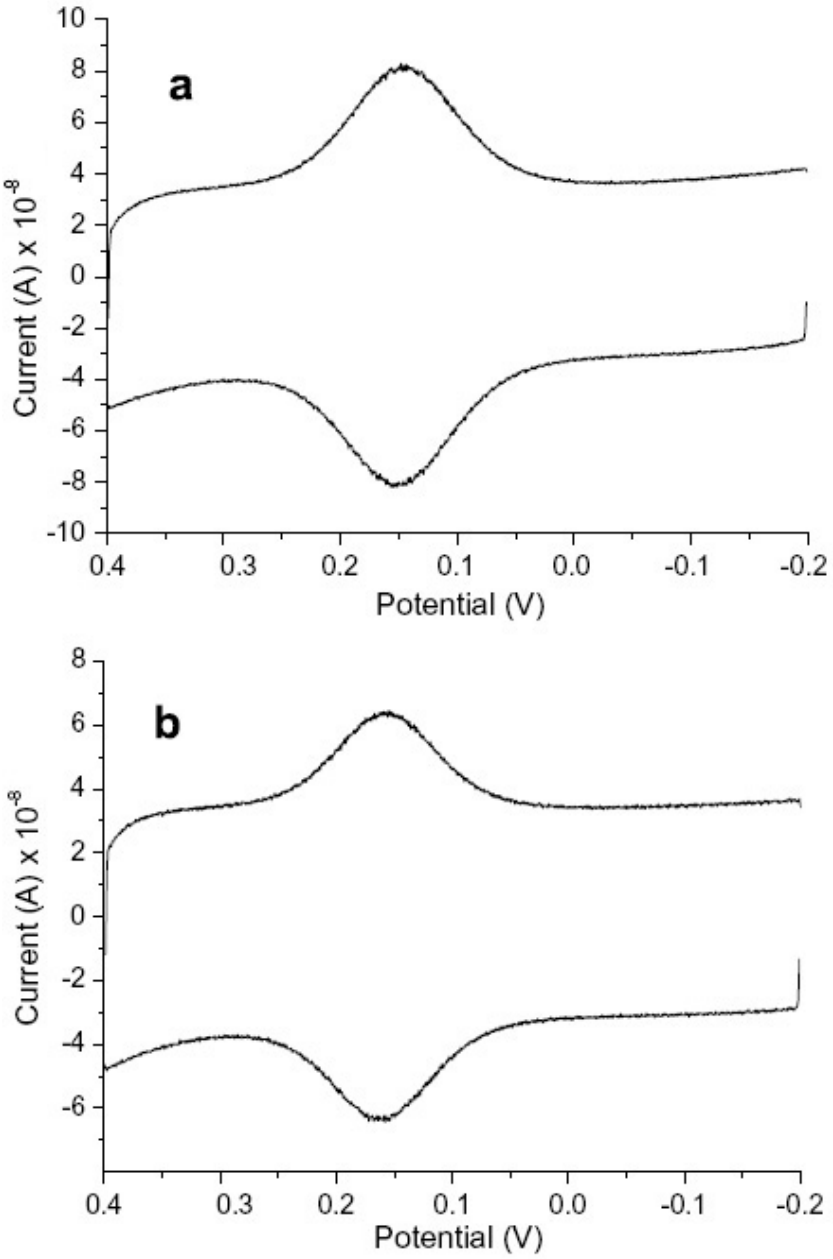

Figure 4.21 Cyclic voltammograms of wild-type (a) and Trp48-all-Phe (b) azurins on a 1:1 $CH_3(CH_2)_8SH$:$HO(CH_2)_8SH$ gold electrode in 100 mM NH_4OAc buffer at pH 4.6.

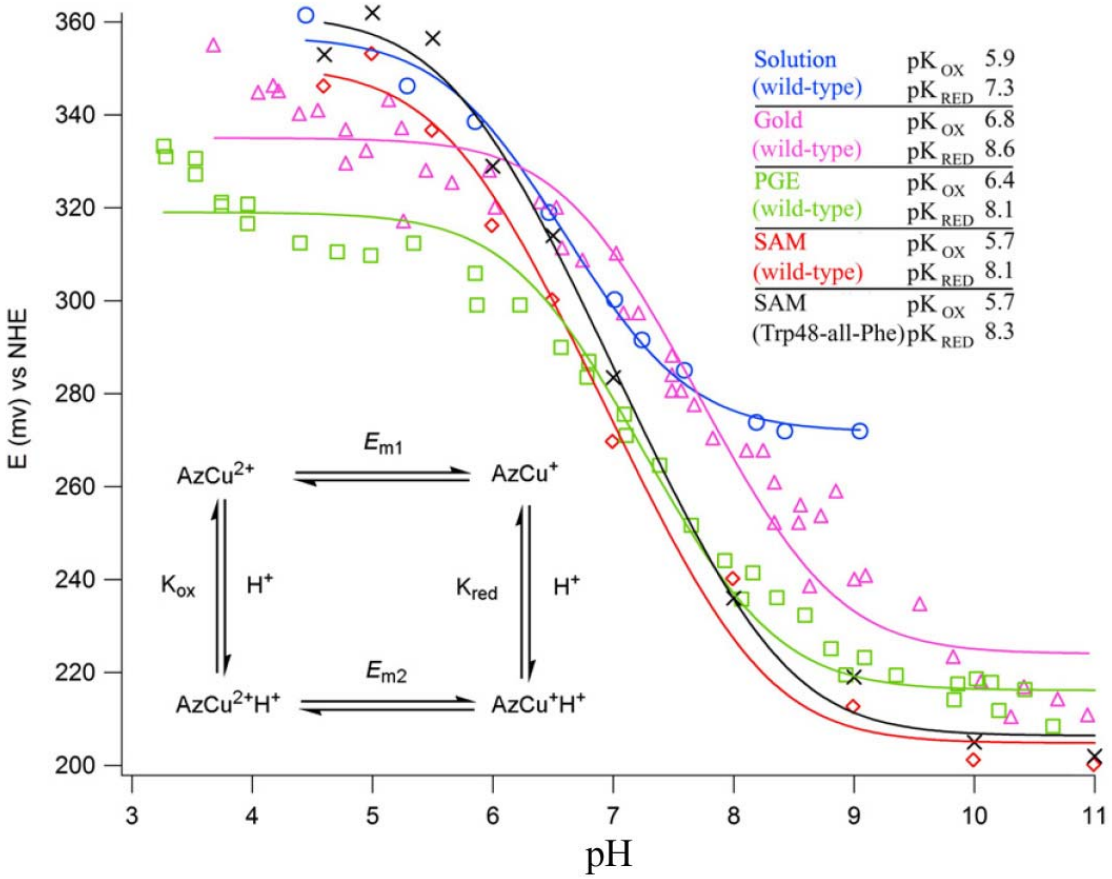

Figure 4.22 Midpoint potentials vs. pH: wild-type and Trp48-all-Phe azurins on a 1:1 $CH_3(CH_2)_8SH$:$HO(CH_2)_8SH$ gold electrode. Other fits are based on literature data: [Solution (wild-type)];[46] and [Gold (wild-type); PEG (wild-type)].[45] Inset: K_{ox} and K_{red} are the protonation constants for the oxidized and the reduced forms of the protein; and Em1 and Em2 are the midpoint potentials at low and high pH.

solution.[9, 46, 47] This variation likely arises from the unique SAM/protein interface. Because H35 is the only non-coordinating histidine present in both the wild-type and W48-all-Phe, it is likely that the observed pKs are attributed to the equilibrium of the imidazole ring.

At pH 11 the CV peak separation for wild-type protein is very small, indicating that electron transfer is more rapid at this high pH.[43] This increase in rate may be due to enhanced coupling of the SAM to N47 caused by deprotonation of a nearby residue.

Future work

Ongoing projects in the group continue to probe a number of topics presented in this chapter. Multiple mutations at position 47 are currently being explored to probe the role of the residue in electron transfer in azurin. While the work on cyt *c* and azurin has been able to elucidate feasible electronic coupling sites on the protein,[31, 48] currently there are no attempts to create Cu_A mutants to elucidate possible coupling spots on this system. However, a variety of projects may prove to be very interesting. Cu_A and the CcO are very well conserved structurally from *Archaebacteria* to mammalian systems (Figures 4.23 and 4.24). This interface to cyt *c* has been part of life's machinery for billions of years untouched. In order to find the coupling "hot spots" on Cu_A a method similar to what was used on cyt *c* should be employed. For example, mutations that will add steric bulk over the proposed coupling site should retard electron transfer and shed light on the site of optimal coupling. Two such point mutations include V112F and G154Y; this mutation may successfully shield the proposed coupling spot (carbonyl oxygen on

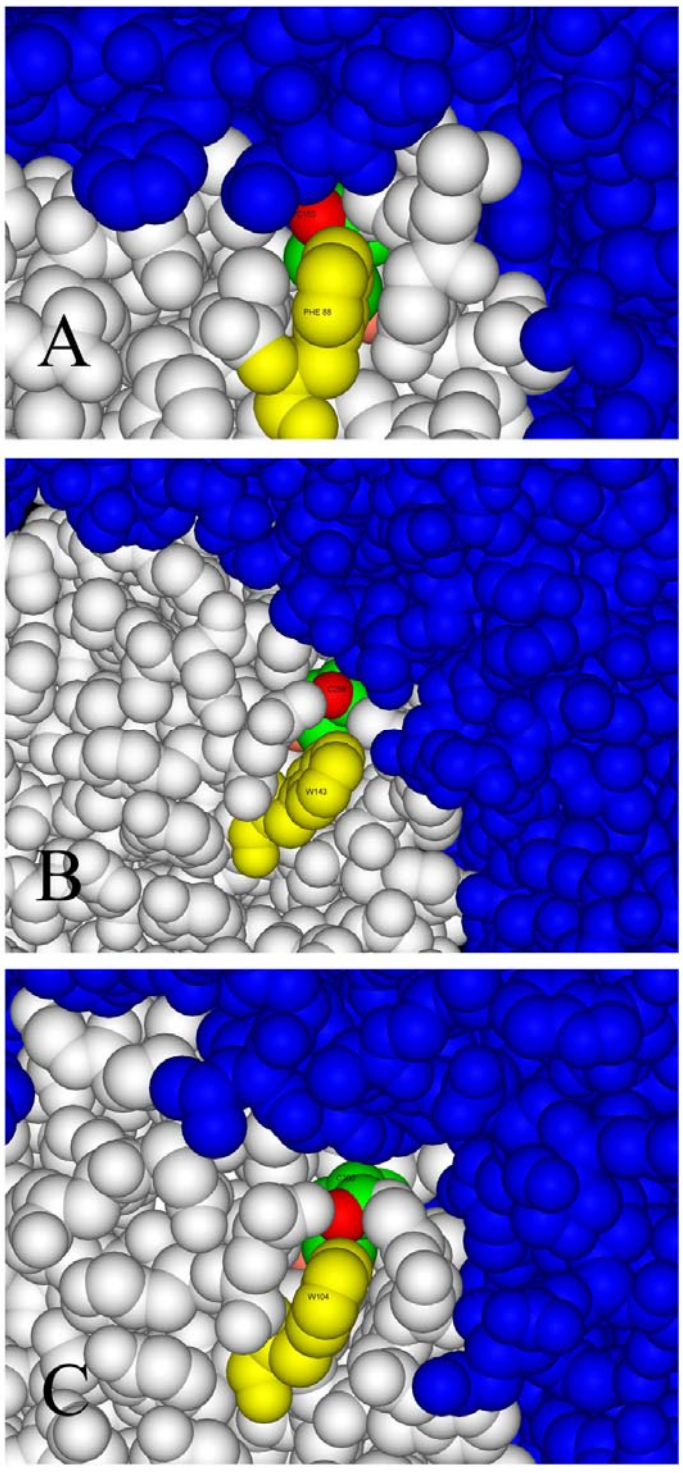

Figure 4.23 Structures of the Cu_A domain (white) and the CcO subunit 1 domain (blue) of (a) *T. thermophilus* (Cys153), PDB code 1EHK (b) *R. Sphaeroides* (Cys256), PDB code 1M56, and (c) bovine (Cys200), PDB code 1OCC, cytochrome *c* oxidase. Capping aromatic residue W104, W148 and F88 in yellow, and ligands C153, C256 and C200 in green, with the cysteine backbone carbonyl in red.

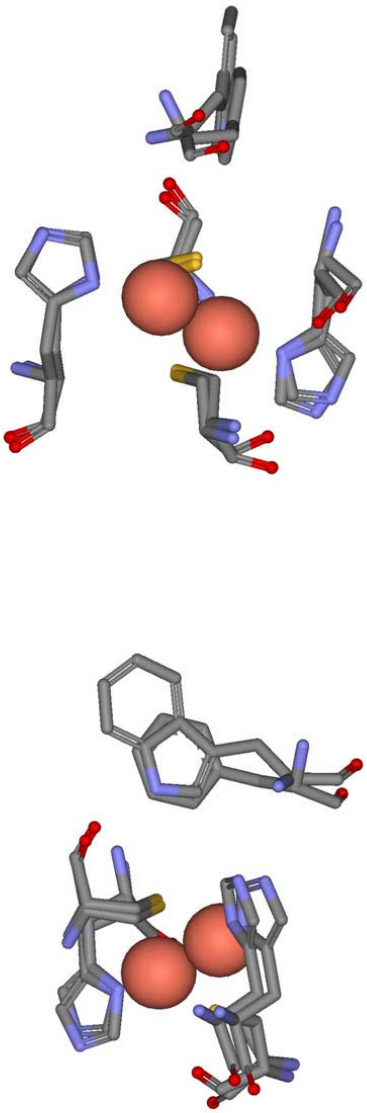

Figure 4.24 Structures of the Cu_A binuclear redox center showing the conserved geometry between *T. thermophilus* and bovine sites. W104 and F88, aromatic capping residues, occupy analogous regions in the protein. Bottom image is a 90 degree rotation of the top image.

ligating cysteine residue C153) (Figure 4.25), resulting in diminished electron transfer rates.

Conclusion

The redox potentials of wild-type azurin, several azurin mutants, and Cu_A have been determined using SAM electrodes (azurin = 0.15 V and Cu_A = 0.10 V vs. Ag/AgCl). The mutants have allowed for the identification of an optimal electronic coupling spot in azurin near N47, which contrasts to what has previously been suggested as the electronic coupling spot (H117). Future work may also elucidate good electronic coupling points in Cu_A.

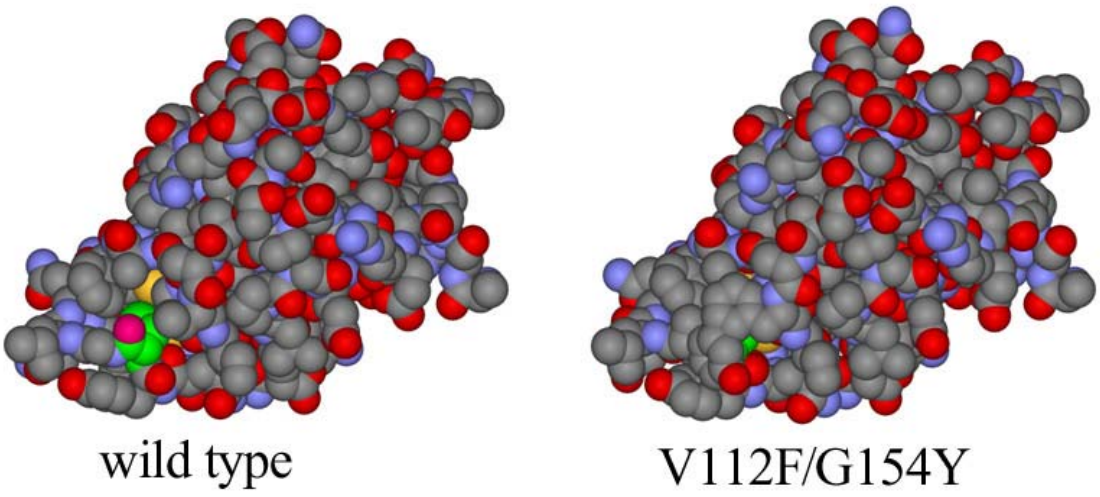

Figure 4.25 Structural models of wild-type Cu_A and the proposed V112F/G154Y mutant. Accessibility to the cysteine residue (green) has been effectively reduced in the V112F/G154Y mutant, and a decrease in electron transfer rate should be observed.

References

1. Verhoeven, W.; Takeda, Y., *In Organic Nitrogen Metabolism*. The Johns Hopkins Press: Baltimore, 1956.
2. Nakamura, T., *Biochim. Biophys. Acta* **1958,** 80, 44.
3. Yamanaka, T.; Kijimoto, S.; Okunuki, K., *J. Biochem., Tokyo* **1963,** 53, 256.
4. Horio, T., *J. Biochem., Tokyo* **1958,** 45, 195.
5. Horio, T., *J. Biochem., Tokyo* **1958,** 45, 267.
6. Coval, M. L.; Horio, T.; Kamen, M. D., *Biochim. Biophys. Acta* **1961,** 51, 246.
7. Sutherland, I. W.; Wilkinson, J. F., *J. Gen. Microbiol.* **1963,** 80, 105.
8. Antonini, E.; Finazzi-Agro, A.; Avigliano, L.; Guerrieri, P.; Rotilio, G.; Mondovi, B., *J. Biol. Chem.* **1970,** 245, 4847.
9. Nar, H.; Messerschmidt, A.; Huber, R.; van de Kamp, M.; Canters, G. W., *J. Mol. Biol* **1991,** 221, 765.
10. Engeseth, H. R.; McMillin, D. R., *Biochemistry* **1986,** 25, 2448.
11. Kabsch, W.; Sander, C., *Biopolymers* **1983,** 22, 2577.
12. Olsson, M. H. M.; Ryde, U., *J. Biol. Inorg. Chem.* **1999,** 4, 654.
13. St Clair, C. S.; Ellis, W. R.; Gray, H. B., *Inorg. Chim. Acta* **1992,** 191, 149.
14. Battistuzzi, G.; Borsari, M.; Loschi, L.; Righi, R.; Sola, M., *J. Am. Chem. Soc.* **1999,** 121, 501.
15. van de Kamp, M.; Canters, G. W.; Andrew, C. R.; Sanders-Loehr, J.; Bender, C. J.; Peisach, J., *Eur. J. Biochem.* **1993,** 218, 229.
16. Feng, Z. Q.; Imabayashi, S.; Kakiuchi, T.; Niki, K. J., *J. Chem. Soc., Faraday Trans.* **1997,** 93, 1367.
17. Avila, A.; Gregory, B. W.; Niki, K.; Cotton, T. M., *J. Phys. Chem. B* **2000,** 104, 2759.
18. Dick, L. A.; Haes, A. M.; Van Duyne, R. P., *J. Phys. Chem. B* **2000,** 104, 11752.
19. Groeneveld, C. M.; Canters, G. W., *J. Biol. Chem.* **1988,** 263, 167.
20. Mikkelsen, K. V.; Skov, L. K.; Nar, H.; Farver, O., *Proc. Natl. Acad. Sci. U.S.A.* **1993,** 90, 5443.
21. Gorren, A. C. F.; den Blaauwen, T.; Canters, G. W.; Hopper, D. J.; Duine, J. A., *FEBS Lett.* **1996,** 381, 140.
22. Farver, O.; Skov, L. K.; Young, S.; Bonander, N.; Karlsson, B. G.; Vänngård, T.; Pecht, I., *J. Am. Chem. Soc.* **1997,** 119, 5453.
23. Farver, O.; Blatt, Y.; Pecht, I., *Biochemistry* **1982,** 21, 3556.
24. Iwata, S.; Ostermeler, C.; Ludwig, B.; Michel, H., *Nature* **1995,** 376, 660.
25. Gaigalas, A. K.; Niaura, G., *J. Colloid Interface Sci.* **1997,** 193, 60.
26. Firstrup, P.; Grubb, M.; Zhang, J.; Christensen, H. E. M.; Hansen, A. M.; Ulstrup, J. J., *J. Electroanal. Chem.* **2001,** 511, 128.
27. Chi, Q.; Zhang, J.; Andersen, E. T.; Ulstrup, J., *J. Phys. Chem. B* **2001,** 105, 4669.
28. Farver, O.; Pecht, I., *J. Am. Chem. Soc.* **1992,** 114, 5764.
29. Chang, T. K.; Iverson, S. A.; Rodrigues, C. G.; Kiser, C. N.; Lew, A. Y. C.; Germanas, J. P.; Richards, J. H., *Proc. Natl. Acad. Sci. U.S.A.* **1991,** 88, 1325.
30. Slutter, C. PhD Thesis, California Institute of Technology, 1996.
31. Tanimura, R.; Hill, M. G.; Margoliash, E.; Niki, K.; Ohno, H.; Gray, H. B., *Electrochem. Solid-State Lett.* **2002,** 5, E67-E70.

32. Widrig, C. A.; Chung, C.; Porter, M. D., *J. Electroanal. Chem.* **1991,** 310, 335.
33. van de Kamp, M.; Silvestrini, M. C.; Brunori, M.; Van Beeumen, J.; Hali, F. C.; Canters, G. W., *J. Biochem.* **1990,** 194, 109.
34. Immose, C.; Hill, M. G.; Sanders, D.; Fee, J. A.; Slutter, C. E.; Richards, J. H.; Gray, H. B., *JBIC* **1996,** 1, 531.
35. Marcus, R. A.; Sutin, N., *Biochim. Biophys. Acta* **1985,** 811, 265.
36. Hsu, C.-P.; Marcus, R. A., *J. Chem. Phys.* **1997,** 106, 584.
37. Smalley, J. F.; Feldberg, S. W.; Chidsey, C. E. D.; Linford, M. R.; Newton, M. D.; Liu, Y.-P., *J. Phys. Chem.* **1995,** 99, 13141.
38. Carter, M. T.; Rowe, G. K.; Richardson, J. N.; Tender, L. M.; Terrill, R. H.; Murray, R. W., *J. Am. Chem. Soc.* **1995,** 117, 2896.
39. Wuttke, D. S.; Bjerrum, M. J.; Winkler, J. R.; Gray, H. B., *Science* **1992,** 256, 1007.
40. Wuttke, D. S.; Bjerrum, M. J.; Chang, I. J.; Winkler, J. R.; Gray, H. B., *Biochim. Biophys. Acta* **1992,** 1101, 168.
41. Gray, H. B.; Winkler, J. R., *Annu. Rev. Biochem.* **1996,** 65, 537.
42. Farver, O.; Lu, Y.; Ang, M. C.; Pecht, I., *Proc. Natl. Acad. Sci. U.S.A.* **1999,** 96, 902.
43. Laviron, E., *J. Electroanal. Chem.* **1979,** 101, 19.
44. Gilardi, G.; Mei, G.; Rosato, N.; Canters, G. W.; Finazzi-Agro, A., *Biochemistry* **1994,** 33, 1425.
45. Jeuken, L. J. C.; Wisson, L.-J.; Armstrong, F. A., *Inorg. Chim. Acta* **2002,** 331, 216.
46. Pettigrew, G. W.; Leitch, F. A.; Moore, G. R., *Biochim. Biophys. Acta* **1983,** 725, 409.
47. Kalverda, A. P.; Ubbink, M.; Gilardi, G.; Wijmenga, S. S.; Crawford, A.; Jeuken, L. J. C.; Canters, G. W., *Biochemistry* **1999,** 38, 12690.
48. Fujita, K.; Nakamura, N.; Ohno, H.; Leigh, B. S.; Niki, K.; Gray, H. B.; Richards, J. H., *J. Am. Chem. Soc.* **2004,** 126, 13954.

Chapter 5

Resonance Raman of the Tryptophan Radical

Introduction

Free radicals and biological systems do not appear to go well together on the surface. Severe damage can be done to DNA[1] or proteins[2] by highly reactive species like superoxide ($O^{\cdot}_2^{-}$) or peroxide ($HOO^{\cdot}$). The first protein discovered to have a radical species associated with its normal catalytic cycle was ribonucleotide reductase (RNR).[3, 4] RNR is a heterodimeric tetramer that catalyzes the conversion of ribonucleoside 5'-diphosphates to deoxyribonucleotide triphosphate via a tyrosyl radical species.[5]

It has been found that many proteins utilize amino acid radicals as part of their catalytic functions;[6] galactose oxidase,[7] amine oxidase,[8] and pyruvate formate lyase[9] are a few examples. Studies of the radical species have primarily been achieved with EPR or time resolved absorbance spectroscopy. There are very few reports of the vibrational structures of amino acid radicals.[10, 11]

Background

Raman spectroscopy is a method used to study the vibrations of a molecule and gain information on structure and local environment.[12, 13] It is an inelastic scattering technique in which the scattered light is shifted to lower or higher energies depending on whether energy is deposited into or removed from a vibrational mode of the molecule. Resonance Raman spectroscopy is a form of Raman spectroscopy where the energy of the incident light is resonant with an electronic transition of the molecule. In this case, scattering from vibrational modes that are coupled to the electronic transition are selectively enhanced.

Resonance Raman spectroscopy has become more prevalent since the invention of the laser, but still has its limitations. Compounds that are highly fluorescent often mask the Raman spectrum of a molecule of interest. For the study of transient species, compounds that are short lived and therefore, cannot be generated in sufficient quantities, are also a challenge for Raman spectroscopy. Radicals in short peptide chains have lifetimes around 400 ns.[14] The radical in DNA photolyase has a lifetime of 10 ms.[15] A mutant of ribonucleotide reductase has been shown to have a relatively long lifetime of 49 seconds.[16] Despite the success with which the radicals can be generated, none of these radicals are sufficiently long lived or can be generated in sufficient quantities for steady-state resonance Raman spectroscopy.

Transient Raman spectra of tyrosine and tryptophan radicals were previously obtained by ionizing the residue in water with a 235 nm excitation beam using a 20-Hz Nd-YAG laser with 5.5 mW average power.[10] Raman spectra were acquired with low and high power densities. The difference between the two spectra was assumed to be that of the radical species (Figure 5.1)

Recently Schelvis *et al.* reported a time resolved resonance Raman study of the neutral radical Trp_{306} in DNA photolyase.[17] They acquired spectra at 0.7 ms and 2 ms after excitation, obtaining a difference spectrum between these two times and assumed it is of the tryptophan radical (Figure 5.2). Their results agree well with normal mode calculations performed on indole rings.[18]

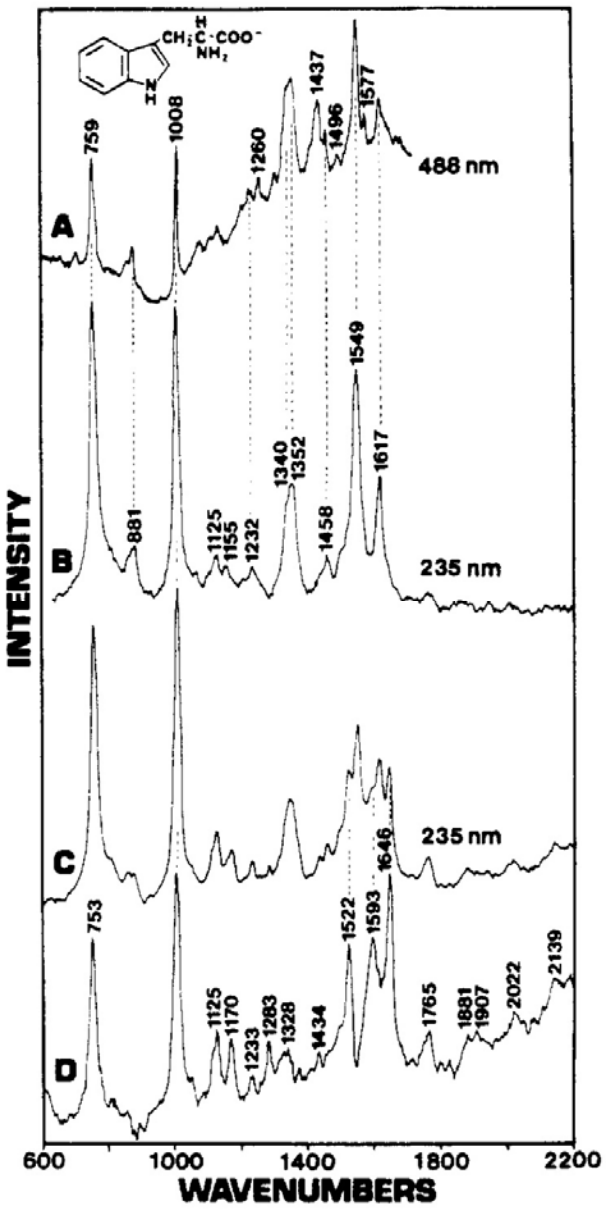

Figure 5.1 (A) Off-resonance Raman spectrum of tryptophan model compound with 488 nm excitation using a CW laser. (B) UV resonance Raman (UVRR) spectrum of a 5 mM tryptophan solution with 235 nm excitation using a 20-Hz Nd-YAG laser (5.5 mW average power) focused above the sample; (C) same conditions as B but with the laser beam focused at the sample; (D) spectrum of the tryptophan transient obtained as the difference spectrum between B and C.[10]

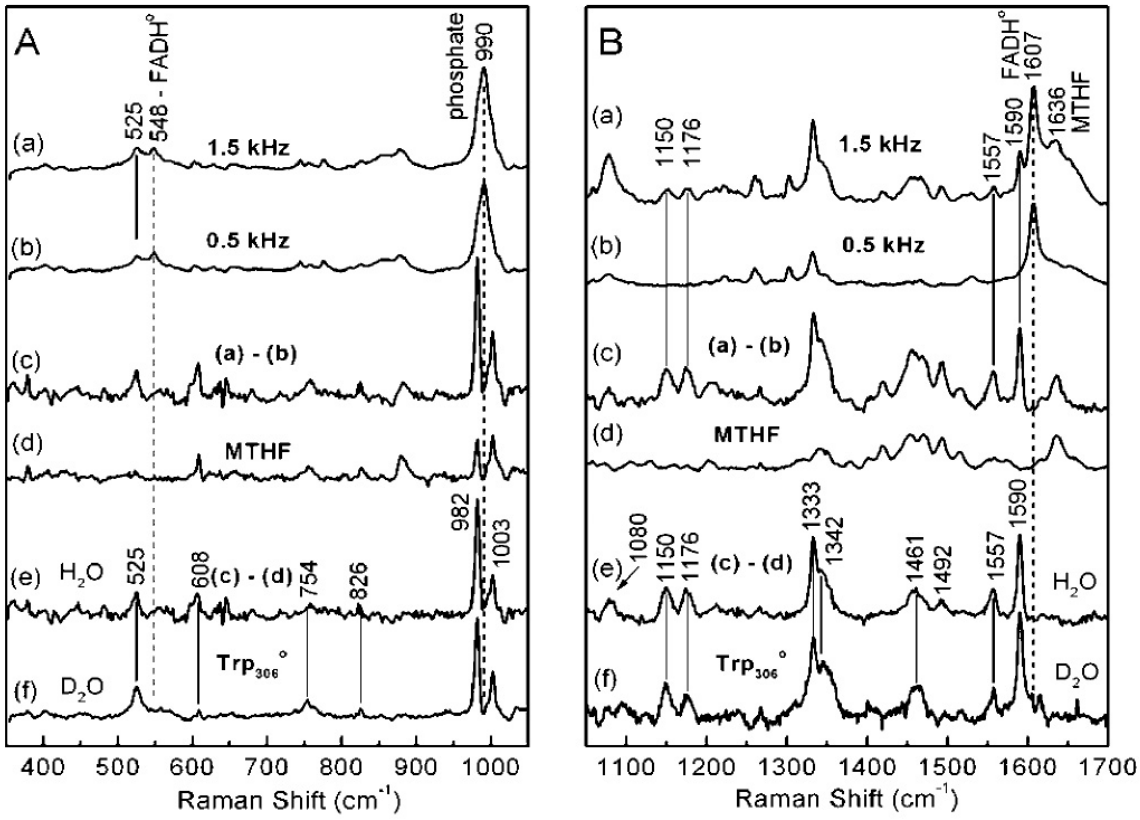

Figure 5.2 Raman spectra of *E. coli* photolyase obtained with 10 mW pulsed excitation at 527 nm at 1.5 (a) and 0.5 kHz (b) repetition rates. (c) 1.5 kHz - 0.5 kHz difference spectra after buffer correction. (d) Reduced photolyase: Raman spectra of MTHF. (e) $Trp_{306}^{\cdot}$: spectrum c corrected for MTHF contributions. (f) $Trp_{306}^{\cdot}$ in D_2O. Dashed lines: removal of $FADH^{\cdot}$ and buffer contributions.[17]

A special tryptophan radical has been discovered in which the lifetime is hours.[19] This radical was discovered by accident in the Gray group. The engineered azurin trp_{108} mutant was supposed to be an exercise in studies of electron hopping. A covalently-bound, oxidized Re metal center created the tryptophan radical, but this radical remained in situ and did not oxidize the Cu center. The radical was characterized by EPR and transient absorption spectroscopy (Figure 5.3).

This long lived tryptophan radical is an excellent candidate to be studied with resonance Raman spectroscopy.

Experimental

Azurin mutant expression

The Q107H/W48F/Y72F/H83Q/Y108W mutant was expressed and purified as described previously in Chapter 4.

Rhenium (I) (1,10-phenanthroline) tricarbonyl η1-tetrahydrofuran triflate synthesis

Rhenium (I) (1,10-phenanthroline) tricarbonyl η1-tetrahydrofuran triflate (DMP-Re) was prepared following a published procedure.[20-22] 0.2 g of 4,7-dimethyl-1,10 phenanthroline (TCI America Boston, MA) was dissolved in 15 ml of dry toluene, under a nitrogen purge with a reflux condenser. 0.3 g of pentacarbonylchloro-rhenium(I) was added, and the resulting mixture was a chalky white. The solution was heated to 60 ºC for an hour. After an hour the solution had a yellow suspension; the solution was filtered through a fine frit and the solid was collected. The solid was washed with toluene, resuspended in methylene chloride, decanted and pumped to dryness. The resulting solid

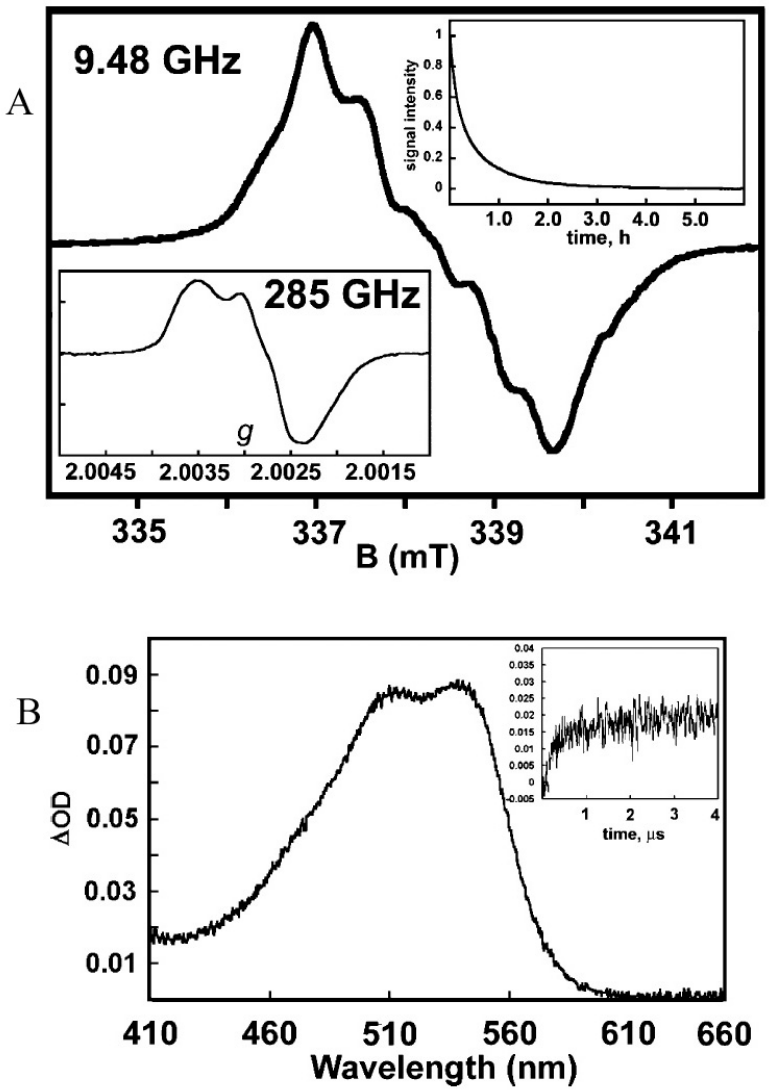

Figure 5.3 A: X-band EPR spectrum of W108 azurin (77 K, pH 7.2 KPi, υ = 9.4753 GHz, modulation amplitude = 0.2 mT, microwave power ≈ 200 μW). Lower left inset: 285 GHz EPR spectrum under nonsaturating conditions (50 K, modulation amplitude = 0.1 mT). Upper right inset: Decay of EPR signal as a function of time. B: Transient absorption spectrum of W108 azurin recorded 20 μs after flash/quench of 63 mM Re(I)Az(W108)Zn(II)/5 mM $[Co(NH_3)_5Cl]Cl_2$ in 50 mM KPi (pH 7.2) at room temperature. Inset: Rise in signal at 520 nm as a function of time delay after excitation. Spectra are from reference.[19]

was resuspended in dry THF (15 ml) under a nitrogen purge with a reflux condenser. Silver trifluoromethanesulfonate (AgOTf) (0.1 g) was added to the solution. This solution was allowed to reflux in the dark for 4 hours. The resulting yellow solution was filtered over celite to remove white precipitate. The THF was removed by vacuum to produce a yellow oil. The oil was redissolved in 5 ml methylene chloride and layered with 50 ml of pentane at 0 ºC. This was then placed stored overnight at -20 ºC. The resulting crystals were collected using a fine glass frit and dried under vacuum overnight to give yellow solid. TLC of the product on silica gel with 9:1 methylene chloride:methanol eluent showed only a single spot. No further purification was pursued (29% yield).

Protein labeling

The azurin to be labeled was transferred to a 25 mM HEPES buffer, pH 7.4 using an Amicon, and concentrated to about 1 mM. This solution was then placed into Eppindorf tubes (1 ml), to which 100 µl of a saturated aqueous solution of DMP-Re was added. This solution was then placed on a heating block at 37 ºC for 1 week in the dark. Excess label was removed using a PD-10 size exclusion column (GE Healthcare Piscataway, NJ).

Labeled protein purification

Labeled azurin was separated from unlabeled protein using an FPLC and an IMAC column (Pharmacia). Following the labeling reaction, the azurin solution was transferred to a 20 mM NaPi, 750 mM NaCl pH 7.2 buffer using an Amicon. The

column was then loaded with 100 mM $CuSO_4$ and washed with 5 column volumes of 20 mM NaPi, 750 mM NH_4Cl pH 7.2 buffer followed by 5 column volumes of 20 mM NaPi, 750 mM NaCl pH 7.2 buffer. About 1 ml of 1 mM azurin was loaded onto the column and run with the IMAC protocol at a flow rate of 1 ml/min (Table 5.1). The labeled protein came off the column immediately while unlabeled protein stuck and came off with the NH_4Cl buffer.

Radical generation

Two methods were found to generate the tryptophan radical. The first method involved a solution of 50 μM labeled protein (Q107H-(DMP-Re)/W48F/Y72F/H83Q/Y108W) and 500 μM pentaamminechlorocobalt(III) chloride (Alfa Aesar Ward Hill, MA). This deoxygenated solution was placed in a glass capillary and exposed to a xenon arc lamp. The 355 nm light from the lamp created the excited-state DMP-Re(I)* which was in turn oxidatively quenched by $Co(NH_3)_5Cl$. The DMP-Re(II) species (1.85 V)[19] then oxidized W108 (1.02 V)[23] creating the long lived trp108 radical.

A second method of creating the radical did not require a metal label. Q107H/W48F/Y72F/H83Q/Y108W azurin (50 μM) was placed in front of a 280 nm laser beam (Spectraphysics FDO Mountain View, CA). The tryptophan residue was directly photolyzed, resulting in the formation of the tryptophan radical and solvated electron. The solvated electron absorption signal (broad peak at ~700 nm) disappeared after ~4 μs and a steady-state difference spectrum was obtained for the radical. When the solvated electron was generated in this fashion, it has three routes for disappearance:

IMAC FPLC Buffer Program

Buffer A 20 mM NaPi, 750 mM NaCl pH 7.2
Buffer B 20 mM NaPi, 750 mM NH_4Cl pH 7.2

ml	%A	%B
0	100	0
12	100	0
15	0	100
25	0	100
27	100	0
32	100	0

Table 5.1 IMAC buffer and eluent composition table.

recombination with the tryptophan radical, reaction with the solvent, or reduction of the Cu^{2+} redox center to Cu^{+}. If the solvated electron recombines with the tryptophan radical, no net signal will be recorded in the steady state spectrum. If the electron reacts with solvent, we will only observe an increase in absorption at 525 nm (tryptophan radical). If the electron reduces the copper center, we expect to see an increase in absorption at 525 nm and a decrease in absorption at 625 nm (Cu^{2+}). As can be seen in Figure 5.4, the last scenario was observed: formation of the tryptophan radical and reduction of the copper center are apparent in the steady-state difference spectrum. This difference spectrum allowed for the calculation of an upper limit to the molar extinction coefficient of the tryptophan radical since more radical species will be generated than there will be loss of Cu^{2+} signal. The resulting upper limit for the extinction coefficient is 1750 M^{-1} cm^{-1}, which is about half of the previously reported value.[19] It is interesting to note that attempts to scavenge the solvated electron with N_2O inhibited all radical generation with direct UV photolysis.

Raman spectroscopy

Resonance Raman data was acquired using the instrumentation in the Beckman Institute Laser Resource Center. The labeled protein sample (Q107H-(DMP-Re)/W48F/Y72F/H83Q/Y108W) was excited with the 514 nm line from a Coherent Innova 70 argon ion laser (Santa Clara, CA). The scattered light was focused onto a 100 μm slit and dispersed in a Spex 750 spectrograph (Edison, NJ). Raman signal was recorded using a Princeton Instruments liquid nitrogen cooled CCD detector (Acton, MA). Power at the sample was less than 1 mW and a 530 nm long pass filter was placed

in front of the entrance slit to remove elastically scattered laser light. Acquisition lasted 5 minutes total (30-second scans), cosmic rays were removed, and difference spectra of pre (Figure 5.5) and post (Figure 5.6) photolysis were generated. Samples were also allowed to equilibrate in D_2O and the same Raman experiments were performed (Figure 5.7).

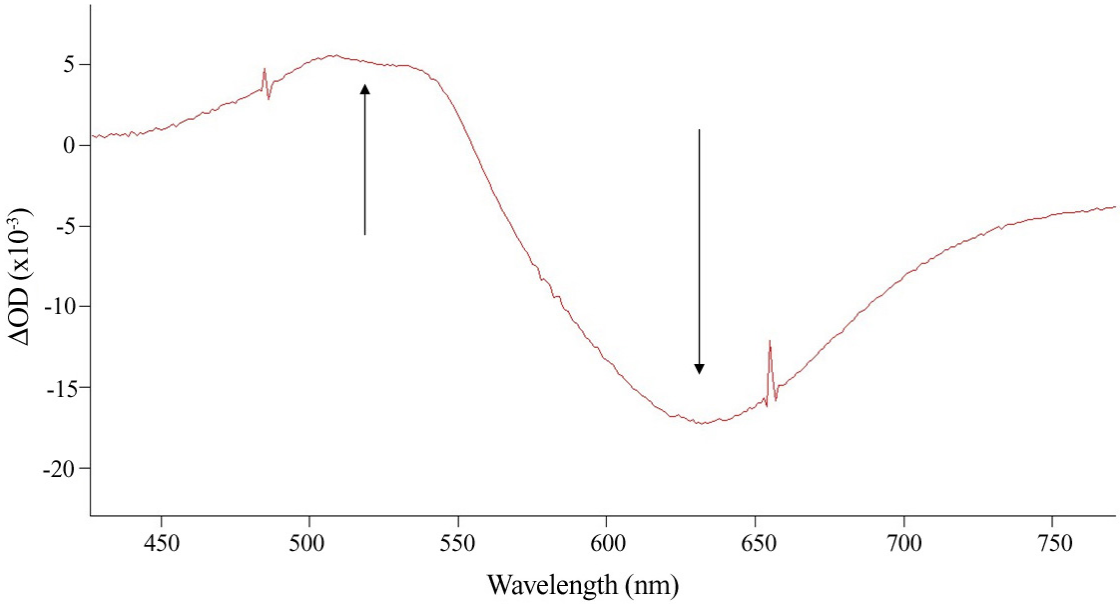

Figure 5.4 Steady-state absorption spectrum of the tryptophan radical and azurin Cu^{2+} bleach.

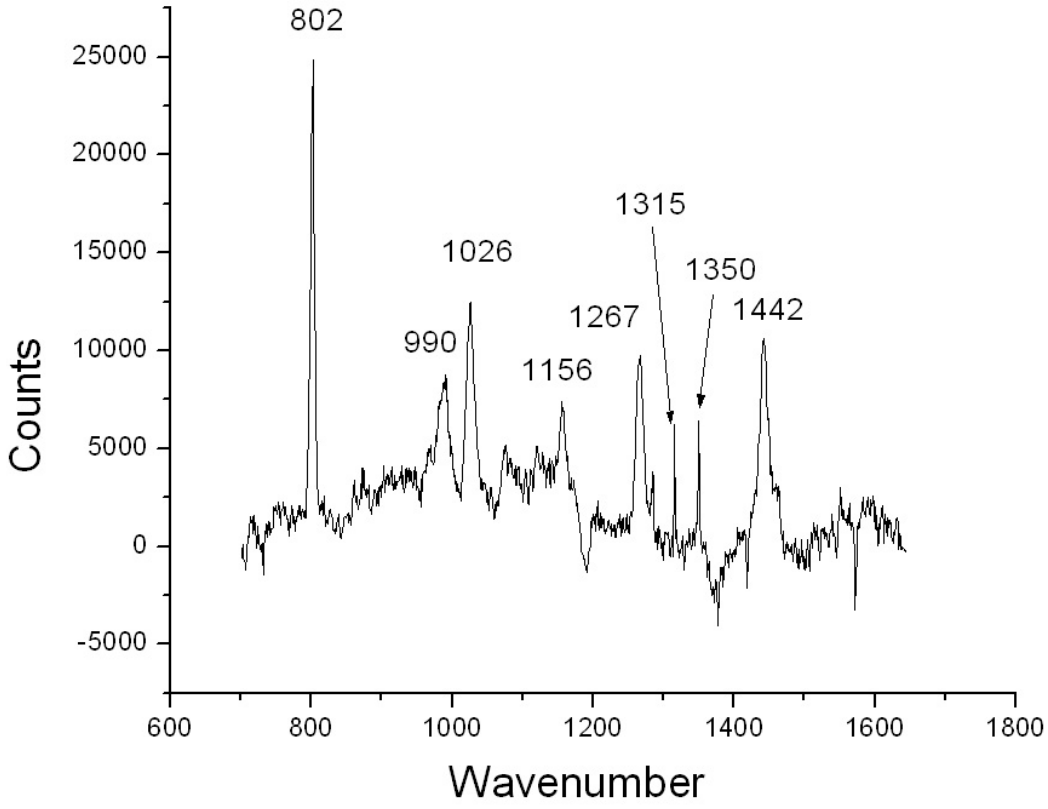

Figure 5.5 Resonance Raman spectrum of Q107H-(DMP-Re) /W48F/Y72F/H83Q/Y108W labeled protein prior to exposure to xenon lamp (355 nm excitation of DMP-Re).

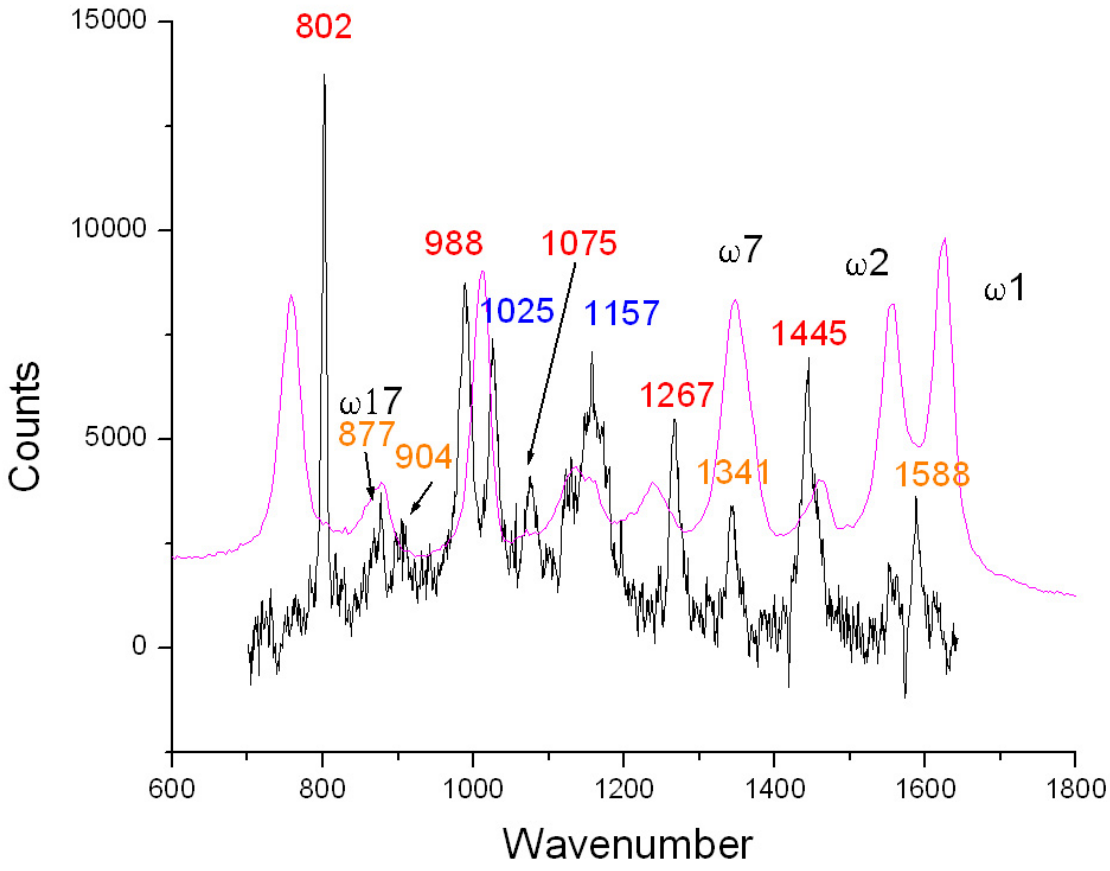

Figure 5.6 Resonance Raman spectrum of Q107H-(DMP -Re) /W48F/Y72F/H83Q/Y108W labeled protein post exposure to xenon lamp (355 nm excitation of DMP-Re); Pre-photolysis peaks (red), new post photolysis peaks (orange), $Co(NH_3)_5Cl$ (blue), UV resonance Raman of tryptophan (purple). Mode labels refer to UVRR spectrum.

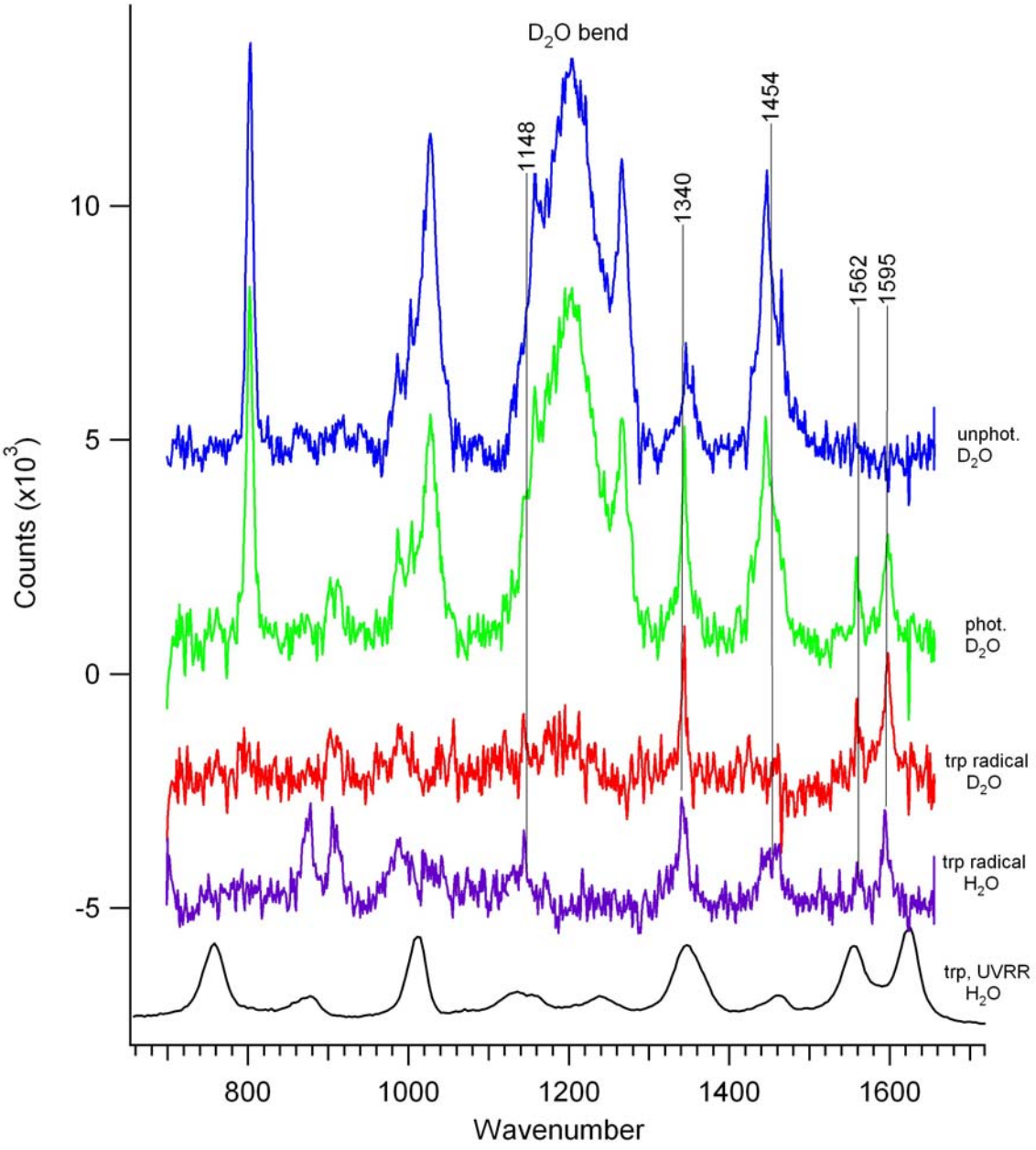

Figure 5.7 Resonance Raman spectra of the D_2O unphotolyzed, D_2O photolyzed, D_2O difference spectrum, H_2O difference spectrum, and UV resonance Raman spectrum of tryptophan.

Discussion

Our results are in good agreement with calculations and previously reported experimental values (Table 5.2). The assignments for the radical in H_2O include a 1595 cm^{-1} peak that corresponds to a normal mode involving C-N stretch and phenyl ring vibrations (W1).[24-26] The 1562 and 1454 cm^{-1} modes primarily involve in-plane vibrations of the phenyl ring (W2 and W4). The 1340 cm^{-1} mode (W7) is attributed to a Fermi resonance between a skeletal stretching fundamental and out-of-plane vibrations of the indole ring. The 1148 cm^{-1} peak is the W3 mode that primarily consists of N-C and C-C stretches in the five-membered ring. A number of tryptophan modes, such as the W3 and W7 modes, have been shown to be sensitive to tryptophan structure and local environment.[24, 25] Preliminary data indicate that the resonance Raman spectrum of the radical in D_2O is very similar to that obtained in H_2O for this mutant. The tentative assignments presented here demonstrate the wealth of information that may be obtained with resonance Raman spectroscopy, and lay important foundations for future studies of amino acid radical intermediates.

Conclusion

The upper limit on the extinction coefficient for a tryptophan radical (Trp108) in an azurin mutant has been calculated to be 1750 M^{-1} cm^{-1}. This radical has been shown to be generated by direct photolysis with UV light; surprisingly, in the presence of the electron scavenger N_2O, the tryptophan radical cannot be generated by direct photolysis. Finally, our Raman peaks for the tryptophan radical are in good agreement with both experimental and computational data.

Mode	Trp_{108}	Trp_{306}	Theory
W1	1595	1590	1583
W2	1562	1557	1560
W4	1454	1461	1434
W7	1340	1342	1351
W3	1148	1150	1317

Table 5.2 Raman shift (wavenumber) of the Trp_{108} radical in H_2O from the current study, Trp_{306} radical from the DNA photolyase study,[17] and calculations.[18] Mode description and assignment from literature.[24-26]

References

1. Keyer, K.; Imlay, J. A., *Proc. Natl. Acad. Sci. USA* **1996,** 93, 13635.
2. Davies, K. J., *J. Biol. Chem.* **1987** 262, 9895.
3. Atkin, C. L.; Thelander, L.; Reichard, P.; Lang, G., *Journal of Biological Chemistry* **1973,** 248, 7464.
4. Brown, N. C.; Canellakis, Z. N.; Lundin, B.; Reichard, P.; Thelander, L., *Eur. J. Biochem.* **1969,** 9, 561.
5. Jordan, A.; Reichard, P., *Annu. Rev. Biochem.* **1998,** 67, 71.
6. Stubbe, J.; van der Donk, W. A., *Chem. Rev.* **1998,** 98, 705.
7. Turner, B. E.; Branchaud, B. P., *Bioorganic & Medicinal Chemistry Letters* **1999,** 9, 3341.
8. Pedersen, J. Z.; El-Sherbini, S.; Finazzi-Agro, A.; Rotilio, G., *Biochemistry* **1992,** 31, 8.
9. Guo, J.-D.; Himo, F., *J. Phys. Chem. B* **2004,** 108, 15347.
10. Johnson, C. R.; Ludwig, M.; Asher, S. A., *J . Am. Chem. Soc.* **1986,** 108, 905.
11. Berthomieu, C.; Boussac, A., *Biospectroscopy* **1996,** 1, 187.
12. Raman, C. V.; Krishnan, K. S., *Nature* **1928,** 121, 501.
13. Raman, C. V.; Krishnan, K. S., *Indian Journal of Physics* **1928,** 2, 399.
14. Jones, G.; Lu, L. N., *J. Org. Chem.* **1998,** 63, 8938.
15. Aubert, C.; Vos, M. H.; Mathis, P.; Eker, A. P. M.; Brettel, K., *Nature* **2000,** 405, 586.
16. Potsch, S.; Lendzian, F.; Ingemarson, R.; Hornberg, A.; Thelander, L.; Lubitz, W.; Lassmann, G.; Graslund, A., *J. Biol. Chem.* **1999,** 274, 17696.
17. Gurudas, U.; Schelvis, J. P. M., *J. Am. Chem. Soc.* **2004,** 126, 12788.
18. Bunte, S. W.; Jensen, G. M.; McNesby, K. L.; Goodin, D. B.; Chabalowski, C. F.; Nieminen, R. M.; Suhai, S.; Jalkanen, K. J., *Chemical Physics* **2001,** 265, 13.
19. Miller, J. E.; Gradinaru, C.; Crane, B. R.; Di Bilio, A. J.; Wehbi, W. A.; Un, S.; Winkler, J. R.; Gray, H. B., *J. Am. Chem. Soc.* **2003,** 125, 14220.
20. Connick, W. B.; Di Bilio, A. J.; Hill, M. G.; Winkler, J. R.; Gray, H. B., *Inorg. Chim. Acta* **1995,** 240, 169.
21. Wrighton, M.; Morse, D. L., *J. Am. Chem. Soc.* **1974,** 96, 998.
22. Sullivan, B. P.; Meyer, T. J., *J. Chem. Soc. Chem. Comm.* **1984**, 1244.
23. Harriman, A., *J. Phys. Chem.* **1987,** 91, 6102.
24. Harada, I.; Takeuchi, H., *Spectroscopy of Biological Systems*. Wiley: Chichester, U.K., 1986.
25. Miura, T.; Takeuchi, H.; Harada, I. J., *J. Raman Spectrosc.* **1989,** 20, 667.
26. Takeuchi, H.; Harada, I., *Spectrochim. Acta* **1986,** 42A, 1069.